A NEW APPROACH TO DETERMINE THE THERMOPHYSICAL PROPERTIES OF SATURATED LIQUID-VAPOR MIXTURE NANOREFRIGERANTS

A THESIS SUBMITTED TO
THE GRADUATE SCHOOL OF NATURAL AND APPLIED SCIENCES
OF
MIDDLE EAST TECHNICAL UNIVERSITY

BY

BİLGEHAN TEKİN

IN PARTIAL FULFILLMENT OF THE REQUIREMENTS
FOR
THE DEGREE OF DOCTOR OF PHILOSOPHY
IN
MECHANICAL ENGINEERING

JULY 2023

Approval of the thesis:

A NEW APPROACH TO DETERMINE THE THERMOPHYSICAL PROPERTIES OF SATURATED LIQUID-VAPOR MIXTURE NANOREFRIGERANTS

submitted by **BİLGEHAN TEKİN** in partial fulfillment of the requirements for the degree of **Doctor of Philosophy** i**n Mechanical Engineering, Middle East Technical University** by,

Prof. Dr. Halil Kalıpçılar
Dean, Graduate School of **Natural and Applied Sciences** _____

Prof. Dr. Mehmet Ali Sahir Arıkan
Head of the Department, **Mechanical Engineering** _____

Prof. Dr. Almıla Güvenç Yazıcıoğlu
Supervisor, **Mechanical Engineering, METU** _____

Examining Committee Members:

Assoc. Prof. Dr. Özgür Bayer
Mechanical Engineering, METU _____

Prof. Dr. Almıla Güvenç Yazıcıoğlu
Mechanical Engineering, METU _____

Prof. Dr. Hakan Ertürk
Mechanical Engineering, Boğaziçi University _____

Prof. Dr. Selin Aradağ Çelebioğlu
Mechanical Engineering, TED University _____

Assoc. Prof. Dr. Feyza Kazanç Özerinç
Mechanical Engineering, METU _____

Date: 11.07.2023

I hereby declare that all information in this document has been obtained and presented in accordance with academic rules and ethical conduct. I also declare that, as required by these rules and conduct, I have fully cited and referenced all material and results that are not original to this work.

Name Last name : Tekin, Bilgehan

Signature :

ABSTRACT

A NEW APPROACH TO DETERMINE THE THERMOPHYSICAL PROPERTIES OF SATURATED LIQUID-VAPOR MIXTURE NANOREFRIGERANTS

Tekin, Bilgehan
Doctor of Philosophy, Mechanical Engineering
Supervisor: Prof. Dr. Almıla Güvenç Yazıcıoğlu

July 2023, 175 pages

With the increasing thermal load in new technological devices and applications, demand for cooling rates increases. Therefore, enhancement in heat transfer efficiency is a vital issue. To increase the thermal performance of the vapor compression refrigeration cycle (VCRC) nanorefrigerants are used. Nanorefrigerant use in refrigerators still needs attention because there are not sufficient data to determine the thermophysical properties of nanorefrigerants. A new approach, based on an analogy to fluidized beds, to determine the thermophysical properties of nanorefrigerants in a two-phase flow of refrigerant is suggested in this study and the approach is verified using Artificial Neural Network (ANN). A case study for an evaporator in an ideal R141b VCRC is performed for four different nanoparticles (Cu, Al, Al_2O_3, CuO) and three mass fraction values, and the increase in COP with nanorefrigerants is reported between 4.15%-13.17%.

Keywords: Nanorefrigerant, Conductivity, Viscosity, ANN, COP

ÖZ

DOYMUŞ SIVI-BUHAR KARIŞIMI NANOSOĞUTKANLARIN TERMOFİZİKSEL ÖZELLİKLERİNİN BULUNMASI İÇİN YENİ BİR YAKLAŞIM

Tekin, Bilgehan
Doktora, Makina Mühendisliği
Tez Yöneticisi: Prof. Dr. Almıla Güvenç Yazıcıoğlu

Temmuz 2023, 175 sayfa

Yeni teknolojik cihaz ve uygulamalarda artan termal yük ile soğutma ihtiyacı daartmaktadır. Bu nedenle, ısı transfer verimliliğindeki artış hayati bir konudur. Buhar sıkıştırmalı soğutma çevriminin termal performansını artırmak için nanosoğutucular kullanılır. Nanosoğutucuların termofiziksel özelliklerini belirlemek için yeterli veri olmadığı için buzdolaplarında nanosoğutucu kullanımı hala dikkat gerektirmektedir. Bu çalışmada, iki fazlı bir soğutucu akışkan akışında nanosoğutucu akışkanların termofiziksel özelliklerini belirlemek için akışkan yataklara benzetmeye dayalı yeni bir yaklaşım önerilmiş ve bu yaklaşım Yapay Sinir Ağı (YSA) kullanılarak doğrulanmıştır. İdeal bir R141b çevrimindeki bir evaporatör için dört farklı nanopartikül (Cu, Al, Al_2O_3, CuO) ve üç kütle fraksiyonu değeri için bir vaka çalışması yapılmış ve nanosoğutucu akışkanlarla performans katsayısındaki (COP) artış %4.15-%13.17 arasında rapor edilmiştir.

Anahtar Kelimeler: Nanosoğutkan, Isıl iletkenlik, Akmazlık, YSA, Performans Katsayısı

Dedication

To My Parents

ACKNOWLEDGMENTS

The author wishes to express his deepest gratitude to his supervisor Prof. Dr. Almıla Güvenç Yazıcıoğlu for her guidance, advice, criticism, encouragements and insight throughout the research.

The student is partially funded by Scientific and Technological Research Council of Türkiye.

TABLE OF CONTENTS

LIST OF TABLES

TABLES

LIST OF FIGURES

FIGURES

LIST OF ABBREVIATIONS

ABBREVIATIONS

Bo : boiling number [-]

c : heat capacity [kJ/K]

c_p : specific heat [kJ/K]

Co : confinement number [-]

COP : coefficient of performance [-]

E : enhancement factor [-]

F : boiling enhancement factor [-]

Fr : Froude number [-]

h : heat transfer coefficient [$W/m^2.K$]

i : enthalpy [kJ/kg]

k : thermal conductivity [W/m.K]

M : molecular weight [kg/kmol]

m : mass [kg]

ρ : density [kg/m^3]

P : pressure [kPa]

Pr : Prandtl number [-]

r : radius [nm]

POE : Polyolester oil [-]

Re : Reynolds number [-]

q" : heat flux [W/m2]

S : suppression factor [-]

t : thickness of nanolayer [nm]

V : Volume [m^3]

X_{tt} : Lockhart-Martinelli parameter [-]

x : quality [%]

Δp_v : vaporization pressure [kPa]

LIST OF SYMBOLS

SYMBOLS

μ : viscosity [Pa.s]

Θ_b : wall superheat [ºK]

φ : volume fraction [%]

ψ : multiplication factor [-]

Subscripts

cb : convective boiling

f : base fluid

l : liquid

lv : vaporization

m : mass fraction

nb : nucleate boiling

nf : nanofluid

nr : nanorefrigerant

p : nanoparticle

pe : effective nanoparticle

r : reduced

v : pool boiling, vapore if it is not necessary

CHAPTER 1

INTRODUCTION and LITERATURE REVIEW

For heat transfer applications with liquid flow, nanoparticles have been used to increase the thermal conductivity of the working fluids in the last few decades. Instead of pure liquids, nanofluids, which are the mixture of base (pure) liquids (such as water, ethylene glycol, engine oil, refrigerants) and nanoparticles [high thermal conductivity materials such as; metals (Ag, Au, Fe, Cu, et al.), metal oxides (CuO, Al_2O_3, ZnO, SiO_2, TiO_2, Fe_3O_4, et al.), Carbides (TiC, SiC, et al.), Nitrides (SiN, AlN, et al.), or carbon forms (graphite, diamond, single and multi wall carbon nanotubes, et al.), are used in various research applications to increase the heat transfer performance. Unfortunately, these nanoparticles lead to an increase in viscosity as well as conductivity. Therefore the pressure drop in the channel increases, leading to exemplified pumping power expenditure in addition to heat transfer. Thus, a thorough study of nanofluids is critical to optimize flow parameters, such as base fluid and nanoparticle type, fraction and size of nanoparticles, working temperature, and pressure. In two-phase flows, quality is also essential.

A nanorefrigerant is a sub-class of nanofluids [Celen et al., 2014]. However, the investigation of nanorefrigerant flow and the optimization problem is much more complex, where three phases (two-phase liquid-vapor refrigerant and solid nanoparticles) of two different materials are present in the mixture. The present literature stresses the need for more studies and a deeper understanding of heat transfer for this specific subject [Zhelezny et al., 2017]. In addition, research on the thermophysical properties of nanorefrigerants is scarce [Sanukrishna, et al., 2018].

In recent decades, the demand for efficient cooling systems [Yu et al., 2019] has grown significantly due to the rapid expansion of industries, the increasing global population, and the ever-advancing technological landscape. However, conventional refrigerants used in cooling systems pose significant environmental challenges, particularly their contribution to global warming and ozone depletion [IPCC, 2013]. As a result, there is an urgent need for innovative and sustainable alternatives [Agyenim et al., 2010] that can address these concerns while maintaining or enhancing the overall energy efficiency of cooling processes.

Nanorefrigerants have emerged as a promising technology in refrigeration and cooling systems [Saidur et al., 2011]. They are a new class of heat transfer fluids that consist of base refrigerants infused with nanoparticles. Integrating nanoparticles into traditional refrigerants aims to enhance thermophysical properties [Halim and Sidik, 2020] and improve overall heat transfer performance. Nanorefrigerants offer the potential for more efficient and effective cooling systems [Patil et al., 2015], contributing to energy savings, environmental sustainability, and improved thermal management [Hai et al., 2023] in various applications.

The nanoparticles employed in nanorefrigerants are typically selected based on their high thermal conductivity, as mentioned above, and stability [Wang et al., 1999]. Examples of commonly used nanoparticles include metals (e.g., silver, copper) [Govindasamy et al., 2022], metal oxides (e.g., aluminum oxide, titanium dioxide, zinc oxide) [Wen and Ding, 2004], carbon-based materials (e.g., carbon nanotubes, graphene) [Ali et al., 2021], and other nanomaterials with unique properties. These carbon nanotube nanoparticles possess a high aspect ratio, large surface area, and superior thermal properties, making them ideal for enhancing heat transfer characteristics in refrigeration systems. SEM images of spherical and cubical ZnO nanoparticles are given in Figures 1.1 and 1.2.

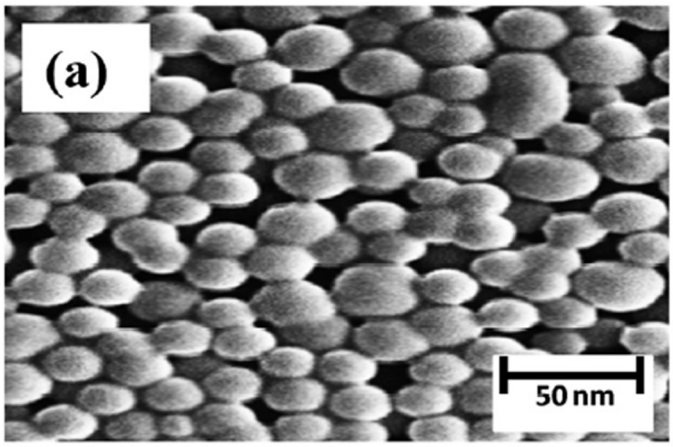

Figure 1.1. SEM image of spherical ZnO nanoparticles [Maheshwary et al., 2018]

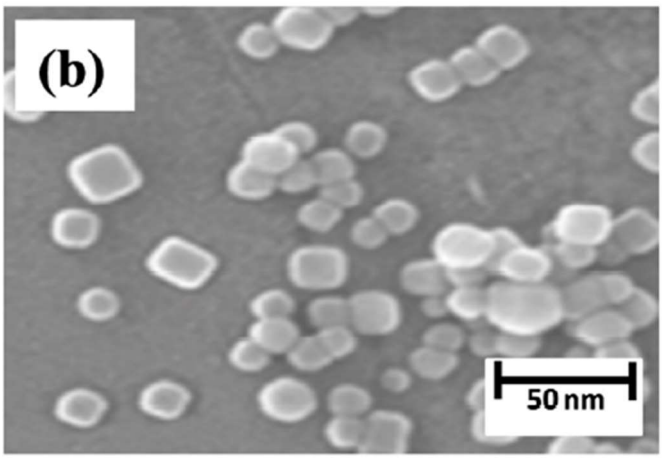

Figure 1.2. SEM image of cubical ZnO nanoparticles [Maheshwary et al., 2018]

The primary objective of incorporating nanoparticles into refrigerants is to enhance their thermophysical properties [Yıldız et al., 2021], such as thermal conductivity [Azmi et al., 2017] and specific heat capacity [Zhou et al., 2010]. As a side effect, viscosity [Wang et al., 1999] also increases. By increasing the thermal conductivity, nanorefrigerants can transfer heat more effectively, enabling better cooling performance and reduced energy consumption. The improved specific heat capacity allows for better thermal storage and temperature regulation. Moreover, the alteration in viscosity influences the fluid flow behavior, affecting heat transfer efficiency and pumping power requirements.

It is essential to consider the potential applications and benefits of nanorefrigerants in various fields. Nanorefrigerants are not limited to traditional cooling systems but extend to emerging technologies [Yu and Xie, 2012] and sectors where efficient thermal management is crucial. One significant application area is electronics cooling [Cremaschi, 2012]. With the ever-increasing power density and miniaturization of electronic devices, effective cooling solutions are essential to prevent overheating and ensure optimal performance and reliability. Nanorefrigerants offer enhanced heat transfer capabilities, allowing for efficient cooling of electronic components and reducing the risk of thermal damage. They can be integrated into heat sinks, heat pipes, or direct liquid cooling systems to improve heat dissipation and maintain stable operating temperatures.

Nanorefrigerants also hold potential in thermal energy storage systems. Thermal energy storage is an essential component of renewable energy technologies [Liu et al., 2016] and can facilitate efficient energy utilization and load management. Incorporating nanorefrigerants into thermal energy storage systems can enhance heat transfer rates and improve overall energy storage and retrieval efficiency [Helvaci and Khan, 2017]. This can contribute to developing more sustainable and effective energy storage solutions for applications such as solar thermal power plants, district heating and cooling, and waste heat recovery [Hu et al., 2018].

Another emerging application area is in the field of aerospace and aviation. Efficient thermal management is critical in these fields to ensure that systems and components are safe and optimal operation [Jixiang et al., 2021]. Nanorefrigerants can improve heat transfer efficiency and reduce weight and size requirements in cooling systems [Awais et al., 2021], which are particularly important in space applications where weight restrictions are significant [Verma et al., 2011]. Using nanorefrigerants can enhance the thermal performance of avionic systems, improve fuel efficiency, and extend the lifespan of critical components [Sonawane, 2023].

Furthermore, nanorefrigerants can affect the field of air conditioning in buildings and refrigeration [Sanukrishna and Vishnu, 2017]. These systems account for a significant portion of global energy consumption. By incorporating nanorefrigerants with enhanced thermophysical properties and improving the energy efficiency of cooling systems, it is possible to reduce electricity consumption and decrease the environmental impact associated with cooling operations [Kasaeian et al., 2018]. This can contribute to achieving energy efficiency goals and promoting sustainable practices in the building sector [Redhwan et al., 2016]. In summary, nanorefrigerants offer a wide range of potential applications in various fields where efficient thermal management is crucial. From electronics cooling to thermal energy storage, aerospace, and building refrigeration, nanorefrigerants can enhance heat transfer efficiency, improve system performance, and contribute to energy savings and environmental sustainability [Azmi et al., 2017]. As research and development efforts continue, it is expected that nanorefrigerants will play an increasingly significant role in shaping the future of cooling and thermal management technologies [Benam et al., 2021]. By harnessing their unique properties and addressing the associated challenges, nanorefrigerants can pave the way for more efficient, reliable, and sustainable cooling solutions across diverse industries and applications [Sanukrishna et al., 2018].

As mentioned above, one of the critical advantages of nanorefrigerants is their ability to enhance the thermal conductivity of base refrigerants. Incorporating nanoparticles, which possess high thermal conductivity values, into the refrigerant matrix can substantially improve heat transfer efficiency [Choi and Eastman, 1995]. The increased thermal conductivity allows for more effective heat dissipation, enabling refrigeration systems to operate at lower temperatures and achieve better cooling performance [Patil et al., 2015]. This is particularly important in applications where heat transfer limitations can hinder the performance of conventional refrigeration systems [Sanukrishna and Vishnu, 2017].

Moreover, nanorefrigerants have the potential to enhance specific heat capacity, which is another crucial thermophysical property [Wang and Mujumdar, 2007]. By altering the composition and structure of the refrigerant through nanoparticle integration, the specific heat capacity of the nanorefrigerant can be significantly modified [Faizan and Han, 2016]. This property enables efficient thermal storage, facilitating heat transfer from warmer to colder regions within the refrigeration system [Chon et al., 2005]. It also contributes to temperature regulation and stability, ensuring optimal operating conditions and reducing the risk of thermal fluctuations [Xiong et al., 2023].

In addition to thermal conductivity and specific heat capacity, the viscosity of nanorefrigerants plays a vital role in determining their overall heat transfer performance [Buongiorno, 2006]. While the addition of nanoparticles can enhance the thermal properties of the refrigerant, it may also lead to an increase in viscosity [Wang and Mujumdar, 2008]. The viscosity of nanorefrigerants influences the fluid flow behavior and pressure drop within the system [Kakaç and Pramuanjaroenkij, 2009]. It is essential to balance the improved heat transfer characteristics and the potential increase in pumping power requirements due to increased viscosity. Optimizing nanoparticle concentration and size can help mitigate the adverse effects on fluid flow and maintain an efficient and reliable refrigeration process [He et al., 2007].

To fully harness the potential of nanorefrigerants, extensive research efforts have been devoted to understanding their thermophysical properties, heat transfer mechanisms, stability, and practical applications [Saidur et al., 2011]. Experimental investigations have been conducted to measure and analyze the thermophysical properties of nanorefrigerants under varying conditions [Wang et al., 1999]. These studies provide valuable insights into the influence of nanoparticle concentration, size, and type on the thermal conductivity, specific heat capacity, and viscosity of nanorefrigerants [Keblinski et al., 2002]. Theoretical modeling and simulation

techniques have also been employed to understand the underlying mechanisms better and optimize the design and application of nanorefrigerants [Das et al., 2003].

Computational fluid dynamics (CFD) simulations [Duangthongsuk and Wongwises, 2009], molecular dynamics simulations [Xiong et al., 2023], and other theoretical approaches have been utilized to investigate the behavior of nanorefrigerants at the molecular and macroscopic levels [Abed et al., 2022]. These simulations help elucidate the fundamental mechanisms of heat transfer enhancement in nanorefrigerants and provide insights into the interplay between nanoparticle characteristics, fluid flow dynamics, and heat transfer efficiency [Wen and Ding, 2004].

Experimental techniques play a crucial role in measuring the thermophysical properties of nanorefrigerants. Various experimental methods, such as transient hot-wire, differential scanning calorimetry, and thermal conductivity analyzers, are employed to find the thermal conductivity and specific heat capacity of nanorefrigerants [Wang et al., 2017]. These techniques involve subjecting the nanorefrigerant samples to controlled heating or cooling and measuring the associated temperature and heat flow changes.

In addition to experimental approaches, theoretical models and numerical simulations are valuable tools for predicting and understanding the thermophysical behavior of nanorefrigerants [Xuan and Li, 2003]. These models consider factors such as nanoparticle concentration, size, and morphology to estimate the effective thermal conductivity and specific heat capacity of the nanorefrigerant mixture [Keblinski et al., 2002].

To ensure the accuracy and reliability of thermophysical property measurements, it is vital to standardize testing methods and establish consistent evaluation procedures. Organizations such as ASTM International and ISO (International Organization for

Standardization) are actively working on developing standard protocols for measuring the thermophysical properties of nanorefrigerants [ASTM E2585-16, 2016] [ASTM D7896-18, 2018] [ISO 22007-4, 2016]. These standards facilitate the comparison of data obtained from different studies, enable a better understanding of nanorefrigerant behavior, and support the development of reliable guidelines for their practical implementation. Therefore, research efforts are focused on exploring the effects of different parameters on the thermophysical properties of nanorefrigerants. Factors such as nanoparticle concentration [Fadhilah et al., 2014], particle size distribution, temperature [Duangthongsuk and Wongwises, 2009-II], pressure, and base fluid composition can significantly influence the properties of nanorefrigerants [Mondejar et al., 2021]. Understanding these effects is crucial for tailoring nanorefrigerant formulations to specific applications and optimizing their performance.

The studies about nanofluids started with the concept of increasing thermal conductivity. The addition of nanoparticles tends to increase viscosity as well as conductivity. The present studies about thermophysical properties usually cover both properties. In addition, the heat transfer and pressure drop characteristics for nanofluid flow are also considered, and many studies are available in the literature with the interests given below.

- Analytical studies: Calculate thermophysical properties and heat transfer (and/or pressure drop) with the available models and correlations, and compare the results with pure fluid flows.
- Numerical studies: Calculate thermophysical properties with the available models, form a model for the problem, solve with available programs or in-house codes, and compare the results with pure fluid flows and/or reference studies to show the enhancement or to validate the flow model.
- Experimental studies: Perform experiments and compare the results with pure fluid flows, offer new correlations, and/or optimize the flow condition.

- Review studies: Investigate the available studies, compare them with the theory/analytical results, and offer new correlations for a specified or any condition.

In the literature, the research about nanofluids in terms of the types of studies given above is mainly performed for liquid-based nanofluids, in which the base fluid is in the liquid phase only. For the nanorefrigerants, the current state of the art focuses on heat transfer in a cycle and flow in a tube or thermophysical properties with a liquid phase flow of refrigerant. The interest in nanorefrigerants is increasing remarkably, and in addition to the property determination studies, flow boiling heat transfer of nanorefrigerants is also taken into account by many research teams. They are performed experimentally or analytically.

Many scientists study enhancement in thermal conductivity. Zhang et al. (2020) investigate the thermal conductivity of nanorefrigerants (in the single phase where the refrigerant is in liquid form), including TiO_2, Al_2O_3, and SiO_2 nanoparticles, with low particle fractions. The study focuses on R141b-based nanorefrigerants and examines the effects of volume fraction, temperature, and particle size on conductivity. Experimental measurements were conducted within a specific temperature range, and a proposed model was developed to explain the thermal conductivity mechanisms, including interfacial layer, nanoparticle aggregation, and Brownian motion. For aggregation, they presented the images of nanorefrigerants in tubes for three different nanoparticles and six different weight fractions of each after 12 hours of preparation, presented in Figure 1.3. The authors claimed that no sedimentation was observed, so they concluded that the dispersion of the nanoparticles inside R141b was stable. The results indicate that increasing temperature and concentration enhance thermal conductivity, while larger particle size decreases it. The model's predictions closely match the experimental data, with a less than 3% deviation. Furthermore, the study finds that dynamic mechanisms play a dominant role in enhancing thermal conductivity for nanorefrigerants with low

concentrations (<0.1 vol.%), while the contribution of the interfacial layer is insignificant.

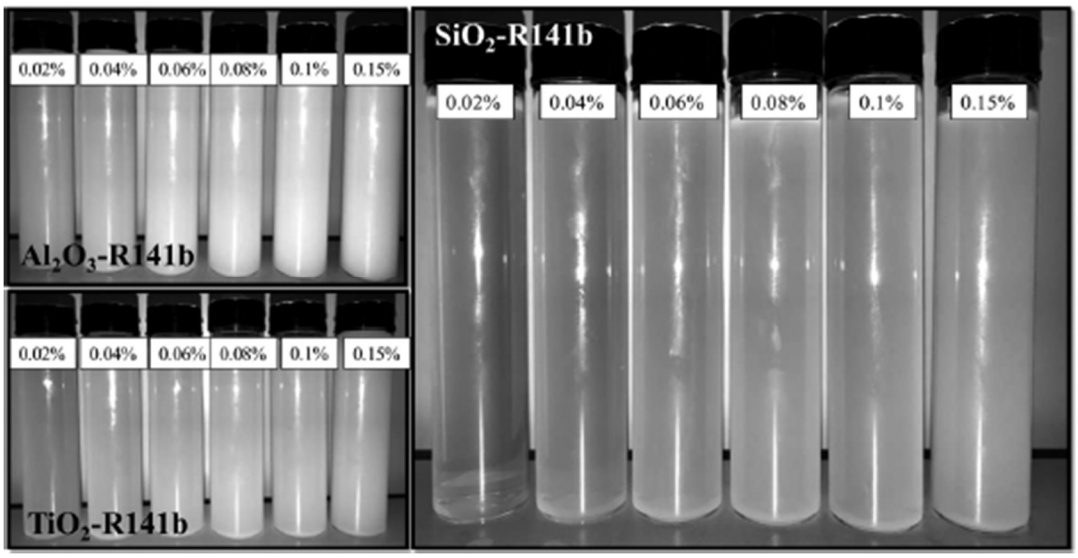

Figure 1.3. Nanorefrigerant tubes 12 hours after preparation [Zhang, et.al., 2020]

The rheological behavior of Al_2O_3-R141b nanorefrigerant was investigated by Mahbubul et al. (2014). The nanorefrigerant exhibited non-Newtonian behavior, specifically shear thickening, at low shear rates while approaching Newtonian behavior at high shear rates. The power-law rheological model was used to analyze the data, confirming the dilatant nature of the nanorefrigerant with a power-law index greater than unity. At higher shear rates, the agglomeration of particles broke down, resulting in a dispersed suspension with near-Newtonian behavior. This property could be advantageous for practical applications of nanorefrigerants in refrigeration cycles, as compressor forces can fracture agglomerations to form a dispersed solution. The viscosity of the nanorefrigerant was found to increase with higher shear rates and volume concentrations but decrease with increasing temperature. This decreasing trend was more pronounced at higher particle concentrations and shear rates. The experimental viscosity values were higher than those predicted by the Brinkman model but consistent with other experimental studies. The Brinkman model is a viscosity model for nanofluids [Brinkman, 1952], which is based on the

Einstein model and derived by considering the effect of adding one solute-molecule to an existing solution. Particles are assumed as spheres, and it is valid for high-to-moderate concentrations. These findings highlight the importance of analyzing rheological properties to understand and optimize the flow characteristics of nanorefrigerants for improved refrigeration and air-conditioning system performance.

In their study, Wang et al. (1999) measured the effective thermal conductivity of several nanofluids using a steady-state parallel-plate method. The liquids tested included water, vacuum pump fluid, engine oil, and ethylene glycol, with the addition of two types of nanoparticles: Al_2O_3 and CuO. The experimental results revealed that the thermal conductivities of the nanoparticle-fluid mixtures were higher than those of the base fluids. However, when comparing the predicted thermal conductivities of the mixtures using existing theoretical models, it was observed that the predicted values were significantly lower than the measured data. This suggests that the current models could be adequate when applied to nanofluids and accurately describe the heat transfer behavior at the nanometer scale. The study also discussed possible mechanisms contributing to enhancing thermal conductivity in these mixtures and highlighted the need for a more comprehensive theory to explain their behavior fully. Additionally, the researchers noted a correlation between the particle size and thermal conductivity increase, indicating that smaller particles result in more significant conductivity enhancement. Furthermore, the dispersion technique employed also influenced the thermal conductivity increase. To effectively utilize nanofluids for heat transfer enhancement, further investigations on heat transfer in fluid flow are required, considering the microscopic motion and structure-dependent behavior associated with particle size and surface properties.

Jiang et al. (2009-1) investigated the thermal conductivity characteristics of CNT (carbon nanotube) nanorefrigerants and developed a model for predicting their thermal conductivities. The experiments focused on the effects of CNT diameter and

aspect ratio on the thermal conductivity of nanorefrigerants using R113 as the host refrigerant. The results revealed that the thermal conductivities of CNT nanorefrigerants were significantly higher than CNT-water nanofluids or spherical nanoparticle-R113 nanorefrigerants. Additionally, it was observed that smaller CNT diameters and larger aspect ratios led to more significant enhancements in thermal conductivity. Existing models for predicting thermal conductivity, such as the Hamilton-Crosser (1962), Yu-Choi (2003), and Xue (2006) models, were validated using experimental data. The Yu-Choi (2003) model exhibited a mean deviation of 15.1% and demonstrated higher accuracy than the other models. A modified Yu-Choi (2003) model was proposed by refining the empirical constant, and it achieved a mean deviation of 5.5% when compared to experimental results. Key findings include the significant increase in thermal conductivities with increasing CNT volume fraction and the influence of CNT diameter and aspect ratio on thermal conductivity. The study recommends the modified Yu-Choi model for predicting the thermal conductivities of CNT nanorefrigerants.

Bhat et al. (2018) studied the thermophysical properties of mixed nanorefrigerants. Three different nanoparticles (Al_2O_3, Cu, and SiC) were synthesized individually and combined with a mixed refrigerant of R290-R600a. The properties examined include density, thermal conductivity, viscosity, and specific heat of the mixed nanorefrigerant. The results indicate that as the volumetric concentration of nanoparticles increases, the density of the mixed nanorefrigerant also increases. The thermal conductivity improves with higher nanoparticle concentrations, while viscosity increases as well. On the other hand, the specific heat of the mixed nanorefrigerant decreases with increasing nanoparticle concentration. These findings demonstrate the impact of nanoparticle concentration on the thermophysical properties of mixed nanorefrigerants.

In the study of Zhang et al. (2022), the characterization of TiO_2-R141b and Al_2O_3-R141b is studied. The thermal conductivities of these nanorefrigerants were

experimentally investigated at various nanoparticle fractions, temperatures, particle sizes, and nanoparticle thermal conductivities. Additionally, with experimental data, five intelligent models ("the radial basis function (RBF), multilayer perceptron, least-squares support-vector machine, dendrite-morphological neural network, and spiking neural network models") were formed to guess the effective thermal conductivities. The findings indicated that the effective thermal conductivity also increased as the concentration, temperature, and thermal conductivity of the nanoparticles increased. Conversely, when the hydrodynamic size of the nanoparticles increased, the effective thermal conductivity decreased. Among the intelligent models, the RBF model demonstrated the highest accuracy and the lowest error, outperforming the other models and theoretical/empirical correlations. The RBF model successfully represented the physical patterns of effective thermal conductivity when the input parameters were altered. Furthermore, sensitivity analysis revealed that nanoparticle concentration had the highest influence on the effective thermal conductivity, followed by temperature, hydrodynamic size, and thermal conductivity of nanoparticles. The experimental results confirmed the feasibility of enhancing thermal conductivities using nanorefrigerants and provided valuable insights into the influence of various parameters. The study emphasized the importance of developing comprehensive databases covering different nanoparticle types, base fluids, and operating conditions to improve the accuracy of intelligent models. The authors suggested integrating intelligent models with optimization algorithms and exploring non-standard methods to enhance prediction capabilities. Additionally, they proposed using ANN to predict microscopic parameters instead of relying solely on experimental measurements. The study concluded that the RBF model could be a foundational tool for predicting the thermal conductivities of different nanorefrigerants, facilitating efficient decision-making processes and reducing time and costs associated with experimental measurements.

The aim of Jiang et al.'s (2009-2) research was to investigate the thermal conductivity of nanorefrigerants and develop a model for predicting the thermal conductivity of

nanofluids. The experimental findings revealed a notable enhancement in the thermal conductivity of nanorefrigerants with increased nanoparticle volume fractions. Initially, five established models were employed to predict the thermal conductivity of nanorefrigerants; however, their predictions deviated from the experimental data by more than 10%. As a result, a novel model was introduced. This new model simulated the three-dimensional arrangement of nanoparticle clusters within the fluid and accounted for the impact of the nanoparticle's adsorption layer thickness. It utilized the resistance network method to calculate the thermal conductivity between interconnected nanoparticles and within nanoparticle clusters and nanofluids. The schematic view of the new model is presented in Figure 1.4. The newly developed model exhibited superior accuracy in forecasting the thermal conductivity of nanorefrigerants in comparison to existing models. Moreover, it also could predict thermal conductivity in traditional nanofluids.

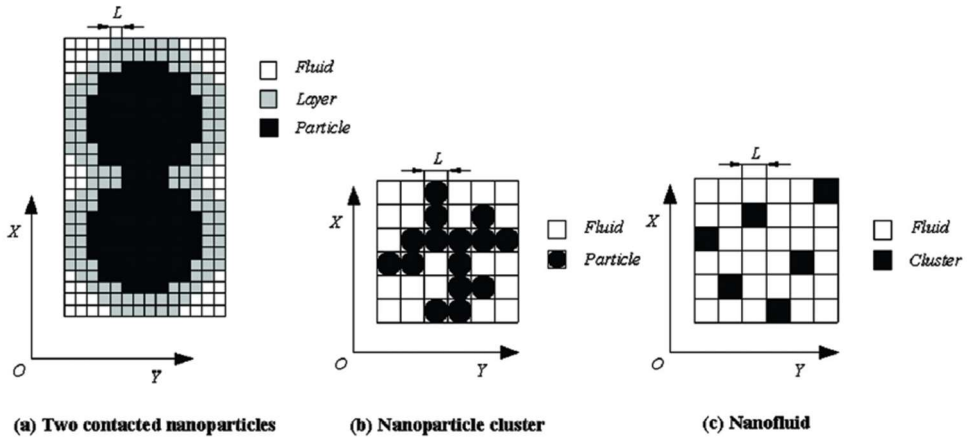

Figure 1.4. The cell segmentation of (a) two connected nanoparticles, (b) a nanoparticle cluster, and (c) nanofluid. [Jiang et al. 2009-2]

The thermal conductivity of nanorefrigerants increased significantly with increasing nanoparticle volume fraction, similar to conventional nanofluids. The thermal conductivities of nanorefrigerants with different nanoparticles were similar when the nanoparticle volume fractions were the same. According to the authors, nanoparticle aggregation and the formation of nanoparticle clusters played a crucial role in

enhancing nanofluids' thermal conductivity. Accurate nanofluid conductivity prediction requires simulating clusters' spatial structure and accounting for the adsorption layer and thermal conductivity between connected nanoparticles. The new model exhibited improved accuracy in predicting nanorefrigerant thermal conductivity compared to existing models. The deviations between the new model's predictions and experimental data ranged from -5% to +5% for nanorefrigerants and from -11% to +8% for other nanofluids. The new model, derived from the refrigerant's single-phase liquid flow, demonstrated good generalization capabilities and could be recommended for predicting thermal conductivity in various nanofluids beyond nanorefrigerants.

Experimental studies are mainly done to determine the heat transfer coefficient in a single tube with nanorefrigerant flow inside. Henderson et al. (2010) conducted experiments to determine the flow boiling heat transfer coefficient increase of SiO_2/R134a and CuO/R134a/POE nanorefrigerants with low vapor quality values. SiO_2 addition increased the heat transfer coefficient up to 55% in comparison to R134a, and CuO-R134a has an effect of more than 100% compared to R134a/POE configuration. Sun and Yang (2014) also performed an experimental study to examine the enhancement of the heat transfer coefficient with four different nanorefrigerants, R141b with Cu, Al, Al_2O_3, and CuO, separately. They altered the vapor quality, volume fraction, and mass flux values. They concluded that nanoparticle addition leads to enhancement with increasing quality, fraction, and flux. An average increase of 27% is reported; the maximum increase was for Cu-R141b, with a 49% increase. Peng et al. (2009) also examined a similar condition with CuO-R113 nanorefrigerant. They selected moderate values for inlet quality and performed experiments. They reported that heat transfer enhancement up to 29.7% had been observed and offered a correlation for the two-phase heat transfer coefficient for nanorefrigerant flow inside a smooth tube. Moreover, they stated that the existing correlations for flow boiling heat transfer underestimate their experimental results.

In their study, Kundan and Singh (2021) aimed to enhance the heat transfer characteristics of a vapor compression refrigeration cycle by using nanorefrigerants composed of R134a and Al_2O_3 nanoparticles (size: 20 nm). They investigated and analyzed various performance parameters, including coefficient of performance, energy consumed, cooling capacity, and temperature differences along the evaporator and condenser. The investigation involved varying the mass fraction of Al_2O_3 nanoparticles (from 0.5 to wt.%) and the flow. Three types of nanorefrigerants were studied: pure R134a, R134a with 0.5 wt.% Al_2O_3, and R134a with 1 wt.% Al_2O_3, with flow rates of 6.5 L/h and 11 L/h. The results showed that the coefficient of performance of the refrigeration system improved with higher nanorefrigerant volumetric flow rates, increasing for 6.5 L/h by 7.20% and for 11 L/h by 16.34% when using 0.5 wt.% Al_2O_3. Using nanorefrigerant (R134a + Al_2O_3) also led to a significant increase in cooling capacity. Additionally, there was a notable temperature drop across the condenser (3.0% to 23.77%) and a temperature increase across the evaporator (4.69% to 39.30%) for the investigated refrigeration system. The experimental study demonstrated the potential application of Al_2O_3 nanoparticles into the R134a refrigerant for vapor compression refrigeration systems. However, when the refrigerant contained one wt.% Al_2O_3, the coefficient of performance decreased at all refrigerant volume flow rates, particularly at low evaporator heat flux. A slight enhancement in the coefficient of performance was observed at a higher refrigerant volume flow rate (11 L/h) and higher evaporator heat flux (at 30-31°C). Moreover, the coefficient of performance decreased as the ambient temperature increased from 21°C to 28°C for both pure refrigerant and nanorefrigerants, indicating that the system operated more efficiently at lower ambient temperatures.

Sanukrishna et al. (2018) offer a comprehensive review of experimental investigations on nanorefrigerants, encompassing their thermophysical and rheological properties, boiling and condensation behaviors, pressure drop

characteristics, aggregation tendencies, migration and degradation properties, as well as their application in HVAC systems. It is well-established that higher levels of nanoparticle dosage lead to increased thermal conductivity and viscosity. Furthermore, the heat transfer rate improves with higher nanoparticle concentration and reduced particle size. Key factors influencing flow boiling and condensation heat transfer in nanorefrigerants include vapor quality, heat flux, mass flux, and particle concentration.

Nanorefrigerants offer the potential for reducing power consumption and increasing freezing speed and HVAC device COP. They enhance the overall performance of heat pumps and heat pipes as working fluids. However, challenges must be addressed before nanorefrigerants find diverse applications. Surfactants and lubricants can impede nanoparticle aggregation, mitigating long-term usage issues. Migration and degradation characteristics of nanoparticles also impact nanorefrigerant heat transfer performance.

In the study of Bi et al. (2011), the performance of TiO_2-R600a nanorefrigerant in a domestic refrigerator was experimentally investigated without any system reconstruction. The researchers conducted energy consumption and freeze capacity tests to assess the refrigerator's performance. The findings have indicated that the TiO_2-R600a nanorefrigerant operates safely within the refrigerator and is deemed valid for use. Moreover, the refrigerator using TiO_2-R600a nanorefrigerant exhibited improved performance compared to the pure R600a system, with a 9.6% reduction in energy consumption when using 0.5 g/L TiO_2-R600a nanorefrigerant. This suggests that the utilization of TiO_2-R600a nanorefrigerant in domestic refrigerators is feasible. The study also noted similarities with previous research that employed TiO_2-R134a as a working fluid, indicating that nanoparticles can enhance the performance of domestic refrigerators.

Nanorefrigerant flow boiling heat transfer is also investigated analytically. Mahbubul et al. (2013-1) studied thermal conductivity, viscosity, and pressure drop in addition to the heat transfer coefficient of Al_2O_3-R134a nanorefrigerant for different volume fraction values. The nanorefrigerant is considered a refrigerant with different thermophysical properties, and these properties are taken from the literature. Then, the flow inside a horizontal tube with a turbulent flow is solved by Excel. The results show that the heat transfer and pressure drop increase with increasing volume fraction. Optimization is not performed, and the authors suggest finding an optimum value for volume fraction. In their second study, Mahbubul et al. (2013-2) conducted a similar study with Al_2O_3-R141b nanorefrigerant to investigate heat transfer and pressure drop in a horizontal tube. This study also is done in Excel. They considered the COP calculations for the nanorefrigerant compared to the base refrigerant. Again, the pressure drop increases even though the heat transfer is enhanced. Therefore, they concluded that optimization is necessary for better cooling capacity and higher energy efficiency.

Habib et al. (2022) examined nanorefrigerants as highly efficient refrigerants that enhance heat transfer in cooling systems. Mathematical modeling was employed to assess the impact of suspended nanoparticles (Al_2O_3, CuO, SiO_2, and ZnO) on the thermophysical properties of R134a. The study focused on thermal conductivity, viscosity, density, and specific heat capacity of the nanorefrigerant within an evaporator pipe. Results showed that Al_2O_3-R134a nanorefrigerant exhibited the highest increase in thermal conductivity, reaching 96.23% at a volume concentration of 0.04. All nanorefrigerant types demonstrated a viscosity enhancement of 45.89%. These properties enhanced heat transfer in the pipe, making nanorefrigerants suitable for cooling units to improve high-temperature transfer characteristics and save energy. The study used mathematical models to discuss the thermal conductivity and rheological behavior of metallic oxide-based nanorefrigerants. For instance, Al_2O_3-R134a coolant exhibited a thermal conductivity of 0.0803 W/m·K at 300K and 0.01 nanoparticle volume fraction. Viscosity showed a notable increase of 10.75% at 0.01

volume fraction. Volume fractions and temperature significantly affected thermal conductivity and viscosity, with viscosity increasing with particle volume fractions but decreasing with temperature. Nanorefrigerants also exhibited improved density and specific heat capacity with increasing nanoparticle volume fraction. These findings highlight their excellent thermal properties that withstand temperature and pressure variations without compromising cooling efficiency, corrosion, or pressure drops in cooling units.

Nair et al. (2020) focused on the numerical analysis of heat transfer and pressure drop in a circular tube of a flooded evaporator chiller using Al_2O_3-R718-based nanorefrigerant, where R718 refers to water, a commonly used secondary refrigerant in HVAC applications. The simulations were conducted for different Reynolds numbers (Re) ranging from 13,000 to 33,000 and three particle volume fractions (ϕ) of 0.25%, 0.5%, and 1.0%. Temperature-dependent thermophysical properties were considered for more accurate results. The results indicated that the surface heat flux was higher for Al_2O_3-R718 nanorefrigerants than water. The average surface heat flux increased with increasing particle volume fraction but was accompanied by increased pumping power. The turbulence in the nanorefrigerant flow was analyzed, showing higher turbulent eddy viscosity but lower turbulent energy dissipation compared to pure R718. Entropy generation analysis revealed that Al_2O_3-R718 nanorefrigerants exhibited lower entropy generation rates than pure R718. The overall performance of the nanorefrigerant was evaluated using thermal performance parameters, and it was found that the nanorefrigerants outperformed the base fluid in all flow scenarios studied. Higher thermal performance parameter for Al_2O_3-R718 nanorefrigerants at higher Reynolds numbers and a particle volume fraction of 1% suggests their suitability for high-capacity chillers with high flow velocities.

Alawi and Sidik (2014) focus on investigating the thermophysical properties and heat transfer performance of nanorefrigerants. Specifically, CuO nanoparticles suspended in R134a are examined. Existing models are used to determine the thermal

conductivity and viscosity of the nanorefrigerants at different particle concentrations (ranging from 1 to 5 vol.%) and temperatures (ranging from 300 to 320 K). The observations reveal that the thermal conductivity and specific heat of the CuO-R134a nanorefrigerant increase as the particle concentrations and temperatures rise. On the other hand, the viscosity and density of the nanorefrigerant experience a significant increase with higher volume fractions, but they decrease with increasing temperature. Therefore, it is vital to consider the optimal particle volume fraction when producing nanorefrigerants to enhance the performance of refrigeration systems. The experimental investigation demonstrates that, similar to other nanofluids, the thermal conductivity of nanorefrigerants increases with higher nanoparticle volume concentrations and temperatures. The increase in thermal conductivity is more pronounced due to nanoparticle concentration compared to the effect of temperature. This characteristic holds promise for practical applications.

In addition to the studies mentioned above, pressure drop studies were also performed for nanorefrigerants, even if they are limited in number. In addition to the previously mentioned Mahbubul et al. (2013-2) study, Peng et al. (2009) also investigated the frictional pressure drop of nanorefrigerant with flow boiling. This study was experimental and mass flux, heat flux, vapor quality, and volume fraction were changed. They calculated the impact factor to compare the nanorefrigerant with pure refrigerant. The results showed that the pressure drop increases with increasing volume fraction. They offered a correlation to predict the frictional pressure loss for a flow-boiling nanorefrigerant configuration.

Alawi et al. (2015) focused on the importance of viscosity, unlike previous research, which focused on thermal conductivity. The effects of volume concentration and temperature on the viscosity of TiO_2-R123 nanorefrigerants are examined using numerical simulations. The experimental conditions include temperature ranges of 300-325 K, nanoparticle concentrations of 0.5%-2%, mass fluxes of 150-200 kg m−2 s−1, inlet vapor qualities of 0.2-0.7, and tube diameters of 6-10 mm. The results

reveal that nanorefrigerant viscosity increases with higher nanoparticle concentrations but decreases with increasing temperature. Additionally, pressure drop significantly increases with higher volume concentrations and vapor quality. Hence, lower volume concentrations are recommended for optimal refrigeration system performance. The study emphasizes the effects of TiO_2 nanoparticles and R123 refrigerant on nanorefrigerant viscosity. It demonstrates that particle volume fractions and temperature play significant roles. Higher particle volume fractions lead to increased viscosity, while higher temperatures result in decreased viscosity. Viscosity also directly affects pressure drop, which rises with higher volume concentrations and vapor quality. Moreover, refrigerant-based nanofluid flow boiling shows a more significant frictional pressure drop than pure refrigerant, increasing nanoparticle mass fraction. The impact factor of nanoparticles on pressure drop is more pronounced at low and high vapor qualities. Lastly, the study reveals a decrease in pressure drop with larger internal microtube diameters.

Since the nanofluids have both positive -heat transfer enhancement- and negative–pressure drop increase- effect, entropy generation, i.e., second law analysis, is an effective way to determine the overall effect. Among studies from the literature, Moghaddami et al. (2011) were interested in the second law analysis of water-based nanofluid pipe flow. They performed a numerical study to calculate entropy generation numbers and covered laminar and turbulent flow conditions. Optimum Reynolds number and volume fraction values are obtained in the range of their study. In a review of entropy generation in nanofluid flow, Mahian et al. (2013) reported studies from the literature where the researchers focused on entropy generation numerically and analytically. These studies mainly focus on entropy generation change with changing volume fraction values for water-based nanofluids. According to the authors, optimization is required, and local entropy generation is an important issue to consider.

Mahbubul et al. (2015) focused on investigating the thermophysical properties and their impact on the coefficient of performance (COP) in refrigeration and air-conditioning systems using Al_2O_3-R134a nanorefrigerant. By adding five vol.% Al_2O_3 nanoparticles to R134a, significant improvements in the thermal conductivity, dynamic viscosity, and density of the nanorefrigerant were observed compared to the base refrigerant. The nanorefrigerant exhibited a remarkable increase of 28.58% in thermal conductivity, indicating its enhanced heat transfer capabilities. Furthermore, the dynamic viscosity and density of the nanorefrigerant showed notable enhancements of approximately 13.68% and 11%, respectively, when compared to the base refrigerant. However, it was observed that the specific heat of the nanorefrigerant was slightly lower than that of R134a. Despite the lower specific heat, the Al_2O_3-R134a nanorefrigerant demonstrated superior COP values to the base refrigerant. The nanorefrigerant exhibited a COP improvement of 15% in thermal conductivity, 3.2% in density, and 2.6% in specific heat, highlighting its potential for enhancing system performance and energy efficiency in refrigeration applications. These findings underscore the promising prospects of utilizing nanorefrigerants to optimize the efficiency and performance of refrigeration systems. The study recommends further investigations and experimental studies to explore the full potential and benefits of incorporating nanorefrigerants. Such research can provide valuable insights into enhancing system performance, energy efficiency, and overall sustainability in refrigeration and air-conditioning.

Kumar et al. (2022) aimed to analyze the thermal performance of a small-scale solar organic Rankine cycle (ORC) system using a flat plate solar collector (FPSC). A mathematical model was developed using experimental data from the FPSC to evaluate the thermal performance of the ORC. A preliminary study compared the performance of R141b with other organic fluids and determined that R141b was the most suitable organic fluid for the ORC. The study also investigated MWCNT + WO3/water nanofluid use in the solar collector and MWCNT-R141b nanorefrigerant in the ORC due to their enhanced thermophysical properties. Parametric analysis was

conducted to assess the energetic and exergetic performance of the ORC under different nanoparticle concentrations and volume flow rates. The results showed that increasing the nanofluid concentration significantly improved energy and exergy efficiency. The study concluded that R141b exhibited the best performance among the tested organic fluids, and the use of nanofluids and nanorefrigerants enhanced the system's thermal performance. The findings suggest the potential for further investigations with different nanorefrigerant combinations, varying mass flow rates, and volume concentrations to optimize operating conditions. Additionally, considering solar irradiance fluctuations and integrating the system with carbon capturing and sequestration technologies could contribute to achieving global net-zero emissions.

Besides the heat transfer and pressure drop effects of nanofluids, the overall effect in terms of energy consumption is an essential aspect of the enhancement subject. Javadi and Saidur (2013) considered the potential energy saving of the nanorefrigerants in the future. They performed an analytical study based on the increased heat transfer mentioned in the available studies in the literature. They concluded a potential energy saving of 10.8 MWh by 2030 in Malaysia, so nanofluids can be named a new field for efficient energy usage. Ewim et al. (2021) mentioned in their review study that nanoparticles used in refrigeration systems face limitations in dispersal in the fluid, which can cause settling and clogging issues. However, these challenges have been largely overcome. Metallic nanofluids have shown higher thermal conductivity than conventional fluids, but clogging and abrasion remain potential issues. The use of smaller nano-sized particles can help reduce these problems. Clustering of nanoparticles can occur if powdered, but controlled ultrasound dispersion can prevent this. There is also a flammability risk associated with hydrocarbon-based nanorefrigerants. Proposed research directions include studying biobased nanorefrigerants, optimizing nanoparticle concentration and properties, developing numerical and analytical models, exploring natural refrigerants and blend refrigerants, and investigating the flow of nanorefrigerants in

different geometries. Most numerical studies on nanorefrigerants have focused on the single-phase approach. However, future research should also explore the challenges and benefits of using the two-phase mixture model, despite its higher computational cost.

In their review, the use of nanorefrigerants in vapor compression refrigeration systems (VCRSs) is examined by Bilen et al. (2022). Adding nanoparticles directly to refrigerants in the gas phase poses challenges, so researchers have explored indirect methods by adding nanoparticles to the compressor oil, which comes into contact with the refrigerant during system operation. Literature findings indicate that nanorefrigerants significantly affect refrigerants' thermal, physical, and heat transfer properties. The heat transfer rate and viscosity increase with higher nanoparticle dosage. Using nanorefrigerants reduces energy consumption and improves the coefficient of performance of refrigeration systems. Experimental studies have shown that concerns about nanoparticle blockages in system components are unfounded due to the small nanoparticle sizes compared to the cross-sectional areas of system elements.

Future research in the field of nanorefrigerants for VCRSs should focus on exploring the use of nanorefrigerants as alternatives to restricted refrigerants, analyzing the behavior of VCRS components when working with nanorefrigerants separately, conducting long-term performance and life cycle analyses of equipment using nanorefrigerants, developing accurate models for determining the thermophysical properties of nanorefrigerants, and investigating the usage of hybrid nanoparticles in VCRSs. These future research directions will enhance our understanding of nanorefrigerants and contribute to improving the performance, safety, and efficiency of VCRSs. They address current limitations and open up new possibilities in the field.

Feroskhan et al. (2022) provide a comprehensive overview of nanorefrigerants, covering various aspects such as fundamental interactions, thermophysical properties, pool boiling mechanisms, and flow boiling studies. The conclusions drawn from the study are as follows: nanorefrigerants can enhance the performance of refrigeration systems, metal, and metal oxide nanoparticles show promise for improving thermal performance, influential parameters include nanoparticle size, shape, type, mass fraction, and heat flux, increasing nanoparticle mass fraction improves heat transfer but also leads to higher pressure drop, surfactants are crucial for stable nanoparticle suspension, heat transfer characteristics during pool boiling can indicate thermal performance in flow boiling conditions, and nanoscale particles modify the heating surface morphology to enhance thermophysical properties and heat flux. To advance research in this field, the following areas should be considered: further investigations on combinations of metal and metal oxide nanoparticles in different refrigerants to establish conclusive findings, more studies on thermophysical properties beyond thermal conductivity and viscosity, identifying the physical mechanisms and sequence during boiling of nanorefrigerants, correlating pool boiling studies with flow boiling using appropriate parameters, extending numerical investigations to estimate physical properties and heat transfer coefficients under various conditions, simulating nanorefrigerant flow processes and mapping flow regimes across evaporator regions, studying long-term stability, thermal performance enhancement, and pumping power loss trade-offs, exploring nanoparticles suitable for retrofitting existing refrigerants, examining nanoparticles' potential in non-vapor compression systems, conducting studies on new generation refrigerants, addressing the research gap in understanding the effects of particle morphology on heat transfer characteristics of nanofluids.

Kumar et al. (2022) review experimental and numerical studies on nanorefrigerants and nanolubricants in their paper. Experimental research is extensive, focusing on enhancing the performance of domestic refrigerators and air conditioners and investigating pool boiling heat transfer. However, there needs to be more numerical

investigations. Key findings indicate that adding nanoparticles to refrigerants and lubricating oil improves performance, reducing energy consumption. Nanoparticles enhance heat transfer coefficients in pool boiling and flow condensation, with size and shape playing essential roles. Optimum nanoparticle volume fractions need to be determined to maximize efficiency. Nanorefrigerants exhibit superior heat transfer capabilities, reducing cooling time and improving systems' freezing or cooling capacity. Numerical studies mainly focus on single-phase simulations, showing rapid increases in heat transfer coefficients at higher nanoparticle concentrations. Pool boiling of nanorefrigerants leads to decreasing nanoparticle mass in liquid form, affecting bubble movements. Applying nanorefrigerants and nanolubricants in heating and cooling systems improves performance. Prospects include synthesizing low boiling point nanorefrigerants, exploring natural refrigerant-based nanorefrigerants, studying boiling heat transfer with low GWP (global warming potential) and ODP (ozone depletion potential) refrigerants, investigating characteristics such as dielectric aspect and surface tension, researching high thermal conductivity nanoparticles, studying flow condensation of nanorefrigerants, and conducting more analytical and numerical studies. Overall, further numerical and experimental investigations are needed to expand the knowledge and application of nanorefrigerants in cooling and heating units.

In their review paper, Xing et al. (2022) expressed that nanorefrigerants have emerged as a promising solution for enhancing the performance of energy-consuming refrigeration cycles. They can be prepared using one-step or two-step methods, with the latter being more common due to its convenience and cost-effectiveness. In vapor compression refrigeration cycles, they offer three ways to improve performance: as nanorefrigerants, nanolubricants, or nanosecondary refrigerants, which are the environmentally harmless than traditional halocarbon refrigerants. These are water, air, ammonia, et al., which are in the liquid phase and used to transfer heat from the interested area to primary refrigerants, which can be kept in a restricted area. By employing nanofluids, heat transfer properties and

compressor energy efficiency can be enhanced, resulting in increased refrigeration capacity, reduced compressor power consumption, and improved overall system performance. In ejection refrigeration systems, using nanorefrigerant improves heat transfer on the refrigerant side, thereby enhancing overall heat transfer and the coefficient of performance by increasing the quality of refrigerant vapor at the evaporator outlet. Nanofluids can also enhance heat transfer characteristics in compound or cascade refrigeration systems. However, the presence of nanoparticles increases pressure drop due to elevated viscosity and density, necessitating consideration of heat transfer coefficient improvement and circulation head loss. Low nanoparticle concentrations are recommended to prevent clogging and ensure better system performance. Further research is required to understand the mechanisms and correlations between different types of nanomaterials and their effects on nanofluid performance in refrigeration systems.

Based on a comprehensive review of nanorefrigerants and their impact on refrigeration system performance, Vamshi et al. (2022) mentioned that nanorefrigerant preparation is challenging and expensive, requiring advanced equipment and chemical treatments for stability. Increasing nanoparticle concentration improves thermal conductivity, particularly with carbon nanotubes. Nanoparticle concentration affects viscosity, leading to increased pressure drop and energy consumption. However, more research is needed to find the optimum concentration. Higher concentrations improve the coefficient of performance, reducing compressor load and energy consumption and increasing freezing capacity. Experimental studies mainly focus on average nanoparticle size, neglecting additives and environmental impacts. Nanoparticles significantly enhance convective and boiling heat transfer coefficients, especially at lower volume fractions. Mass flux, vapor quality, heat flux, and nanoparticle size influence heat transfer. Most experiments treat nanoparticle additions as single-phase flows, but considering them two-phase flows is crucial. Surfactant concentration, nanoparticle shape, and size impact thermal conductivity, viscosity, and lubricant friction. While nanorefrigerants

are promising to improve system efficiency and serve as environmentally friendly alternatives, further research is needed. This includes developing compelling correlations and models for thermophysical property calculations, investigating two-phase flow heat transfer coefficients, understanding nanoparticle behavior during phase change, assessing corrosion tendencies, studying lubricant properties, analyzing nanoparticle aggregation mechanisms, and exploring energy-efficient and cost-effective methods.

Some of the experimental studies in the literature are summarized and tabulated in Table 1.1. In addition, three numerical studies from the literature are tabulated in Table 1.2.

In summary, nanorefrigerants have garnered significant attention for their potential to enhance heat transfer and overall efficiency in refrigeration systems. Studies have shown that adding nanoparticles to refrigerants increases thermal conductivity and heat transfer coefficients, improving system performance. However, this enhancement comes with challenges, including increased viscosity and pressure drop, which need to be carefully managed to ensure practical application.

Experimental studies have demonstrated the significant impact of nanorefrigerants on heat transfer in various refrigeration systems. Nanorefrigerants can enhance heat transfer coefficients by up to 100% compared to conventional refrigerants. However, new research must address nanoparticle aggregation, migration, and system clogging to exploit nanorefrigerants' benefits fully.

To optimize nanorefrigerant performance, accurate modeling, and simulation techniques are essential to predict thermal conductivity accurately. Further research is needed to develop reliable correlations for thermophysical properties and understand two-phase flow heat transfer coefficients. Research should be directed to

explore energy-efficient and cost-effective methods for nanorefrigerant synthesis and application.

Therefore, nanorefrigerants promise to improve refrigeration system efficiency, but practical limitations must be addressed through ongoing research and optimization. Proper management of nanoparticle characteristics and challenges associated with their usage will be crucial for the successful integration of nanorefrigerants in refrigeration systems.

Table 1.1 Experimental studies in the literature

Study	Author(s)	Ref.	Particle	Size	Fraction	x	P	T	Comments
Cycle	Bi et.al. (2011)	R600a	TiO_2	50 nm	0.1g/L 0.5g/L	Single-phase study	0.6 bar	-25ºC evap. 5ºC storage -18ºC freezer	TiO_2-R600a is used in refrigerator directly in replacement of R600a, the overall performance for a 24-h time is investigated. 9.6% less energy used with 0.5 g/L TiO_2-R600a.
Bath	Jiang et.al. – (2009)	R113	CNT	d=15 nm d=80 nm L= 1.5 µm L= 10 µm	0.2-1.0% vol.	Single-phase study	101 kPa	303 K	Experimental "k" measured, compared with Hamilton-Crosser, Yu-Choi, Xue models. 15.1% deviation from Yu-Choi, 5.5% deviation from modified Yu-Choi. For 4 "k" of CNT-R113, "k" increased 82%, 104%, 43% and 50%, respectively.
Cycle	Bi et.al. – (2008)	R134a	TiO_2	50 nm	0.06% wt* 0.10% wt	Single-phase study	0.8-0.9 bar	-30ºC evap. 5ºC storage -18ºC freezer	TiO2-POE-R134a is used in refrigerator directly in replacement of POE-R134a, the overall performance for a 24-h time is investigated. 26.1% less energy used with 0.1% mass fraction TiO_2-R600a.
Tube 8.12 mm ID	Peng et.al. - 2009	R113	CuO	40 nm	0.1% wt 0.2% wt 0.5% wt	0.2-0.7 (0.15 change)	78.25 kPa evap.pres.	N/A	Existing correlations underestimate the heat transfer coefficient enhancement, a new correlation is proposed, 93% agreement is gathered.29.7% HTC enhancement, 93% agreement with new correlation

Table 1.1 Experimental studies in the literature (continued)

Study	Author(s)	Ref.	Particle	Size	Fraction	x	P	T	Comments
Tube 8.12 mm ID	Peng et.al. (2009)	R113	CuO	40 nm	0.1% wt 0.2% wt 0.5% wt	0.2-0.7 (0.15 change)	78.25 kPa evap.pres.	N/A	Friction coefficient increase is examined, an impact factor equation and a new friction coefficient correlation is proposed, 99% and 92% agreement is gathered.20.8% friction coefficient increase, 92% agreement with new correlation
Tube 7.9 mm ID	Bartelt et.al. (2008)	R134a	CuO	30 nm	0.5% wt 1.0% wt 2.0% wt	2.44-6.33%	N/A	3.6-41.0ºC	CuO-POE-R134a is used instead of POE-R134a for heat transfer enhancement. Pressure drop does not have any significant change. It is unclear. Heat transfer coefficient: 0.5% wt, no effect; 1% wt, 42-82% enhancement; 2% wt, 50-101% enhancement
Cycle	Subramani and Prakash (2011)	R134a	Al_2O_3	< 50 nm	0.06% wt	Single-phase study	0.2 MPa (evap)	-6ºC evap. 28ºC cooling load	SUNISO 3GS-Alumina-R134a is used in refrigerator directly in replacement of POE-R134a, the overall performance is investigated. Theoretical and actual COP are found. 25% decrease in power consumption, 33% increase in COP, 1.53 energy. enhancement factor in evap.
Tube 7.9 mm ID	Henderson et.al. (2010)	R134a	SiO_2 CuO	200-300 nm SiO_2, 30 nm CuO	0.5% and 0.05% SiO_2 0.02-0.08% CuO	x< 20%	N/A	N/A	CuO-POE-R134a and SiO2-R134a are used instead of POE-R134a and pure R134a in a 7.9 mm horizontal tube for heat transfer enhancement. Pressure drop does not have any significant change. It is unclear. HTC: SiO_2-R134a: up to 55% decrease CuO-POE-R134a: up to 100% increase

Table 1.1 Experimental studies in the literature (continued)

Study	Author(s)	Ref.	Particle	Size	Fraction	x	P	T	Comments
Tube 10 mm ID	Sun and Yang (2013)	R141b	Cu Al Al_2O_3 CuO	40 nm	0.1% wt 0.2% wt 0.3% wt	0.3-0.8	1 atm	32ºC	Cu-R141b, Al-R141b, Al2O3-R141b, CuO-R141b are used instead of R141b in 10 mm horizontal tube. As x increases, HTC increases but nanoparticle impact factor decreases. HTC: Max. enhancement: 49%, average increase: 27%
Tube 7.72 mm ID	Abdel-Hadi et.al. (2011)	R134a	CuO	15-70 nm	0.05-1.0% wt	Single-phase study	N/A	q": 10-40 kW/m²	Cu-R134a is used instead of R134a. As wt increases, HTC increases up to certain values.
Tube 6 mm ID	Mahbubul et.al. (2012)	R123	TiO_2	21 nm	Up to 2% vol.	0.2-0.7	91.359 kPa	5-20ºC	Viscosity is measured for constant wall heat flux within 6 mm tube. Compared with viscosity models in the literature. Pressure drop increases with vol. fraction and x values
Shaker	Mahbubul et.al. (2013)	R141b	Al_2O_3	13 nm	0.1-0.4% vol.	Single-phase study	N/A	5-20ºC	Conductivity, viscosity and density are measured and compared with available results from models and software in literature. k increases with wt and T, more with wt, μ increases with wt

Table 1.1 Experimental studies in the literature (continued)

Study	Author(s)	Ref.	Particle	Size	Fraction	x	P	T	Comments
Tube 8.22 mm ID	Sun & Yang (2013)	R141b	Cu Al Al_2O_3 CuO	40 nm	0.1% wt 0.2% wt 0.3% wt	0.3-0.8	1 atm	32ºC	Cu-R141b, Al-R141b, Al2O3-R141b, CuO-R141b are used instead of R141b in 8.22 mm horizontal copper tube with internal thread. As x increases, HTC increases but the maximum increase in HTC is observed for x=0.5-0.6. Heat transfer coefficient: Max. enhancement: 17-25%, average increase: 3-20%. Max inc. @ x=0.5-0.6
Shaker	Mahbubul et.al. (2014)	R141b	Al_2O_3	13 nm	0.05-0.15% vol.	Single-phase study	1 atm	4-16ºC	They performed experiments with R141b and Al2O3 and found that viscosity increases with shear rates and volume concentrations but decreases with temperature. Viscosity is found to be larger than Brinkman equation. @low shear rates, nanorefrigerant non-Newtonian (shear-thickening) @ high shear rates, Newtonian.
Beaker	Dhindsa et.al. (2013)	R11	Al_2O_3	20 nm & 40 nm Shape: spherical & elongated	0.02-0.10% wt.	Single-phase study	1 atm	4-16ºC	Experiments for thermal conductivity. 5 different wt. are used. Hamilton Crosser model is suitable for k enhancement calculation. For 20 nm, 11% mean deviation; for 40 nm, 6% mean deviation is observed. Feasible to use Al2O3 in ref. up to 0.08% of 20 nm. Max k increase 42%, k elongated > k spherical, k decreases with T, HC model is suitable.

Table 1.2 Numerical studies in the literature

Study	Author(s)	Ref.	Particle	Size	Fraction	x	P	T	Comments
Tube 8.12 mm ID	Mahbubul et.al. (2013)	R134a	Al_2O_3	5-25 nm	1-5% vol.	0.2-0.7	706 kPa	300-325 K	Sitprasert conductivity and Brinkman viscosity are used, solution is by Excel. k,μ,ΔP and h are studied. k increases with vol.frac. and temp., decreases with np size, μ increases with vol.frac., ΔP increases after 3% vol.frac. h increases for 1% most.
Tube 6 mm ID	Mahbubul et.al. (2013)	R141b	Al_2O_3	13 nm	1-5% vol.	0.2-0.7	78.535 kPa	T=25ºC	Properties are taken from REFPROP, no surfactant was considered. Characteristics are investigated by Excel. Peng equation is used to calculate impact factor, Saitoh equation is used for pure h calculations. h and ΔP increase with wt optimum wt should be desired
Cycle	Javadi & Saidur (2013)	R134a	TiO_2 Al_2O_3	N/A	0.06-0.1 %	Not given	N/A	N/A	Data analysis and calculations are performed according to reference studies and potential energy saving is determined .0.1% TiO_2/mineral oil reduces power cons. 10,863 MWh by 2030.

CHAPTER 2

MOTIVATION and OBJECTIVE

2.1 Motivation

The field of nanorefrigerants has witnessed significant advancements in recent years, with researchers exploring their potential in various applications, including air conditioning, refrigeration, and heat exchangers. These nanoscale particles dispersed in traditional refrigerants have shown promise in enhancing refrigerant fluids' thermophysical properties and heat transfer characteristics. However, when it comes to studying the thermophysical properties of nanorefrigerants in two-phase flow conditions, particularly in the liquid and gas phases, there needs to be more comprehensive research in the existing literature.

Understanding the behavior and performance of nanorefrigerants in two-phase flow is crucial for the efficient design and optimization of cooling systems. The refrigerant flows through liquid and gas phases in many practical cooling applications, such as heat exchangers, evaporators, and condensers. However, most of the studies conducted on nanorefrigerants have primarily focused on single-phase flow, neglecting the intricate dynamics and interactions between the liquid and gas phases. This knowledge gap poses a significant challenge in accurately predicting the performance of cooling systems employing nanorefrigerants and hampers their optimal utilization.

The limited literature on nanorefrigerants in two-phase flow often needs more comprehensive investigations into fundamental thermophysical properties, such as

conductivity and viscosity, as a function of the quality or vapor fraction. These properties play a critical role in determining the heat transfer efficiency, pressure drop, and overall performance of cooling systems. A thorough understanding of how these properties vary with changing quality levels makes it easier to model and optimize cooling systems that employ nanorefrigerants accurately. Moreover, the behavior of nanorefrigerants in two-phase flow conditions is influenced by various factors, including particle size distribution, concentration, and surface chemistry. These parameters, along with the quality level, affect the thermophysical properties of nanorefrigerants and their interaction with the surrounding liquid and gas phases. However, the literature needs comprehensive studies that systematically investigate these relationships and provide a deeper understanding of the complex behavior exhibited by nanorefrigerants in two-phase flow.

Therefore, the primary motivation of this research is to address the existing knowledge gap by conducting a thorough investigation into the thermophysical properties of nanorefrigerants in a two-phase flow system. Focusing on conductivity and viscosity as critical properties aims to gain valuable insights into the heat transfer characteristics, flow behavior, and overall performance of nanorefrigerants in practical cooling applications. This research will bridge the gap between single-phase and two-phase flow studies and provide a comprehensive understanding of the behavior of nanorefrigerants under realistic operating conditions.

Nanorefrigerants exhibit enhanced heat transfer characteristics compared to pure refrigerants [Henderson et al., 2010]. Conventional heat transfer coefficient models designed for pure refrigerants do not accurately capture the behavior of nanorefrigerants due to the presence of nanoparticles. The thermophysical properties of nanorefrigerants, such as thermal conductivity and viscosity, are altered by the nanoparticles, especially in two-phase flow conditions. These changes significantly impact the overall heat transfer coefficient during boiling and condensation [Cheng and Liu, 2013]. Experimental studies have demonstrated substantial heat transfer rate

improvements in nanorefrigerants attributed to nanoparticles' unique dispersion and interaction with the fluid during two-phase flow [Bobbo et al., 2010].

To ensure accurate predictions and optimal design of cooling systems, it is essential to incorporate the influence of nanoparticle dispersion on thermophysical properties into heat transfer coefficient models. Researchers are developing empirical correlations and theoretical models tailored explicitly to nanorefrigerants, accounting for the nanoparticle effects in nanofluids [Zhang et al, 2022]. So far, these efforts for viscosity and conductivity determination are directed to single-phase refrigerant flow of nanorefrigerants. By considering the unique characteristics of nanorefrigerants and their two-phase conductivity and viscosity, these efforts can provide more reliable and accurate heat transfer coefficient formulations for flow boiling applications. Such advancements will enable the efficient utilization of nanorefrigerants and harness their enhanced heat transfer performance for improved cooling systems.

In addition to nanoparticle dispersion, the two-phase nanorefrigerant thermophysical properties have importance in aspects like nonlinear behavior, phase-changing effects, heat transfer mechanisms, critical heat flux, optimization and efficiency, and experimental validation.

1. Nonlinear Behavior [Cheng, 2009]: Nanofluids often exhibit nonlinear behavior concerning thermal conductivity and viscosity, especially at higher nanoparticle concentrations. In the two-phase flow regime, the presence of nanoparticles can result in varying conductivity and viscosity values depending on the phase change conditions. Ignoring the nonlinear effects may lead to inaccuracies in estimating heat transfer coefficients.

2. Phase Change Effects: During two-phase flow, nanorefrigerants undergo phase change processes such as evaporation and condensation [Wang et al.,

2007]. These phase changes introduce additional complexities due to the interaction of nanoparticles with the changing liquid-vapor interface. The resulting changes in thermophysical properties affect the local heat transfer coefficients, necessitating the consideration of two-phase conductivity and viscosity.

3. Enhanced Heat Transfer Mechanisms: Nanorefrigerants exhibit higher heat transfer rates than traditional refrigerants. The enhanced heat transfer mechanisms are intricately linked to the nanofluid's conductivity and viscosity during two-phase flow. Neglecting these properties may underestimate the potential heat transfer enhancements achievable with nanorefrigerants [Bobbo et al., 2010].

4. Critical Heat Flux Improvement: One of the significant advantages of nanorefrigerants is their ability to improve the critical heat flux (CHF) during boiling. CHF is a crucial parameter in high-heat flux applications [Cheng et al., 2007]. The unique properties of nanorefrigerants, including two-phase conductivity and viscosity, contribute to this improvement, highlighting the importance of studying these properties.

5. Optimization and Efficiency: Accurate prediction of two-phase flow properties, including conductivity and viscosity, is essential for optimizing nanorefrigerant formulations and cooling system designs. Understanding these properties enables engineers to tailor nanorefrigerants for specific applications, leading to more efficient and reliable cooling systems.

6. Experimental Validation: Theoretical models using saturated liquid and vapor properties might only partially capture the real-world behavior of nanorefrigerants. Experimental validation of nanorefrigerant behavior during two-phase flow, including conductivity and viscosity measurements, is

essential to confirm the accuracy of predictions and the necessity of considering these properties.

By bridging the gap between single-phase and two-phase flow studies, this research will contribute to the existing body of knowledge regarding nanorefrigerants, specifically in the context of two-phase flow systems. The outcomes of this study will enable engineers, researchers, and manufacturers to optimize the design and operation of cooling systems, leading to more efficient, reliable, and environmentally sustainable cooling technologies.

2.2 Objective

This study aims to determine the thermophysical properties, specifically thermal conductivity and viscosity, of nanorefrigerants in a two-phase flow system consisting of liquid and gas phases. A systematic approach consisting of several steps will be followed to achieve this objective. The steps involved in the study are as follows:

1. Providing existing thermophysical property determination models for the liquid flow of the base fluid: The first step of the study involves reviewing and analyzing the existing thermophysical property determination models for the liquid flow of the base fluid. These models, developed for conventional nanofluids, serve as a foundation for understanding the behavior of the base liquid in the presence of nanoparticles. By examining these models, we can establish a benchmark for comparison and evaluate their suitability for the two-phase refrigerant flow case of nanorefrigerants.

2. Modeling an ideal vapor compression refrigeration cycle with the pure refrigerant flow: An ideal vapor compression refrigeration cycle will be modeled to evaluate the practical implications of the thermophysical properties calculated by existing models. The cycle will be simulated using the thermodynamic properties of pure

refrigerant flow, considering a commonly used refrigerant. Then the thermophysical properties of nanorefrigerant with the two-phase refrigerant flow will be determined.

3. Showing the underestimation of these models for the two-phase refrigerant flow case of nanorefrigerants: In this step, the limitations and underestimation of the existing thermophysical property determination models for nanorefrigerants in two-phase flow conditions will be highlighted. By comparing with the experimental data available in the literature, it will be demonstrated that the existing models fail to accurately predict the thermophysical properties in the presence of nanoparticles, particularly in the two-phase flow regime. This step will emphasize the need for a new model tailored explicitly for nanorefrigerants.

4. Suggesting a new model by making an analogy with fluidized beds: Based on the observed shortcomings of the existing models, a new model will be proposed in this step. The new model will be developed by drawing an analogy between the behavior of nanorefrigerants in two-phase flow and the fluidized bed phenomenon. The fluidized bed concept has been successfully applied in various fields, and by adapting it to the specific characteristics of nanorefrigerants, a novel model can be formulated. This step will outline the theoretical basis and assumptions underlying the new model.

5. Using the model to determine the thermophysical properties: In this step, the newly proposed model will be employed to determine the thermophysical properties, namely thermal conductivity and viscosity, of nanorefrigerants in a two-phase flow system. The model will be applied to experimental data obtained from the literature.

6. Validating the model using Artificial Neural Network (ANN): To ensure the reliability and generalizability of the proposed model, it will be validated using an ANN approach. The ANN will be trained using experimental data from literature and model predictions as inputs and the measured heat transfer coefficient as the output.

This validation step will provide further confidence in the applicability and accuracy of the proposed model.

7. Remodeling the ideal vapor compression refrigeration cycle with the pure refrigerant flow for nanorefrigerant calculations: An ideal vapor compression refrigeration cycle will be modeled to evaluate the practical implications of the determined thermophysical properties. The cycle will be simulated using the thermodynamic properties of pure refrigerant flow, considering a range of commonly used refrigerants. This step will establish a baseline for assessing the impact of nanorefrigerants on the performance of the refrigeration cycle.

8. Calculating the change in Coefficient of Performance (COP) of the cycle with different nanorefrigerants: Finally, the newly developed model will be utilized to determine the thermophysical properties of different nanorefrigerants. The calculated properties will then be used to evaluate the change in the COP.

CHAPTER 3

THERMOPHYSICAL PROPERTIES OF NANOREFRIGERANTS

Various approaches and models calculate the thermophysical properties of nanofluids. The amount of nanoparticles in the base fluid is the primary variable that affects the properties. The nanorefrigerants are a particular case of nanofluids, yet most of the property models are developed for water-based nanofluids and then applied to nanorefrigerants. Therefore, the general expressions for nanofluids have been used in the calculations.

The thermophysical properties of nanofluids are calculated with either simple, empirical, or mixture models as a result of analytical/numerical studies. The formulations are given in this chapter to calculate the thermophysical properties of nanofluids.

3.1 Volume Fraction

The volume fraction is the ratio of the volume of nanoparticles to the total volume of the nanofluid. For nanofluids, the volume fraction is an important parameter determining the concentration or amount of nanoparticles dispersed within a fluid volume. The volume fraction of nanofluids can vary depending on the application and desired properties. Typically, volume fractions of nanofluids range from small values (less than 1%) to moderate values (up to 10%). However, higher volume fractions can also be achieved in some cases.

$$\varphi = \frac{V_p}{V_p + V_f} \tag{1}$$

Here, V is the volume and p and f are subscripts for nanoparticles and base fluid (the refrigerant), respectively.

3.2 Mass Fraction

Mass fraction is the ratio of the mass of the nanoparticles to the total mass of the nanofluid. In the case of nanofluids, the mass fraction measures the concentration or amount of nanoparticles present in a given fluid mass. Similar to volume fraction, the mass fraction of nanofluids can vary depending on the specific application and desired properties. Mass fractions of nanofluids also typically range from small values (less than 1%) to moderate values (up to 10%), and higher mass fractions can also be achieved in some instances.

$$\varphi_m = \frac{m_p}{m_p + m_f} \tag{2}$$

Here m is the mass.

3.3 Density

The density of a nanorefrigerant is calculated by using the simple mixture model.

$$\rho_{nf} = \frac{m_p + m_f}{V_p + V_f} = \frac{\rho_p V_p + \rho_f V_f}{V_p + V_f} = \varphi\rho_p + (1 - \varphi)\rho_f \tag{3}$$

Here ρ is density, and nf is the subscript for nanofluid.

3.4 Heat Capacity

The heat capacity (c) of the nanorefrigerant is calculated by assuming thermal equilibrium between nanoparticles and the base refrigerant [Khanafer and Vafai, 2011].

$$(\rho c)_{nf} = \rho_{nf}\left(\frac{Q}{m\Delta T}\right)_{nf} = \rho_{nf}\frac{Q_p+Q_f}{(m_p+m_f)\Delta T} = \rho_{nf}\frac{(mc)_p\Delta T+(mc)_f\Delta T}{(m_p+m_f)\Delta T} =$$

$$\rho_{nf}\frac{(\rho c)_p V_p+(\rho c)_f V_f}{\rho_p V_p+\rho_f V_f} \tag{4}$$

Then,

$$c_{nf} = \frac{\varphi\rho_p c_p+(1-\varphi)\rho_f c_f}{\rho_{nf}} \tag{5}$$

3.5 Thermal Conductivity

Among all other thermophysical properties, thermal conductivity, k, is the most significant and controversial one, along with dynamic viscosity, for heat transfer and pressure drop calculations. With the addition of nanoparticles to the base fluid, the thermal conductivity is aimed to increase compared to the pure fluid at the same flow conditions, such as mass flux, heat flux, and pressure drop; however, the viscosity is also increased due to the presence of solid particles inside the bulk flow.

For the thermal conductivity calculations of nanofluids, some critical physical factors affect thermal conductivity. In his study, Buongiorno [2006] considered seven-slip mechanisms that lead to slip velocity between nanoparticles and the base fluid. These mechanisms are inertia, Brownian motion, thermophoresis, diffusiophoresis, Magnus effect, fluid drainage, and gravity. Brownian motion is the random motion of nanoparticles inside the base fluid, and continuous collisions between nanoparticles and base fluid molecules are present due to this motion. Thermophoresis is the diffusion of nanoparticles with the presence of a temperature gradient. Diffusiophoresis is the diffusion with the presence of a concentration gradient. Magnus effect is the rotation of the particles around the axis perpendicular to the bulk flow direction under the effect of shear stress. Fluid drainage is the resistance by draining fluid film at the wall to the particle. After performing an order of magnitude analysis among these seven mechanisms, Buongiorno [2006] concluded that Brownian motion and thermophoresis are the only significantly

effective ones. This critical conclusion has directed the literature to focus on these two effects for thermal conductivity and heat transfer studies.

In this section, the thermal conductivity models for nanofluids are reported. First, the classical models are mentioned, then the other mixture models based on other theories and approaches are presented. Finally, the models considering the nano-layer effect and the models with the Brownian motion effect on thermal conductivity are given.

Some of these models are applied to nanorefrigerants, and some are mainly derived and used for water-based nanofluids. The thermal conductivity of nanofluids is presented as a ratio of nanofluid conductivity over base fluid conductivity to indicate the enhancement obtained through using nanofluids more clearly.

The classical models have been developed for mixtures of solids and fluids before the invention of nanofluids. These models have been used for nanofluids before specific models were developed. Maxwell Garnett (1904) and Hamilton-Crosser (1962) are the most familiar classical models. The Maxwell Garnett model (1904) for the thermal conductivity of nanofluids is based on practical medium theory. The model considers the heat transfer occurring through two parallel pathways: the base fluid and the solid particles. The model assumes that the particles are uniformly distributed within the fluid and that there is no interaction or clustering between the solid particles. It also assumes no interfacial thermal resistance between the particles and the base fluid.

The Hamilton-Crosser model (1962) calculates the effective thermal conductivity of the mixture by combining the contributions from the solid particles and the liquid matrix. The model incorporates a correction term considering the interfacial thermal resistance between the solid particles and the liquid.

The Maxwell Garnett model (1904) is a simplified version of the Hamilton-Crosser model (1962) that assumes spherical particles and neglects certain complexities. When the Hamilton-Crosser model is applied with the assumption of spherical particles, the correction term in the model becomes simplified, and the resulting equation becomes equivalent to the Maxwell Garnett model given below for thermal conductivity.

$$\frac{k_{nf}}{k_f} = \frac{k_p + 2k_f + 2\varphi(k_p - k_f)}{k_p + 2k_f - \varphi(k_p - k_f)} \tag{6}$$

This is one of the first thermal conductivity models for solid-liquid mixtures, but the particles are relatively large compared to nanoparticles. It is based on the random suspension of stationary spheres, and the heat conduction equation is solved to achieve the model.

The Bruggeman model can also be considered classical [Bruggeman, 1935]:

$$\frac{k_{nf}}{k_f} = \frac{(3\varphi - 1)\frac{k_p}{k_f} + [3(1-\varphi) - 1] + \sqrt{\Delta}}{4} \tag{7}$$

Here Δ is:

$$\Delta = \left\{(3\varphi - 1)\frac{k_p}{k_f} + [3(1-\varphi) - 1]\right\}^2 + 8\frac{k_p}{k_f} \tag{8}$$

This model is applicable for large volume fractions to estimate the thermal conductivity of composites and is based on differential effective medium (DEM) theory. For low-volume fraction values, it converges to the Maxwell Garnett model.

Like the Maxwell Garnett model, the Jeffrey model (1973) is also derived by solving the conduction equation through the stationary spheres' random suspensions. The higher-order terms are for pair interactions of spherical particles dispersed randomly. It is also mentioned to be accurate to order φ^2.

$$\frac{k_{nf}}{k_f} = 1 + 3\eta\varphi + \varphi^2\left(3\eta^2 + \frac{3\eta^2}{4} + \frac{9\eta^2}{16}\frac{\kappa+2}{2\kappa+3} + \cdots\right) \quad (9)$$

Here $$\kappa = \frac{k_p}{k_f} \quad (10)$$

And $$\eta = \frac{\kappa-1}{\kappa+2} \quad (11)$$

The nanolayer effect is the presence of a solid-like layer between nanoparticles and the base fluid, as presented in Fig. 3.1. It is reported by Fu and Gao (2012) to have a vital role in the thermophoresis of nanoparticles in nanofluids. Therefore, the nanolayer effect can be considered an approach to investigate the thermophoresis effect on thermal conductivity.

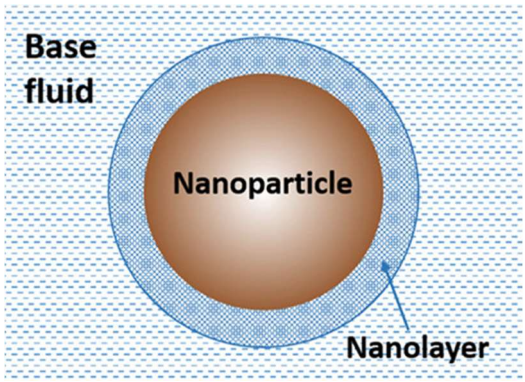

Figure 3.1. The schematic view of the nanolayer between base fluid and nanoparticle [Fan and Zhong, 2020]

One of the many models in the literature considering the nanolayer effect is by Yu and Choi (2003). This model is valid for both spherical and non-spherical particles.

$$\frac{k_{nf}}{k_f} = \frac{k_{pe}+2k_f+2\varphi(k_{pe}-k_f)(1+\beta)^3}{k_{pe}+2k_f-\varphi(k_{pe}-k_f)(1+\beta)^3} \quad (12)$$

k_{pe} is the equivalent thermal conductivity of equivalent particles based on effective medium theory (Yu and Choi, 2003)

Here $$k_{pe} = \frac{2(1-\gamma)+(1+\beta)^3(1+2\gamma)\gamma}{-(1-\gamma)+(1+\beta)^3(1+2\gamma)} k_p \quad (13)$$

and $\beta = \frac{t}{r_p}$ and $\gamma = \frac{k_{layer}}{k_p}$. k_{layer} is the nanolayer thermal conductivity, t is the nanolayer thickness and r_p is the radius of the nanoparticle.

$$k_{layer} = k_p - \frac{k_p - k_f}{t} t_i \quad (14)$$

where t_i where is the calculated position of the interest along the nanolayer and $t_i \in [0, t]$.

The average value of k_{layer} is reduced to:

$$k_{layer} = \frac{k_p - k_f}{2} \quad (15)$$

In addition to the nanolayer effect, the Brownian effect also inspired scientists and researchers to conductivity model determination. The remaining models, by Koo and Kleinstreuer (2004) and Jang and Choi (2004), are based on the Brownian motion of nanoparticles.

The Koo and Kleinstreuer model (2004) is also based on the Maxwell Garnett (1904) model: the authors used a curve-fitting method for the available experimental data. They determined the effect of Brownian motion on thermal conductivity. They considered randomly moving particles surrounded by fluid.

$$k_{nf} = k_{static} + k_{Brownian} = \frac{k_p + 2k_f + 2\varphi(k_p - k_f)}{k_p + 2k_f - \varphi(k_p - k_f)} k_f + 5x10^4 \beta \varphi \rho_p c_p \sqrt{\frac{k_B T}{\rho_p D}} f(T, \varphi) \quad (16)$$

Here k_B is the Boltzmann constant.

Jang and Choi (2004) formed their model by considering four heat transfer mechanisms: the collision of fluid molecules, diffusion of particles, the collision of particles due to Brownian motion, and thermal interactions of particles with fluid molecules.

$$k_{nf} = k_f(1-\varphi) + k_p\varphi + 3C\frac{d_f}{d_p}k_f {Re_{d_p}}^2 Pr\varphi \tag{17}$$

3.6 Viscosity

The viscosity models are also presented as models formed from classical solid-fluid mixtures and new models derived from Stokes flow and Taylor Series expansion. The Einstein model (1906) and the Lungren model (1972) are considered classical mixture models, whereas the Batchelor (1977) model is derived from Stokes flow.

The Einstein model (1906) equation is based on the hydrodynamic equations and the acceptance of infinitely dilute suspensions of spheres. It is more accurate for volume fractions smaller than 2%:

$$\mu_{nf} = (1 + 2.5\varphi)\mu_f \tag{18}$$

Here μ_{nf} and μ_f are the viscosity of nanofluid and base fluid, respectively.

The Batchelor model (1977) is based on the reciprocal theorem in Stokes flow, which is used to obtain the bulk stress due to thermodynamic forces. It consists of both hydrodynamic and Brownian effects. The constant 6.2 adds 5.2 from hydrodynamic effects and 1.0 from Brownian motion.

$$\mu_{nf} = (1 + 2.5\varphi + 6.2\varphi^2)\mu_f \tag{19}$$

The Lundgren model (1972) is based on the Taylor Series expansion of φ. A dilute concentration of spheres is accepted.

$$\mu_{nf} = \frac{1}{(1-2.5\varphi)}\mu_f \tag{20}$$

CHAPTER 4

MODELING OF AN IDEAL VAPOR COMPRESSION REFRIGERATION CYCLE (VCRC)

The previous chapter provides the existing models to determine nanofluids' thermophysical properties. The applicability of these models to two-phase refrigerant flow with the presence of nanoparticles is considered next.

To investigate the nanorefrigerant performance in an ideal vapor compression refrigeration cycle (VCRC), first, the ideal VCRC needs to be modeled. The study conducted by Björk and Palm (2006) is the reference for determining the parameters and modeling the cycle. For the ideal VCRC, one compressor and one compartment refrigerator modeling are selected. As shown in Figure 4.1, the heat transfer in the evaporator and the condenser is assumed to be at constant pressure, the compressor operates isentropically, and there is no pressure or heat loss in the piping. The refrigerant is selected to be R134a since it is the most widely used base fluid for the nanorefrigerants in the literature. For this cycle, the four ideal processes are:

1-2: isentropic compression in a compressor
2-3: isobaric heat rejection in a condenser (state 2’ is the saturated vapor state)
3-4: throttling in an expansion device
4-1: isobaric heat absorption in an evaporator

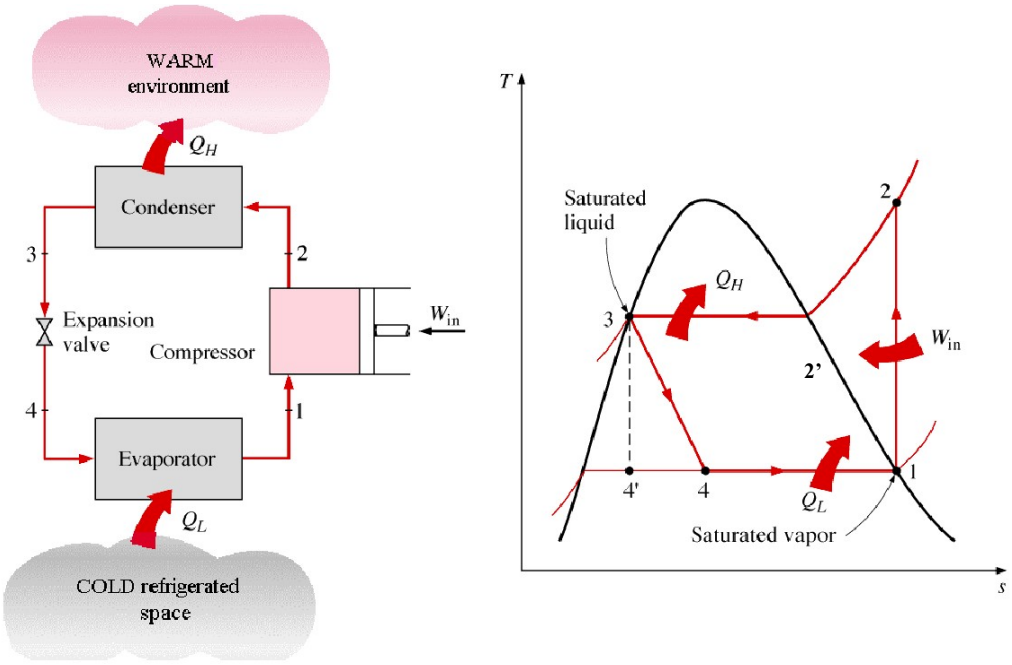

Figure 4.1. Schematic view of a vapor compression refrigeration cycle (VCRC) and T-s diagram for an ideal VCRC [Çengel and Boles, 2006]

The governing energy rate balance equations are as below:

$$\dot{Q}_L = \dot{m}(i_1 - i_4) \tag{21}$$

$$\dot{W}_{in} = \dot{m}(i_2 - i_1) \tag{22}$$

$$\dot{Q}_H = \dot{m}(i_2 - i_3) \tag{23}$$

$$i_3 = i_4 \tag{24}$$

$$COP = \frac{\dot{Q}_L}{\dot{W}_{in}} = \frac{(i_1 - i_4)}{(i_2 - i_1)} \tag{25}$$

Here $\dot{Q}_L$ and $\dot{Q}_H$ are the heat rate removed from refrigerated space and heat rejected from the cycle, respectively. $\dot{W}_{in}$ is the compressor power input and $\dot{m}$ is the mass flow rate of the refrigerant. i is the enthalpy and the subscripts are the corresponding states given in Figure 4.1. COP is the coefficient of performance, which is the measure for the 1st law efficiency of the cycle.

The thermodynamic parameters for modeling the ideal VCRC are given in Table 4.1, which are to be used to determine the mass flow rate, the states, and the sizing of the evaporator and the condenser.

Table 4.1 Input thermodynamic parameters for Ideal VCRC modeling

T_H	20	ºC
T_L	4	ºC
$\dot{W}$	30	W
$\dot{Q}_L$	60	W
P_1	101.325	kPa
$\dot{Q}_H$	90	W

As given in Table 4.1, the hot reservoir temperature, T_H, which is the ambient room temperature, is chosen as 20°C and the cold reservoir temperature, T_L, which is the air temperature inside the refrigerator is taken as 4°C (freezer section is omitted). A larder refrigerator, a refrigerator without any freezer compartment, is selected to be modeled. The COP in the reference paper [Björk and Palm, 2006] is 1.5, whereas it is selected to be 2 here. The COP for a typical refrigerator is between 1.5 and 3; since this is the modeling of an ideal cycle, a slightly larger value for COP is acceptable.

The cooling capacity is given as a maximum of 119 W [Björk and Palm, 2006]. Half of this value is chosen for an average calculation because only the fridge part (the compartment where the temperature is not below 0°C) is to be modeled in a larder refrigerator. The pressure of the low-pressure side, which is the evaporator pressure for a refrigerator, is known to be between 0.8 and 1.5 bar for the evaporation temperature to be below the temperature of the refrigerated space, so a typical value, which is 1 atm, is assumed for the evaporation pressure.

4.1 Evaporator

The evaporator is to be modeled first since the low-pressure side and the cooling capacity are known.

$$\dot{Q}_L = (UA)_{evap}\Delta T_{LM,evap} = (UA)_{evap}(T_1 - T_L) \tag{26}$$

$$\frac{1}{(UA)_{evap}} = \frac{1}{(hA)_{ref,evap}} + \frac{1}{(hA)_{air,evap}} \tag{27}$$

$$\frac{1}{U_{ref,evap}} = \frac{1}{h_{ref,evap}} + \frac{A_{ref,evap}}{h_{air,evap}A_{air,evap}} \tag{28}$$

Here $\Delta T_{LM,evap} = T_1 - T_L$, since temperatures of both sides remain constant in the evaporator. $U_{ref,evap}$ is the overall heat transfer coefficient based on the refrigerant side area, $h_{ref,evap}$ and $A_{ref,evap}$ are the heat transfer coefficient and area of the refrigerant side, and $h_{air,evap}$ and $A_{air,evap}$ are the heat transfer coefficient and area of the air side, which is the refrigerator's inner compartment. There is heat transfer by free convection at inner compartment, therefore the air side heat transfer coefficient, $h_{air,evap}$, is calculated with the following equations [Incropera and De Witt, 2002]:

$$h_{air,evap} = \frac{\overline{Nu}_{air}k_{air}}{L} \tag{29}$$

$$\overline{Nu}_{air} = \begin{cases} \left\{0.825 + \frac{0.387{Ra_L}^{1/6}}{\left[1+(0.492/Pr)^{9/16}\right]^{8/27}}\right\}^2, for\ Ra_L > 10^9 \\ 0.68 + \frac{0.670{Ra_L}^{1/4}}{\left[1+(0.492/Pr)^{9/16}\right]^{4/9}}, for\ Ra_L \leq 10^9 \end{cases} \tag{30}$$

$$Ra_L = Gr_L Pr \tag{31}$$

$$Gr_L = \frac{g\beta(T_w - T_\infty)L^3}{\nu^2} \tag{32}$$

$$\beta \cong \frac{1}{T_m} = \frac{1}{\left(\frac{T_w + T_\infty}{2}\right)} \tag{33}$$

Here $\overline{Nu}_{air}$ is the average Nusselt number, k_{air} is thermal conductivity, L is the effective length (height of the heat transfer area for the air side), Ra_L is Rayleigh number, $Gr_L$is Grashof number, Pr is Prandtl number, g is gravitational acceleration, β is volumetric thermal expansion coefficient, T_w and T_∞ are the wall temperature and temperature of the air outside the thermal boundary layer, and ν is the kinematic viscosity of air. All properties are calculated at mean temperature, T_m, which is the average of T_w and T_∞.

The refrigerant side heat transfer coefficient, $h_{ref,evap}$, is calculated with the following four equations and their average is used in further calculations. These equations are formulated for two-phase flow boiling [Kakaç and Liu, 2002]. They cover conditions of boiling within full range, which means they include extreme conditions such as single-phase of liquid at the entrance of the evaporator and two-phase flow along the evaporator [Kakaç and Liu, 2002]. Since there is a two-phase saturated flow of the refrigerant inside the VCRC at the evaporator and condenser sections, these correlations are needed to predict the heat transfer coefficient.

Güngör and Wınterton Correlatıon [Kakaç and Liu, 2002]

Güngör and Winterton correlation was formed by covering a wide database of flow-boiling of halocarbon refrigerants [Kakaç and Liu, 2002].

$$\bar{h}_{TP} = E\bar{h}_l + S\bar{h}_p \tag{34}$$

Here, $\bar{h}_{TP}$ is the heat transfer coefficient for two-phase flow, E is an enhancement factor, $\bar{h}_l$ is the heat transfer coefficient for the liquid phase at the specified condition, S is the suppression factor and $\bar{h}_p$ is the term of pool boiling. $\bar{h}_l$ can be calculated from any single-phase heat transfer coefficient formula available in the literature according to the flow type and Re limitations. For the present configuration, the flow is laminar with constant wall temperature, so Nusselt number

for $\bar{h}_l$ is taken as 3.66 [Kakaç and Liu, 2002]. The calculation of E, the enhancement factor, is given below.

$$E = 1 + 2.4 \times 10^{-4} Bo^{1.16} + 1.37(1/X_{tt})^{0.86} \tag{35}$$

In equation (35), Bo is the boiling number and $1/X_{tt}$ is the Lockhart-Martinelli Parameter, which are defined in Eqns. (36) and (37), respectively.

$$Bo = \frac{q"}{G \cdot i_{lv}} \tag{36}$$

$$\frac{1}{X_{tt}} = \frac{x}{(1-x)^{0.9}} \left(\frac{\rho_l}{\rho_v}\right)^{0.5} \left(\frac{\mu_v}{\mu_l}\right)^{0.1} \tag{37}$$

In equations (36) and (37), q"is the heat flux, G is the mass flux, i_{lv} is the vaporization enthalpy of the refrigerant, ρ is the density and μ is the viscosity, and l and v are the subscripts for the liquid and vapor phases. For the equation (34), S and $\bar{h}_p$ are the remaining unknowns. S is defined as:

$$S = \left(1 + 1.15 \times 10^{-6} E^2 {Re_l}^{1.17}\right)^{-1} \tag{38}$$

In this equation, Re_l is the Reynolds number for the liquid and it is defined as:

$$Re_l = \frac{2G(1-x)r_i}{\mu_l} \tag{39}$$

The remaining term, $\bar{h}_p$, is the pool boiling term:

$$\bar{h}_p = 55 {p_r}^{0.12} (-log p_r)^{-0.55} M^{-0.5} {q"}^{0.67} \tag{40}$$

Here, p_r is the reduced pressure, and M is the molecular weight of the fluid.

Chen Correlation [Kakaç and Liu, 2002]

This correlation combines the nucleate boiling, $\bar{h}_{nb}$, and convective boiling, $\bar{h}_{cb}$, terms by calculating them separately. It covers both low and high-quality flows and is developed for saturated flow-boiling. The two-phase boiling heat transfer coefficient is given below.

$$\bar{h}_{TP} = \bar{h}_{cb} + \bar{h}_{nb} = \bar{h}_l F_o + \bar{h}_p S \tag{41}$$

$\bar{h}_l$ and S are the same as defined for Eqn. (34). The boiling enhancement factor, F_o is calculated from:

$$F_o = F(1 - x) \tag{42}$$

$$F = \begin{cases} 1, for\ 1/X_{tt} \leq 0.1 \\ 2.35(0.213 + 1/X_{tt})^{0.736}, for\ 1/X_{tt} > 0.1 \end{cases} \tag{43}$$

$\bar{h}_p$ is the pool boiling term and it is calculated through the:

$$\bar{h}_p = 0.00122 \frac{{k_l}^{0.079} {c_{p,l}}^{0.45} {\rho_l}^{0.49} {\theta_b}^{0.24} {\Delta p_v}^{0.75}}{\sigma^{0.5} {\mu_l}^{0.29} (i_{lv} \rho_v)^{0.24}} \tag{44}$$

θ_b is the wall superheat, σ is the surface tension, and Δp_v is the pressure for vaporization of the liquid at the specified conditions. Δp_v is calculated from the Clapeyron Equation, given below.

$$\Delta p_v = \frac{\theta_b i_{lv} \rho_v}{T_{sat}} \tag{45}$$

Shah Correlation [Shah, 1982]

Shah correlation [Shah, 1982] is given in equation (46) as the heat transfer coefficient of the liquid phase which is calculated by a modified Dittus-Boelter correlation [Incropera and De Witt, 2002], equation (47), multiplied by a factor, ψ, presented in equation (48). It is used to predict the flow-boiling heat transfer coefficient for pipe

flow according to four dimensionless numbers which are Fr (Froude number), Co (convection number), Bo (boiling number) and, F (enhancement factor). The flow is characterized by these numbers. The heat transfer coefficient is:

$$\bar{h}_{TP} = \psi \bar{h}_l \tag{46}$$

$$\bar{h}_l = 0.023 \left[\frac{G(1-x)D}{\mu_l}\right]^{0.8} Pr_l \frac{k_l}{D} \tag{47}$$

Here D is the diameter of the tube.

$$\psi = \begin{cases} \psi_{cb}, for\ \psi_{nb} \leq \psi_{cb} \\ \psi_{nb}, for\ \psi_{cb} < \psi_{nb} \end{cases} \tag{48}$$

Here ψ_{cb} and ψ_{nb} are convective and nucleate boiling multiplication factors and they are:

$$\psi_{cb} = 1.8/N^{0.8} \tag{49}$$

$$\psi_{nb} = \begin{cases} \begin{cases} 230Bo^{0.5}, for\ Bo > 0.3x10^{-4} \\ 1 + 46Bo^{0.5}, for\ Bo \leq 0.3x10^{-4} \end{cases} for\ N > 1.0 \\ FBo^{0.5} \exp(2.74N^{-0.1}), for\ 0.1 < N \leq 1.0 \\ FBo^{0.5} \exp(2.74N^{-0.15}), for\ N \leq 0.1 \end{cases} \tag{50}$$

Here factors N and F are given by:

$$N = \begin{cases} 0.38{Fr_L}^{-0.3} Co, for\ Fr_L \leq 0.04 \\ Co, for\ Fr_L > 0.04 \end{cases} \tag{51}$$

$$F = \begin{cases} 14.7, for\ Bo \geq 11x10^{-4} \\ 15.43, for\ Bo < 11x10^{-4} \end{cases} \tag{52}$$

Here Fr_L and Co are Froude and Confinement numbers:

$$Fr_L = \frac{G^2}{\rho_l{}^2 gD} \tag{53}$$

$$Co = \left(\frac{1}{x} - 1\right)^{0.8} \left(\frac{\rho_v}{\rho_l}\right)^{0.5} \tag{54}$$

Kandlikar Correlation [Kandlikar, 1990]

Kandlikar (1990) added a fluid dependent factor to the nucleate boiling term of Shah's correlation [KakaçandLiu, 2002] and formed his correlation as below.:

$$\frac{\bar{h}_{TP}}{\bar{h}_l} = C_1 Co^{C_2} (25 Fr_L)^{C_5} + C_3 Bo^{C_4} F_{fl} \tag{55}$$

Here $\bar{h}_l$ is calculated by eqn. (47), F_{fl} is a constant dependent on the fluid type (1.25 is assumed for R134a since it is not available in the literature and the average of other refrigerants is calculated) and C_n is dependent on the convective ($Co < 0.65$) or nucleate ($Co \geq 0.65$) boiling dominance. C_n values are provided in Table 4.2.

Table 4.2 C_n values for Kandlikar correlation

	$Co < 0.65$	$Co \geq 0.65$
C_1	1.1360	0.6683
C_2	-0.9	-0.2
C_3	667.2	1058.0
C_4	0.7	0.7
C_5	0.3	0.3

The geometry of the evaporator is taken as a starting point from the reference paper [Björk and Palm, 2006] but the air-side heat transfer area is modified after the calculations to reach the reference heat transfer value. In Table 4.3, the final geometry of the evaporator is given.

In Figure 4.2, the flow chart for evaporator calculations is presented. With the fixed values of State 1 (see Fig. 4.1) and $\dot{Q}_L$, the geometry of the evaporator in Björk and Palm (2006) is a reference for the refrigerant side hydraulic diameter and the air side (refrigerated space) heat transfer area. The refrigerant tube's length and the air-side area's size are finalized after iterations with the procedure described in the figure.

The initial values for the heat transfer coefficients of the air and refrigerant sides are guessed and iterated with the calculated results. The iterations are repeated until the calculated heat load is the same as the design value.

Table 4.3 The geometry of the evaporator to be used in calculations

$A_{air,evap}$	0.5188	m^2
$L_{ref,evap}$	8.2	m
$d_{ref,evap}$	3.2	mm
$A_{ref,evap}$	0.0824	m^2

In Table 4.3, $L_{ref,evap}$ is the refrigerant tube length, $d_{ref,evap}$is the refrigerant tube diameter for the evaporator.

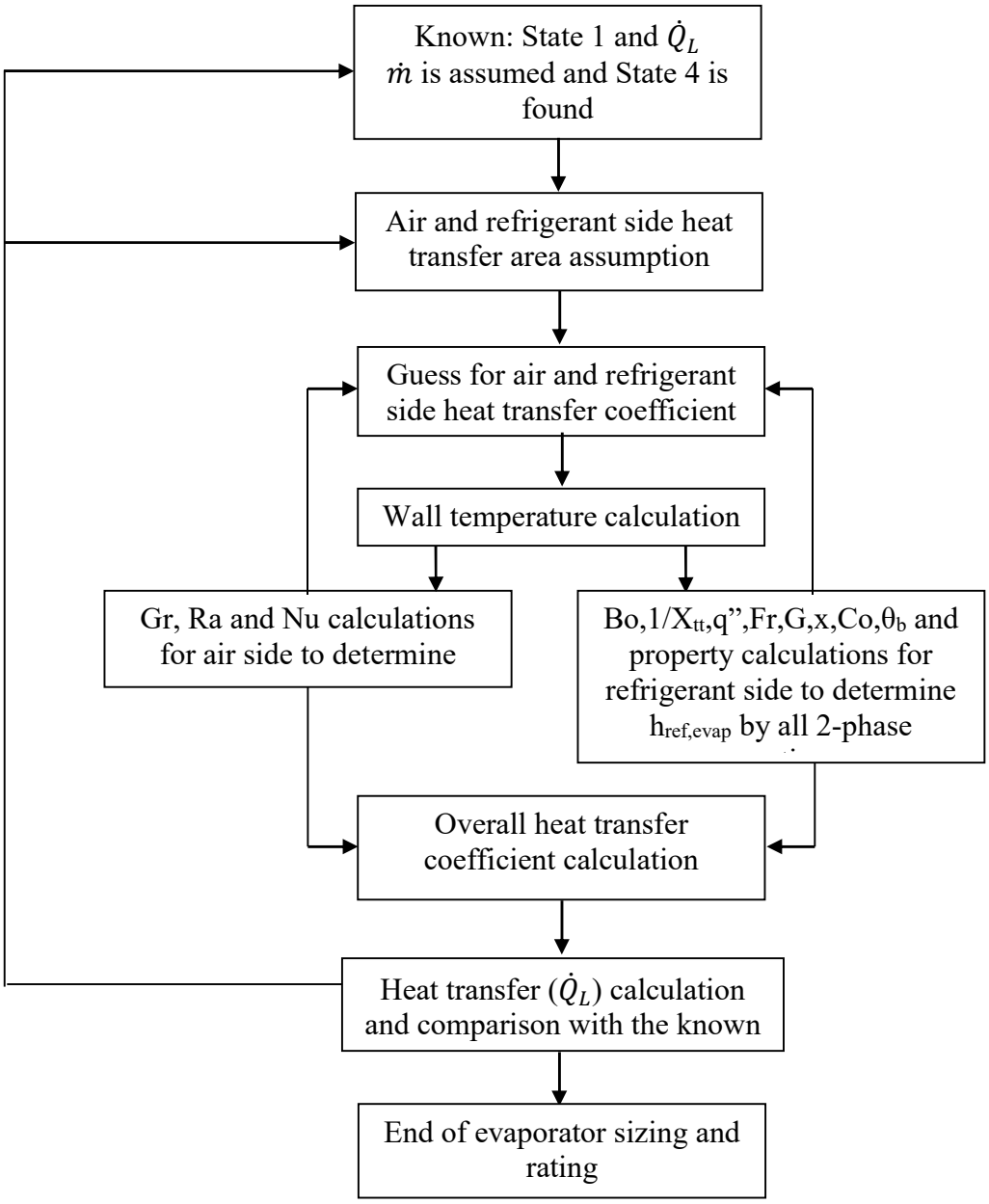

Figure 4.2. Flow chart for evaporator calculations

4.2 Condenser

After the evaporator sizing and rating is performed, state 4 (see Fig. 4.1) is known. Therefore, the enthalpy of state 3 is also known. With the assumption of an ideal cycle, state 3 is saturated liquid. Therefore, the pressure and temperature of state 3 are also found. Eqn calculates the enthalpy of state 2. (22) since mass flow rate and power input are also present. The pressure of state 2 is the same as that of state 3. Therefore, two independent conditions are gathered to determine state 2. The following equations are used to determine the size of the condenser.

$$\dot{Q}_H = (UA)_{cond} \Delta T_{LM,cond} = (UA)_{cond} \frac{(T_2 - T_1) - (T_3 - T_1)}{ln\frac{(T_2 - T_1)}{(T_3 - T_1)}} \tag{56}$$

$$\frac{1}{(UA)_{cond}} = \frac{1}{(hA)_{ref,cond}} + \frac{1}{(hA)_{air,cond}} \tag{57}$$

$$\frac{1}{U_{ref,cond}} = \frac{1}{h_{ref,cond}} + \frac{A_{ref,cond}}{h_{air,cond} A_{air,cond}} \tag{58}$$

Here

$$\Delta T_{LM,cond} = \frac{(T_2 - T_1) - (T_3 - T_1)}{ln\frac{(T_2 - T_1)}{(T_3 - T_1)}} \tag{59}$$

since $T_1 = T_4$. $U_{ref,cond}$ is the overall heat transfer coefficient based on the refrigerant side area, $h_{ref,cond}$ and $A_{ref,cond}$ are the heat transfer coefficient and area of the refrigerant side, and $h_{air,cond}$ and $A_{air,cond}$ are the heat transfer coefficient and area of the air side. $h_{air,cond}$ is calculated with Eqns. (29-33).

The geometry of the condenser is taken as a starting point from the reference paper [Björk and Palm, 2006]. However, the air-side heat transfer area and the length of the refrigerant side are modified after the calculations to reach the reference heat transfer value, as was done for the evaporator. In Table 4.4, the final geometry of the condenser is given.

Table 4.4 The geometry of the condenser to be used in calculations

$L_{ref,cond}$	11.91	m
$d_{ref,cond}$	3.5	mm
$A_{ref,cond}$	0.1310	m^2
Width of condenser	460	mm
Height of condenser	1810	mm
Distance between refrigerant tubes	80	mm
Wire # on each side of the tube	79	mm
$A_{air,cond}$	1.3476	m^2

In Table 4.4, $L_{ref,cond}$ is the refrigerant tube length, $d_{ref,cond}$is the refrigerant tube diameter.

Since state 2 (see Fig. 4.1) is superheated vapor, the heat transfer calculations are divided into two sub-groups to determine the heat transfer coefficients of the air and refrigerant side and the overall heat transfer coefficient. State 2' is introduced, the saturated vapor state at the same pressure as states 2 and 3. The single-phase heat load is found with known enthalpy of states 2' and 2, and the Dittus-Boelter correlation, Eqn. (60) is used to determine the heat transfer coefficient of the refrigerant side in single-phase flow.

$$\bar{h}_l = 0.0265 {Re_D}^{0.8} {Pr_l}^{0.3} \frac{k_l}{D} \tag{60}$$

The two-phase region heat transfer coefficient calculations are performed with the same four equations given in Section 4.1. The air side is also divided into two parts since the wall temperature would alter for two because the superheated vapor and saturated liquid-vapor temperatures are different for the refrigerant side. Both for the air and refrigerant sides, the length of the single-phase heat transfer region for the

refrigerant side and the ratio of the single-phase heat transfer length to the total length for the air side are compared during the calculations. Iterations are made to equate the ratios of lengths of single-phase (saturated vapor) and two-phase (saturated liquid-vapor mixture) to the total length. After that, the area/length-based average heat transfer coefficients for both sides are determined, and the overall heat transfer coefficient is found.

In Figure 4.3, the flow chart for condenser calculations is presented. With the fixed values of State 3 and $\dot{W}$, the geometry of the evaporator in Björk and Palm (2006) is taken as a reference in terms of the refrigerant side hydraulic diameter and the air side (condenser coils) heat transfer area. The refrigerant tube's length and the air-side area's size (with the number of coil wires) are finalized after iterations with the procedure provided in Figure 4.4. The initial values for the heat transfer coefficients of the air and refrigerant sides are guessed, and they are also iterated with the calculated results; the iterations are repeated until the calculated heat load is the same as the design value.

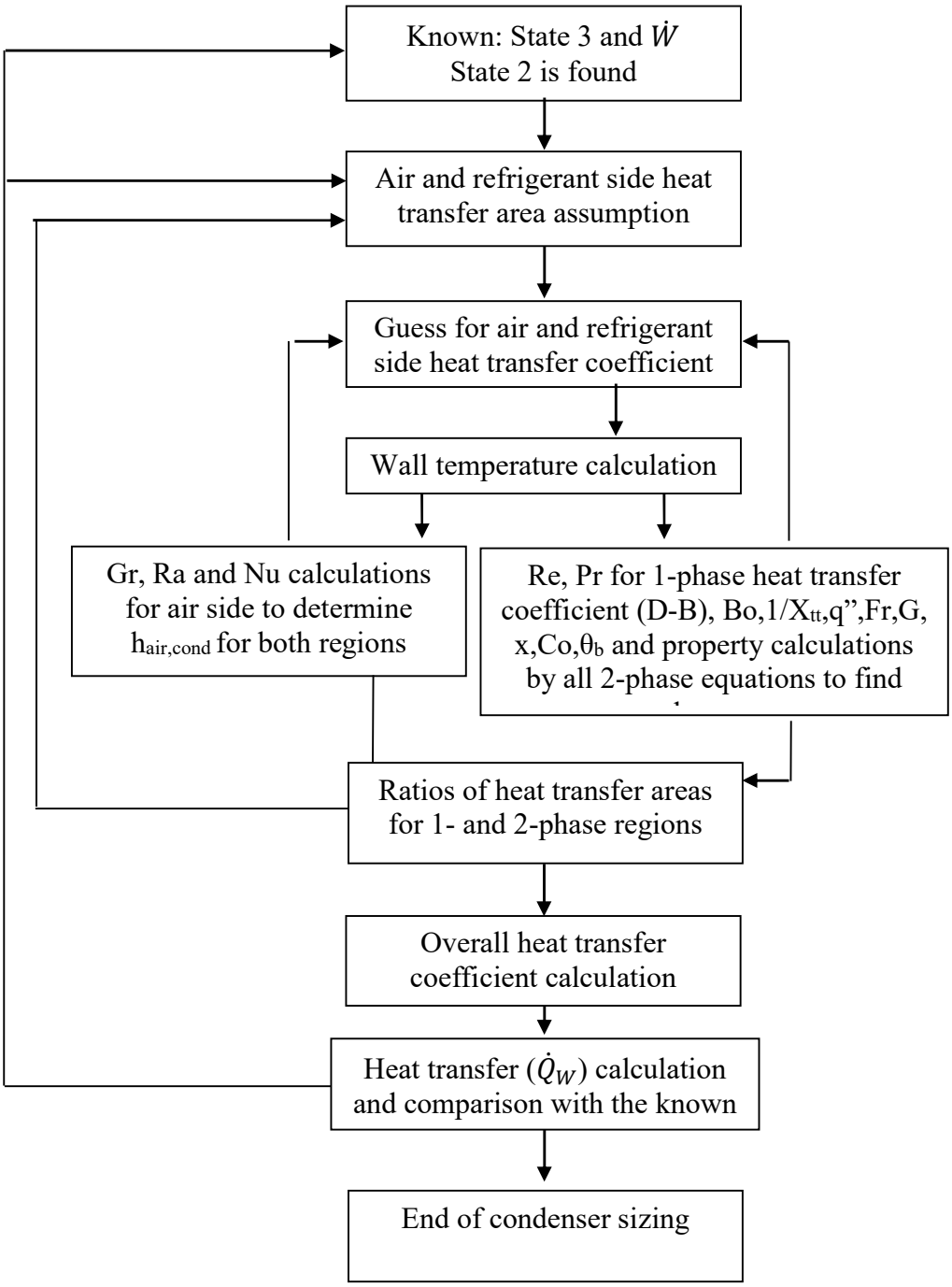

Figure 4.3. Flow chart for condenser calculations

4.3 Ideal VCRC Results

The Ideal VCRC is modeled with the parameters provided in the previous sections. Incropera and De Witt (2002) and Ethermo (2009) are used for the thermophysical properties. The cycle overview is presented in Table 4.1. The cycle is formed with these parameters and the flow charts of the evaporator and condenser. The mass flow rate, $\dot{m}$, is determined as 0.45 g/s.

The following tables (Tables 4.5-4.7) provide the states of the cycle (see Fig. 4.1) and the results of evaporator and condenser analyses. The methodology and equations explained in Sections 4.1 and 4.2 are used to determine the results presented in Tables 4.5, 4.6, and 4.7.

Table 4.5 The states of the cycle

	1	2	2'	3	4
P [kPa]	101.325	883.24	883.24	883.24	101.325
i [kJ/kg]	382.16	448.83	417.3	248.83	248.83
T [K]	246.7	337.9	307.8	307.8	246.7
x	1	-	1	0	0.38
s [kJ/kgK]	1.7453	1.7453	1.7139	1.1673	1.2053

In Table 4.5, the hot and cold reservoir temperatures, which are the ambient room temperature and the temperature of the refrigerated space, the final mass flow rate, and the power input values and heat loads in the evaporator and condenser, are given.

The results presented in Table 4.6 and Table 4.7 are determined iteratively using a model prepared in Microsoft Excel 2010. The evaporator analysis in Table 4.6 is done simultaneously by sizing and rating. The initial value of the heat transfer rate

is fixed, and the iteration is done till the calculated heat transfer rate value matches the initial value. The mass flow rate and the geometry are determined using the heat transfer coefficient of the refrigerant side, calculated by the average of four two-phase correlations mentioned in the table. Among the four equations used for two-phase heat transfer coefficient prediction, Chen's correlation deviated from the other three equations. It highly depends on the wall temperature value, which calculates the wall superheat given in Equations (44) and (45). The wall temperature is calculated by assuming no heat loss between the two fluids and no conduction along the wall (constant temperature wall for both analyses).

Table 4.6 Evaporator analysis

Ref.	$T_{in} = T_4$	246.7	K	$h_{ref,Güngör}$	2697.6	W/m^{2}K
	$T_{out} = T_1$	246.7	K	$h_{ref,Chen}$	1318.7	W/m^{2}K
Air	$T_{air} = T_L$	277	K	$h_{ref,Shah}$	2083.0	W/m^{2}K
$\dot{Q}_L$		60	W	$h_{ref,Kandlikar}$	1921.4	W/m^{2}K
$\Delta T_{LM,evap}$		30.30	K	$h_{ref,evap}$	2005.200	W/m^{2}K
$U_{A,ref,evap}$		24.021	W/m^{2}K	$h_{air,evap}$	3.864	W/m^{2}K
$A_{air,evap}$		0.519	m^2	$UA_{ref,evap}$	1.9803	W/K
$L_{ref,evap}$		8.2	m	$\dot{Q}_{L,calculated}$	60.00	W
$d_{ref,evap}$		3.2	mm			
$A_{ref,evap}$		0.0824	m^2			

The condenser analysis given in Table 4.7 is done by sizing. The initial value of the heat transfer rate and the mass flow rate are fixed, and the iteration is done till the calculated heat transfer rate value matches the initial value. The geometry is determined using the heat transfer coefficient of the refrigerant side, calculated by the average of four two-phase correlations mentioned in the table for the two-phase region and by the Dittus-Boelter correlation for the superheated vapor region.

. Table 4.7 Condenser analysis

Ref.	$T_{in} = T_2$	337.9	K	$L_{ref,cond}$	11.91	m
	$T_{out} = T_3$	307.8	K	$d_{ref,cond}$	3.5	mm
	T_{av}	322.8	K	$A_{ref,cond}$	0.1310	m^2
Air	$T_{air} = T_H$	293	K	Width	460	mm
$\dot{Q}_H$		90	W	Height	1810	mm
$\dot{Q}_{1,phase}$		14.2	W	Dis. Tubes	80	mm
$\dot{Q}_{2,phase}$		75.8	W	Wire #	79	mm
$\Delta T_{LM,cond}$		27.12	K	$A_{air,cond}$	1.3476	m^2
$U_{A,ref,cond}$		25.344	W/m^2K			
$h_{ref,1-phase}$		219.01	W/m^2K			
$h_{ref,Güngör}$		1057.2	W/m^2K			
$h_{ref,Chen}$		1773.5	W/m^2K			
$h_{ref,Shah}$		760.0	W/m^2K			
$h_{ref,Kandlikar}$		707.0	W/m^2K			
$h_{ref,2-phase}$		1074.4	W/m^2K			
$h_{ref,cond}$		985.8	W/m^2K			
$h_{air,cond}$		2.527965	W/m^2K			
$UA_{ref,cond}$		3.3192	W/K			
$\dot{Q}_{H,calculated}$		90.00	W			

1st Law Efficiency for Ideal Cycle

$$\eta_I = COP = \frac{\dot{Q}_L}{\dot{W}_{in}} = \frac{60}{30} = 2 \quad (61)$$

4.4 Nanorefrigerant Calculations with the Ideal VCRC

For the designed ideal cycle, CuO is selected as the nanoparticle to be formed as CuO-R134a nanorefrigerant. The thermal conductivity and viscosity are calculated for a selected volume fraction value.

Maxwell Garnett (1904), Bruggeman (1935), Jeffrey (1973), and Yu and Choi (2004) models are selected to calculate two-phase nanorefrigerant conductivity, and Einstein (1906), Batchelor (1977), and Lungren (1972) models are selected to calculate two-phase nanorefrigerant viscosity for the evaporator and the condenser.

Table 4.8 presents the selected nanoparticle, CuO, properties, and the selected mass fraction value. The mass flow rate for the refrigerant is recalculated for the desired fraction to keep the total mass flow rate constant.

Table 4.8 Nanoparticle (CuO) properties and selected mass fraction

M	79.545	g/mol
ρ_p	6.32	g/cm^3
k_p	32.9	W/mK
c_p	0.729	J/g-K

m_T	0.45	g/s
φ_m	30%	%
d_p	40	nm

For the evaporator and the condenser, volume fraction, density, heat capacity, conductivity, and viscosity calculations for two-phase are performed by dividing the two-phase region into sub-regions of 5% difference in quality and all properties are calculated as the weighted average of these sub-regions. The properties change between these data points is assumed linear (5% increments). The region between 38%-100% for the evaporator is considered since the quality at the inlet is 38%. For the condenser, as in the pure R134a calculations, the same two regions are considered single- and two-phase R134a flow regions. For the single-phase region, base fluid

properties are taken as the average of states 2 and 2' (see Fig. 4.1). The nanorefrigerant properties for the selected mass fraction, prepared following the abovementioned procedure, are given in Table 4.9.

Table 4.9 Property enhancement of CuO-R134a for the parameters in Table 4.8

		Evaporator	Condenser	
		2-phase	1-phase	2-phase
Volume Fraction	φ	0.054%	0.269%	1.31%
Density	ρ_{nf}/ρ_f	42.78%	42.472%	43.13%
Heat capacity	c_{nf}/c_f	-6.54%	-9.339%	-13.62%
Conductivity k_{nf}/k_f	Maxwell Garnett	0.16%	0.810%	4.06%
	Bruggeman	0.16%	0.814%	4.38%
	Jeffrey	0.16%	0.810%	4.09%
	Yu and Choi	0.19%	0.938%	4.72%
Viscosity μ_{nf}/μ_f	Einstein	0.14%	0.674%	3.28%
	Batchelor	0.14%	0.678%	3.55%
	Lundgren	0.14%	0.678%	3.59%

The models used here underestimate the conductivity and viscosity enhancement because even for larger mass fractions (calculated at 30%), the results in Table 4.9 are much smaller than the empirical results in the literature for liquid-based nanofluids. Normalization of the models in terms of single-phase/two-phase point of view and/or new models should be prepared from the available limited experimental studies.

4.5 Problems of Determining Properties

In the previous section, the first approach to determine the nanorefrigerant conductivity and viscosity was to use the models for water-based nanofluids. Conductivity and viscosity calculations in the evaporator and the condenser were performed using the existing correlations derived for liquid-based nanofluids, where the base fluid is only in the liquid phase. The enhancement in these two properties is incompatible with the studies of nanorefrigerant heat transfer in the literature.

As was provided in Tables 1.1 and 1.2, the studies in the literature show a much higher enhancement in conductivity, viscosity, heat transfer coefficient, and overall cycle performance. Among many studies concentrating on the conductivity of the nanorefrigerant with the single-phase refrigerant flow, Jiang et al. (2009) conducted an empirical study and showed a 43%-104% increase in conductivity with a 1.0% volume fraction of nanoparticles. Bartelt et al. (2008) also performed experiments about conductivity and reported up to 101% increase with a 2% mass fraction. Similarly, the predicted viscosity enhancement in the current work is also entirely below the reported data. Habib et al. (2022) reported a 10.75% increase in viscosity for even a 0.01% volume fraction of Al_2O_3 nanoparticles in R134a refrigerant. In addition, Mahbubul et al. (2015) confirmed a 13.68% increase in viscosity for a 5.0% volume fraction again for Al_2O_3-R134a nanorefrigerant. The thermal conductivity and viscosity enhancement results in Table 4.9 are significantly below those available in the literature. In addition to research about thermophysical properties, a heat transfer coefficient increase in the two-phase flow of the refrigerant with the presence of nanoparticles is observed. Henderson et al. (2010) discovered a 55%-100% increase in heat transfer coefficient for quality values less than 0.2 with nanoparticles volume fraction less than 0.5%. Also, Sun and Yang (2014) performed experiments for different nanorefrigerants with less than 0.3% mass fraction for quality values between 0.3-0.8. They came up with the result that increases the heat transfer coefficient up to 49%. Peng et al. (2009) revealed up to 30% increase in heat

transfer coefficient with particle mass fraction up to 0.50%. Among many studies in the literature about cycle performance, Bi et al. (2008) claim 26.1% less energy consumption, Subramani, and Prakash (2011) report 25% less energy consumption and a 33% increase in COP, while Bi et al. (2011) shows 9.6% decrease in energy consumption in VCRC.

The predicted conductivity and viscosity values in Chapter 4.5 are dramatically lower than expected and observed in the literature. As a result, it is concluded that the existing nanofluid correlations for thermophysical properties are not valid for two-phase nanorefrigerant flow conditions. Moreover, enhancement of the heat transfer coefficient and COP are interpreted to have a much higher thermal conductivity than the results in Table 4.9.

Moreover, as it is seen from Equations (34), (41), (46), and (55), the two-phase heat transfer coefficient depends on numerous parameters such as enhancement factor, boiling number, Lockhart-Martinelli parameter, boiling enhancement factor, convective and nucleate boiling multiplication factors, Froude and Confinement numbers, various thermophysical properties, flow conditions, constants, and so on. Therefore, formulizing the heat transfer coefficients as functions of conductivity or viscosity or any other thermophysical property is impossible while neglecting other parameters.

An alternative approach is considered using the results of existing experimental studies, which have been reviewed in Chapter 1, for thermophysical properties. However, since none of the studies in the literature focus on the thermophysical properties of the two-phase flow of nanorefrigerants, it is not possible to manage a proper formulation in the current work using this approach, either. Therefore another way to determine the thermophysical properties of nanorefrigerants is needed.

CHAPTER 5

THE NEW APPROACH TO DETERMINE THE THERMOPHYSICAL PROPERTIES OF NANOREFRIGERANTS

Nanorefrigerants with a two-phase flow of refrigerants consist of three phases of materials: the liquid and gas phases of the refrigerant and the solid phase of nanoparticles. Similar conditions are valid for fluidized beds with gas-liquid-solid fluidization systems in which three phases coexist. These three phases are coal particles, sand particles acting as the liquid phase, and the air blown inside the mixture in the gas phase. While the two systems seem analogous, one significant difference is that not all three phases are different materials for nanorefrigerants. Moreover, the interactions between the three phases are only physical in nanorefrigerants, while there are chemical and physical interactions in fluidized bed systems. The three phases of nanorefrigerants are solid nanoparticles and liquid and gas phases of refrigerant. Since the liquid-gas phase transition only changes the quality of the refrigerant and it has not directly affected the nanoparticle interaction (mentioned in detail in the next paragraph), the analogy does not cause a problem accordingly. The absence of chemical interactions in nanorefrigerants also has no adverse effect because the phenomena in nanorefrigerants do not include the combustion process. The interest is only in physical interactions.

As mentioned in some of the significant studies about three-phase fluidization systems [Zhang et al., 2000], [Yang et al., 2007], [Zhang and Ahmedi, 2005] and [Muroyama and Fan, 1985], the direct interactions between gas and solid particles is very low. In the general methodology, gas-solid interactions are neglected, and it is assumed that the liquid is in contact and interaction with the gas. In addition, liquid-solid fluidization with gas phase results in similar conditions as in gas-liquid systems where the liquid-solid stream acts like a liquid. However, this condition is not valid

for wake regions and when the solid-solid collisions cannot be neglected [Zhang et al. 2000], [Yang et al. 2007], [Zhang and Ahmedi, 2005] and [Muroyama and Fan, 1985].

With the acceptance of differences in material types and neglecting the solid-solid interactions/collisions, an analogy for the interactions of gas-solid particles is offered. The flow is taken as horizontal flow, assumed to be bubbly flow for low-quality and wavy and slug flow for high-quality flows [Nuclear Power, 2023]. The liquid phase of refrigerant with nanoparticles flows on the bottom side, whereas the vapor phase of refrigerant flows on the top without any nanoparticle interaction. In this analogy, the nanoparticles in the solid phase are assumed to be in a homogeneous stream/mixture with the liquid phase refrigerant and not to interact with the gas phase refrigerant. Therefore, the main idea of the new approach is to consider the nanorefrigerant with the two-phase refrigerant flow as a mixture of nanorefrigerant with the liquid phase of the base fluid and nanoparticles and the pure gas phase of the refrigerant.

For a thermophysical property such as enthalpy or entropy, the change in the value in the saturated liquid-gas mixture phase is linear as a function of quality, x.

$$i(x) = i_f + x\left(i_g - i_f\right) \tag{62}$$

Here "i" is the enthalpy, "f" and "g" are subscripts for the liquid and gas phase. Thus, for such properties of nanorefrigerants, when the liquid phase property with nanoparticles is determined and the pure gas phase property is known, the two-phase property of the nanorefrigerant can be found with a similar approach.

For the modeled ideal cycle where the saturation pressures for the condenser and evaporator were 883 kPa and 101 kPa, respectively, the thermophysical properties for pure refrigerant in terms of quality are considered. The enthalpy and entropy are

linear, as mentioned above. However, density, ρ, conductivity, k, and viscosity, μ, are nonlinear. Density can be written as a reciprocal of specific volume, which is also linear. These values are gathered from Etermo (2009) and are presented in Figure 5.1-5.5; the resolution for quality is 5% from saturated liquid to saturated gas conditions. The specific volume variation for both saturation pressures for pure R134a is given in Figure 5.1.

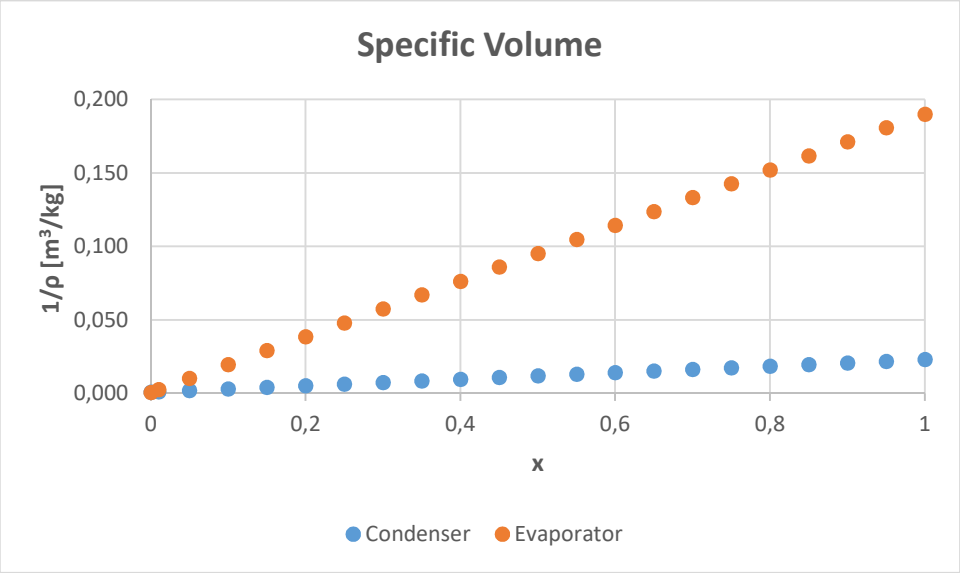

Figure 5.1. Variation of R134a specific volume with quality for condenser and evaporator saturation pressures (P_{evap}= 101.325 kPa, P_{cond}= 883.24 kPa)

As seen in Figure 5.1, the change in specific volume and quality is linear. Also, the specific volume values for the condenser are smaller than those for the evaporator. The saturation pressure of the condenser is much higher than the evaporator; therefore, this is expected. The change of specific volume with quality is given in equations (63) and (64) as functions of saturated liquid and vapor densities, and specific volume, respectively.

$$v(x) = \frac{1}{\rho(x)} = \frac{1}{\rho_f}(1-x) + \frac{1}{\rho_g}x \tag{63}$$

$$v(x) = v_f + x\left(v_g - v_f\right) \tag{64}$$

The graphs for conductivity are given in Figures 5.2 and 5.3 for condenser and evaporator, respectively. These values are also gathered from Etermo (2009). For condenser and evaporator saturation pressures, the conductivity tends to decrease with increasing quality up to a certain amount, which is about 0.35 for the condenser and 0.2 for the evaporator. This interesting and unexpected phenomenon may occur because of a transition in the boiling regime from bubbly/slug flow to slug/annular flow.

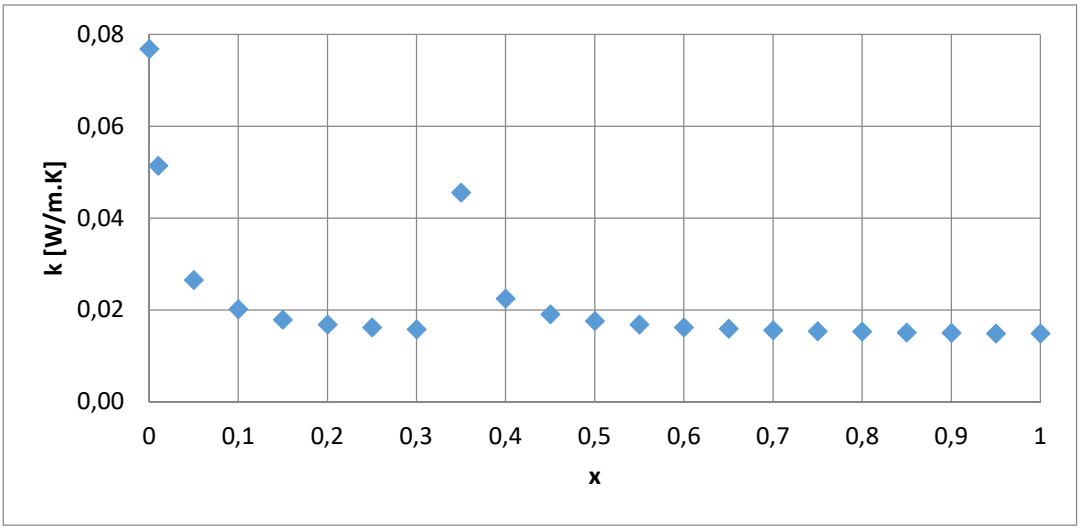

Figure 5.2. Variation of R134a conductivity with quality for condenser saturation pressure (P_{sat}=883.24 kPa)

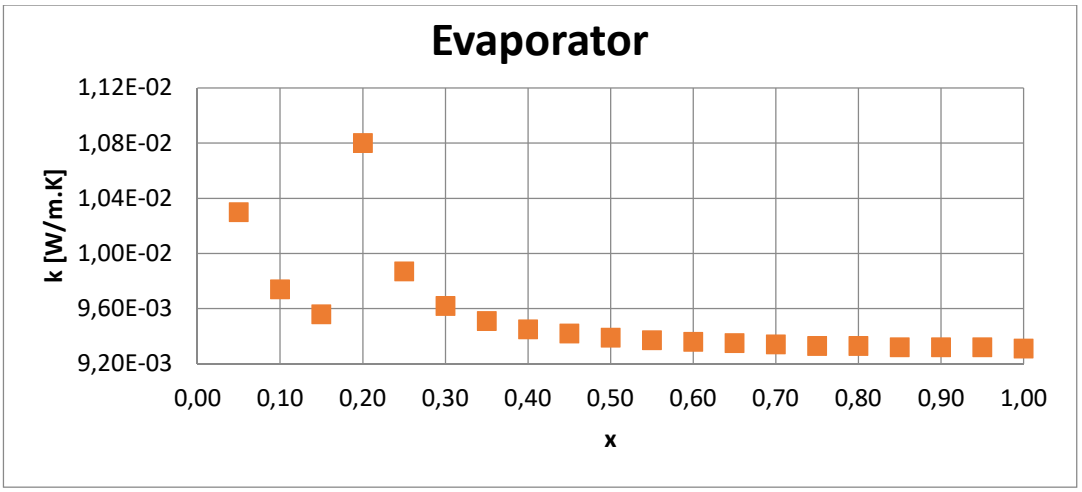

Figure 5.3. Variation of R134a conductivity with quality for evaporator saturation pressure (101.325 kPa)

The viscosity graphs are given in Figures 5.4 and 5.5 for condenser and evaporator, respectively. The change in viscosity for the condenser and evaporator shows a different tendency. While it decreases for the condenser with increasing quality, there is an increase in evaporator viscosity values. The reason may be the change in saturation pressures. With lower pressure, the increase in quality may increase the viscous effects.

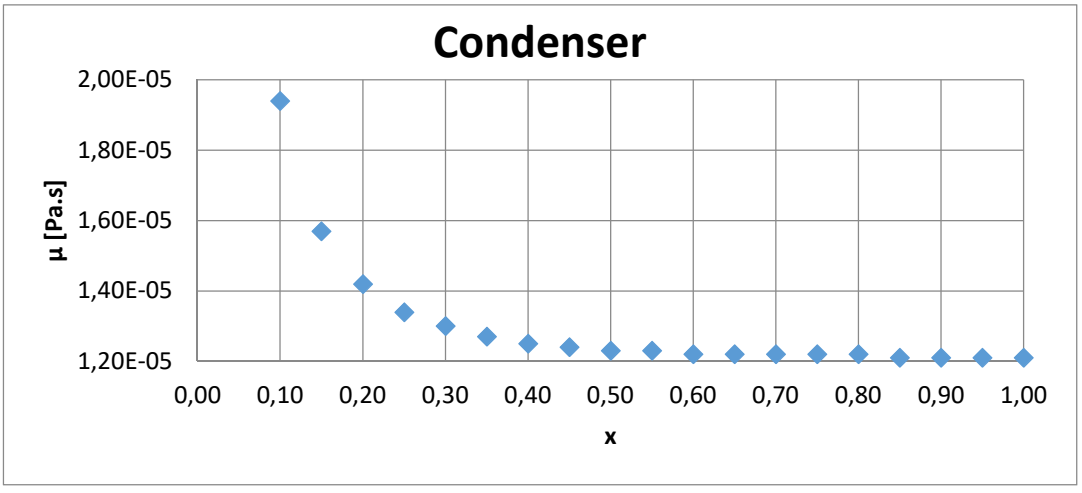

Figure 5.4. Variation of R134a viscosity with quality for condenser saturation pressure (P_{sat}=883.24 kPa)

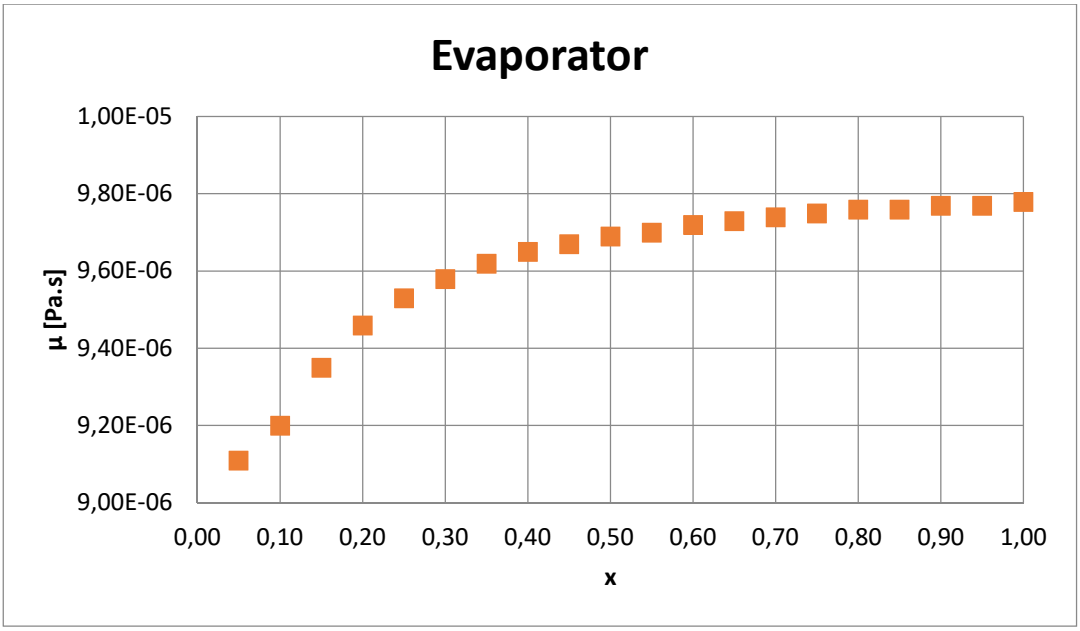

Figure 5.5. Variation of R134a viscosity with quality for evaporator saturation pressure (P_{sat}=101.325 kPa)

From Figure 5.2-5.5, it is observed that thermal conductivity and viscosity are non-linear with respect to quality, therefore they cannot simply be formulated in the following form.

$$a(x) = f(x, a_f, a_g) \tag{65}$$

Here "a" is one of the properties mentioned. Thus, a different approach is applied for the property calculations. Specific volume is linear but since conductivity and viscosity are not linear in the two-phase region, the following method is suggested [Tekin and Yazıcıoğlu, 2016]:

$$a(x) = a_f + x(a_g - a_f) + {c_x}^a \tag{66}$$

Here ${c_x}^{\nu}$ is "0" for specific volume since it is linear along quality. In this formula, the corresponding property is modeled with a linear change with respect to quality, and the deviation from linear behavior is compensated with a constant for each quality value of the given property. For 5% quality resolution, these constants are calculated for each of two properties – conductivity and viscosity – at condenser and evaporator pressures. The formulations are given in the following equations.

$$k(x) = k_{linear}(x) + {c_x}^{k} = k_f + x\left(k_g - k_f\right) + {c_x}^{k} \tag{67}$$

$$\mu(x) = \mu_{linear}(x) + {c_x}^{\mu} = \mu_f + x\left(\mu_g - \mu_f\right) + {c_x}^{\mu} \tag{68}$$

The constants of deviation from linear assumption are found for pure two-phase refrigerant R134a at condenser and evaporator pressures, with known property values at saturated liquid and saturated gas states and property values at each of the 5% increment qualities. Pure refrigerant viscosity and conductivity values are gathered from Etermo (2009). The calculated constants for the properties of condenser and evaporator pressures are tabulated in Tables 5.1 and 5.2.

For the nanorefrigerant property calculations, in a similar manner as in Equations (67-68), the following formulations are used:

$$\nu_{nr}(x) = \nu_{nf} + x\left(\nu_g - \nu_{nf}\right) \tag{69}$$

$$k_{nr}(x) = k_{nf} + x\left(k_g - k_{nf}\right) + {c_x}^{k} \tag{70}$$

$$\mu_{nr}(x) = \mu_{nf} + x\left(\mu_g - \mu_{nf}\right) + {c_x}^{\mu} \tag{71}$$

Table 5.1 Constants for condenser properties

x	μ	μ_{linear}	c^{μ}	k	k_{linear}	c^{k}
-	Pa.s			W/mK		
0	1.72E-04	1.72E-04	0.00E+00	7.69E-02	7.69E-02	0.0000
0.01	9.08E-05	1.70E-04	-7.96E-05	5.14E-02	7.63E-02	-0.0249
0.05	3.16E-05	1.64E-04	-1.32E-04	2.65E-02	7.38E-02	-0.0473
0.10	1.94E-05	1.56E-04	-1.37E-04	2.02E-02	7.07E-02	-0.0505
0.15	1.57E-05	1.48E-04	-1.32E-04	1.79E-02	6.76E-02	-0.0497
0.20	1.42E-05	1.40E-04	-1.26E-04	1.68E-02	6.45E-02	-0.0477
0.25	1.34E-05	1.32E-04	-1.19E-04	1.62E-02	6.14E-02	-0.0452
0.30	1.30E-05	1.24E-04	-1.11E-04	1.58E-02	5.83E-02	-0.0425
0.35	1.27E-05	1.16E-04	-1.03E-04	4.56E-02	5.52E-02	-0.0096
0.40	1.25E-05	1.08E-04	-9.55E-05	2.25E-02	5.21E-02	-0.0296
0.45	1.24E-05	1.00E-04	-8.76E-05	1.91E-02	4.90E-02	-0.0299
0.50	1.23E-05	9.21E-05	-7.98E-05	1.76E-02	4.59E-02	-0.0283
0.55	1.23E-05	8.41E-05	-7.18E-05	1.68E-02	4.28E-02	-0.0260
0.60	1.22E-05	7.61E-05	-6.39E-05	1.62E-02	3.97E-02	-0.0235
0.65	1.22E-05	6.81E-05	-5.59E-05	1.59E-02	3.66E-02	-0.0207
0.70	1.22E-05	6.01E-05	-4.79E-05	1.56E-02	3.35E-02	-0.0179
0.75	1.22E-05	5.21E-05	-3.99E-05	1.54E-02	3.04E-02	-0.0150
0.80	1.22E-05	4.41E-05	-3.19E-05	1.53E-02	2.73E-02	-0.0120
0.85	1.21E-05	3.61E-05	-2.40E-05	1.51E-02	2.42E-02	-0.0091
0.90	1.21E-05	2.81E-05	-1.60E-05	1.50E-02	2.11E-02	-0.0061
0.95	1.21E-05	2.01E-05	-8.00E-06	1.49E-02	1.80E-02	-0.0031
1	1.21E-05	1.21E-05	0.00E+00	1.49E-02	1.49E-02	0.0000

Table 5.2 Constants for evaporator properties

x	μ	μ_{linear}	c^{μ}	k	k_{linear}	c^{k}
-	Pa.s			W/mK		
0	3.79E-04	3.79E-04	0.00E+00	1.04E-01	1.04E-01	0
0.01	1.93E-05	3.75E-04	-3.56E-04	1.70E-02	1.03E-01	-0.0861
0.05	9.11E-06	3.61E-04	-3.51E-04	1.03E-02	9.93E-02	-0.089
0.1	9.20E-06	3.42E-04	-3.33E-04	9.74E-03	9.45E-02	-0.0848
0.15	9.35E-06	3.24E-04	-3.14E-04	9.56E-03	8.98E-02	-0.0802
0.2	9.46E-06	3.05E-04	-2.96E-04	1.08E-02	8.51E-02	-0.0743
0.25	9.53E-06	2.87E-04	-2.77E-04	9.87E-03	8.03E-02	-0.0705
0.3	9.58E-06	2.68E-04	-2.59E-04	9.62E-03	7.56E-02	-0.066
0.35	9.62E-06	2.50E-04	-2.40E-04	9.51E-03	7.09E-02	-0.0613
0.4	9.65E-06	2.31E-04	-2.22E-04	9.45E-03	6.61E-02	-0.0567
0.45	9.67E-06	2.13E-04	-2.03E-04	9.42E-03	6.14E-02	-0.052
0.5	9.69E-06	1.94E-04	-1.85E-04	9.39E-03	5.67E-02	-0.0473
0.55	9.70E-06	1.76E-04	-1.66E-04	9.37E-03	5.19E-02	-0.0426
0.6	9.72E-06	1.57E-04	-1.48E-04	9.36E-03	4.72E-02	-0.0378
0.65	9.73E-06	1.39E-04	-1.29E-04	9.35E-03	4.25E-02	-0.0331
0.7	9.74E-06	1.21E-04	-1.11E-04	9.34E-03	3.77E-02	-0.0284
0.75	9.75E-06	1.02E-04	-9.23E-05	9.33E-03	3.30E-02	-0.0237
0.8	9.76E-06	8.36E-05	-7.39E-05	9.33E-03	2.82E-02	-0.0189
0.85	9.76E-06	6.52E-05	-5.54E-05	9.32E-03	2.35E-02	-0.0142
0.9	9.77E-06	4.67E-05	-3.69E-05	9.32E-03	1.88E-02	-0.0095
0.95	9.77E-06	2.82E-05	-1.85E-05	9.32E-03	1.40E-02	-0.0047
1	9.78E-06	9.78E-06	2.20E-20	9.31E-03	9.31E-03	0

In Equations (69-71), subscripts nr and nf are nanorefrigerant and nanofluid, respectively. Here nanofluid properties are calculated according to the formulas given in Chapter 3 for specific volume, conductivity, and viscosity. Therefore, the existing correlations for the nanofluids are applied to the nanofluid calculations. Since the approach assumes no solid-vapor interaction, the saturated vapor properties of pure refrigerant are used for the gas phase of the refrigerant. Then nanorefrigerant properties are calculated for the corresponding quality values. The constants of deviation from linear variation for pure refrigerant are assumed to be the same for

nanorefrigerant calculations, which is the primary assumption in the current new model. Linear variation is just used to formulate the change of the corresponding property in the two-phase region. Another approach, like polynomial, exponential, or logarithmic change, can be assumed to eliminate these constants. The linear approach is selected for simplicity. The main idea behind it is that the mixture is formed of a nanofluid (nanoparticle + liquid refrigerant) and pure refrigerant vapor. Nanofluid conductivity calculation includes factors affecting nanofluid conductivity, such as Brownian motion, thermophoresis, and nanolayer effect. Therefore, the linear approach does not omit the consideration of these factors.

The mass fraction values are selected for the saturated liquid refrigerant phase, and the volume fraction values are calculated for the reference mass fraction. With increasing quality and decreasing liquid mass, the mass and volume fractions are recalculated for each quality value. The mass flow rate of the refrigerant is taken as in the ideal modeled cycle, which is 0.45 g/s. With increasing quality, the mass flow rate of the liquid refrigerant decreases, so the mass and volume fraction of the nanofluid increases. For the condenser, the mass and volume fraction for three mass fraction values are given in Appendix Tables A.1-A.3. For the evaporator, and similar tables are prepared and presented in Tables A.4-A.6.

For the saturated gas state, since there is no refrigerant in the liquid phase, the mass and volume fraction values are calculated as 100% with the assumption of no interaction between nanoparticles and the gas phase of nanorefrigerant. This is the singular point of the model that it fails to cover. The specific volume values of the nanorefrigerant, which are calculated with the suggested model, are determined for each mass fraction value and are given in Tables A.7-A.9 for the condenser and A.10-A.12 for the evaporator.

The other nanofluid properties are needed for further calculations. The conductivity and viscosity models for water-based nanofluids are used because of the fact that

nanoparticles are assumed to be in interaction with the liquid phase refrigerant only. Conductivity results for the condenser and evaporator for three different mass fraction values are tabulated in Tables A.13-A.15 and A.16-A.18, respectively. Finally, viscosity results for the condenser and evaporator for three different mass fraction values are tabulated in Tables A19-A.21 and A.22-A.24, respectively.

5.1 Discussion about the First Results

The results for the thermophysical properties of CuO-R134a nanorefrigerant are presented in Appendix A. Three different mass fraction values at saturated liquid refrigerant are used. The calculations are done for both the condenser and evaporator of the modeled ideal cycle. The same mass flow rate of pure refrigerant is used for the nanorefrigerant calculations. The density, thermal conductivity, and viscosity of the nanorefrigerant are obtained using the proposed approach and model.

The results in Tables A.7-A.12 are presented in Figure 5.6 and Figure 5.7 for the condenser and the evaporator, respectively. They show that the specific volume of the nanorefrigerant decreases with increasing mass and volume fraction values, as expected. In addition, the effect of nanoparticles increases with increasing quality values since with increasing amount of gas mass percentage, the specific volume of the refrigerant increases, and the nanoparticles lead to a higher increase in density change. When the condenser and evaporator specific volume values of the nanorefrigerants are compared, while the effect of nanoparticle presence shows a similar decrease in specific volume for low-quality values, the effect is much higher for the evaporator at moderate and high-quality values since the evaporator pressure is much lower than condenser pressure, so the specific volume of two-phase refrigerant tends to show a more dramatic increase than the condenser.

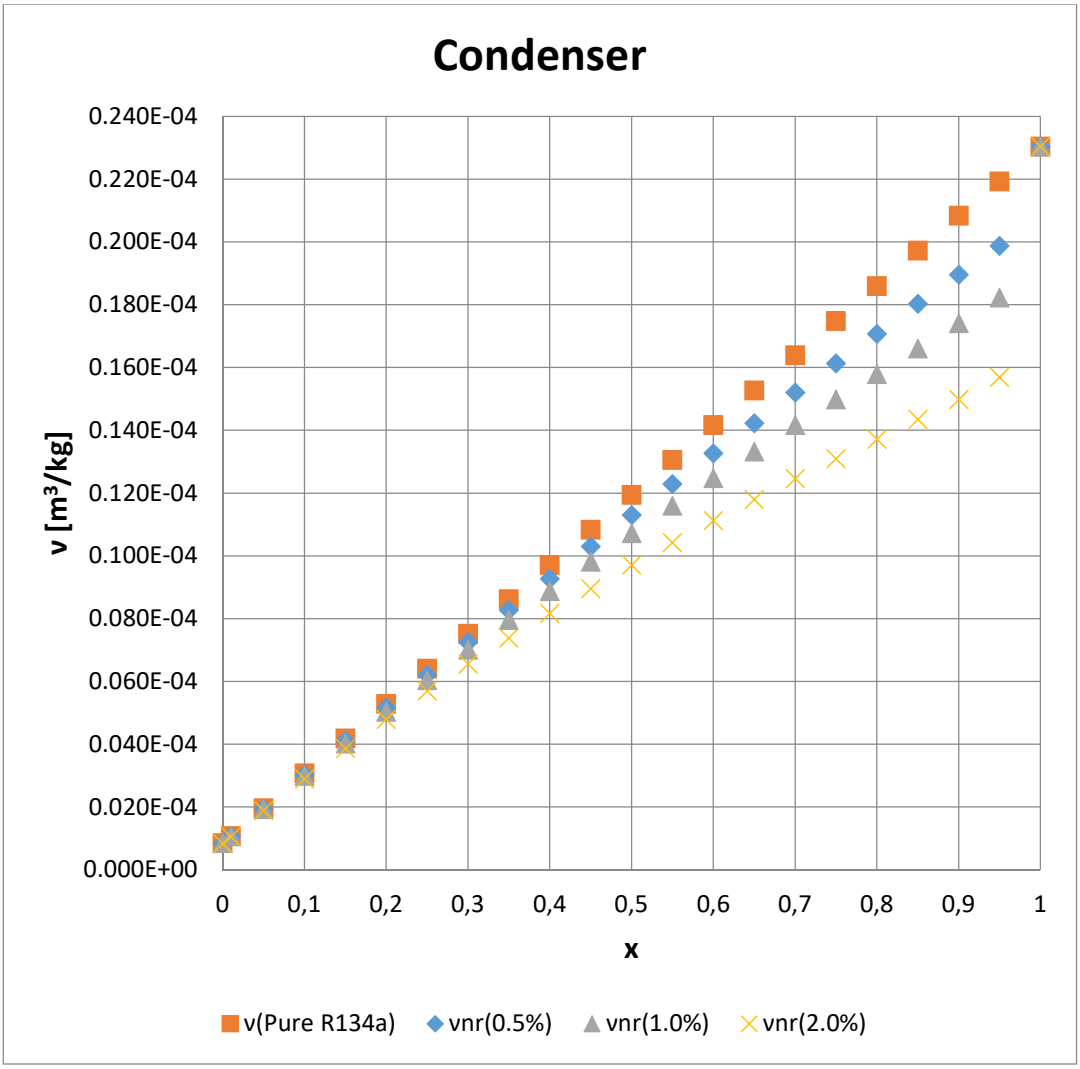

Figure 5.6. Specific volume change of Cu-R134a nanorefrigerant with quality for condenser for three mass fraction values (P_{sat}=883.24 kPa)

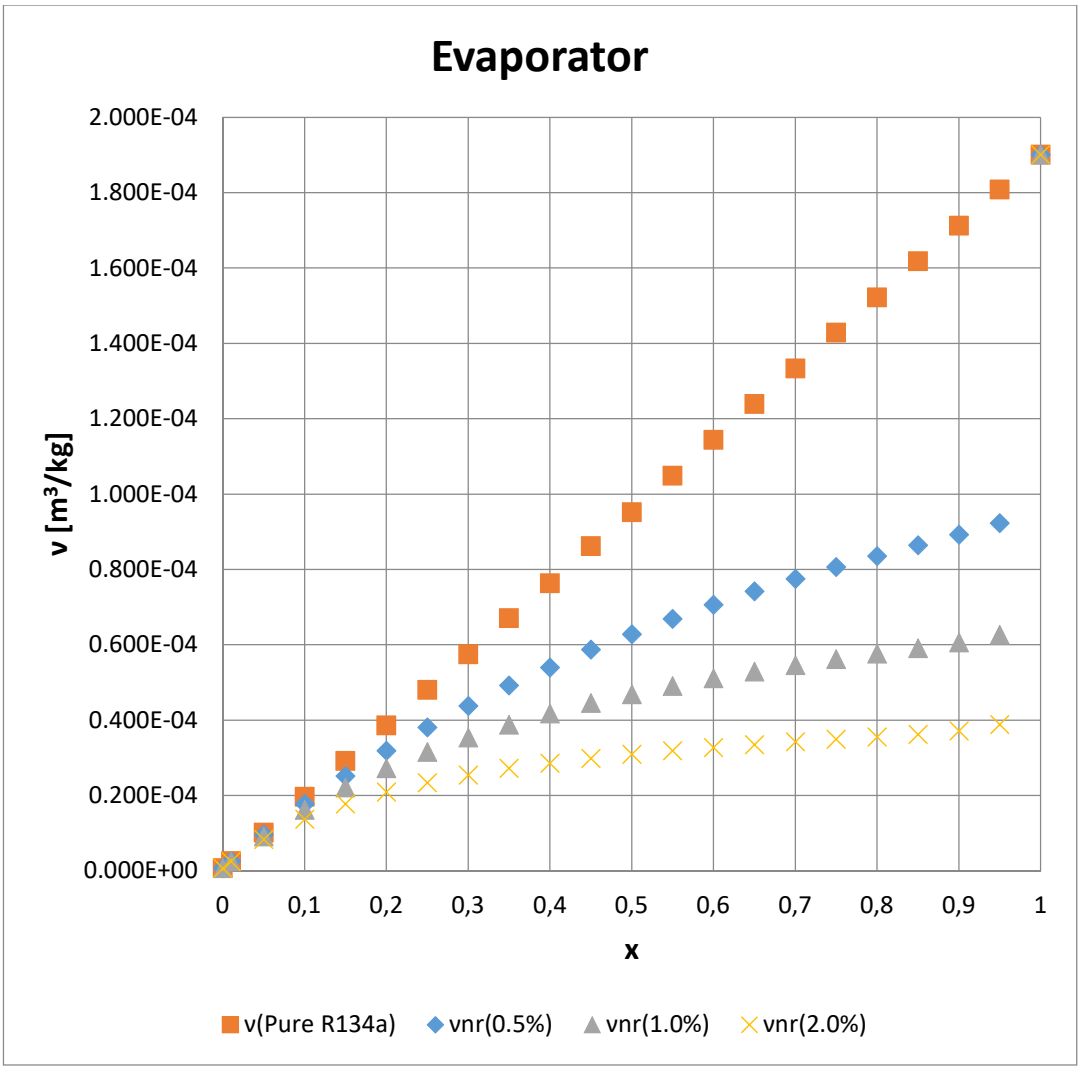

Figure 5.7. Specific volume change of Cu-R134a nanorefrigerant with quality for evaporator for three mass fraction values (P_{sat}=101.325 kPa)

Among the three models used, Bruggeman predicts a higher increase than Maxwell Garnett and Jeffrey's models, as seen in Tables A.13-A.18, while this difference is not significant. Nanoparticles increase conductivity for the evaporator than for the condenser because of the similar condition in density. The increase is up to 15% for a 2% mass fraction. As mentioned in Chapter 1, the studies in the literature are performed for the single-phase flow of refrigerant. Dhindsa et al. (2013) reported a 42% conductivity increase, while Jing et al. (2009) revealed 43-104%, and Bartelt et

al. (2008) observed a 101% increase. The change may occur because of vapor presence in two-phase flow, which decreases conductivity compared to liquid form.

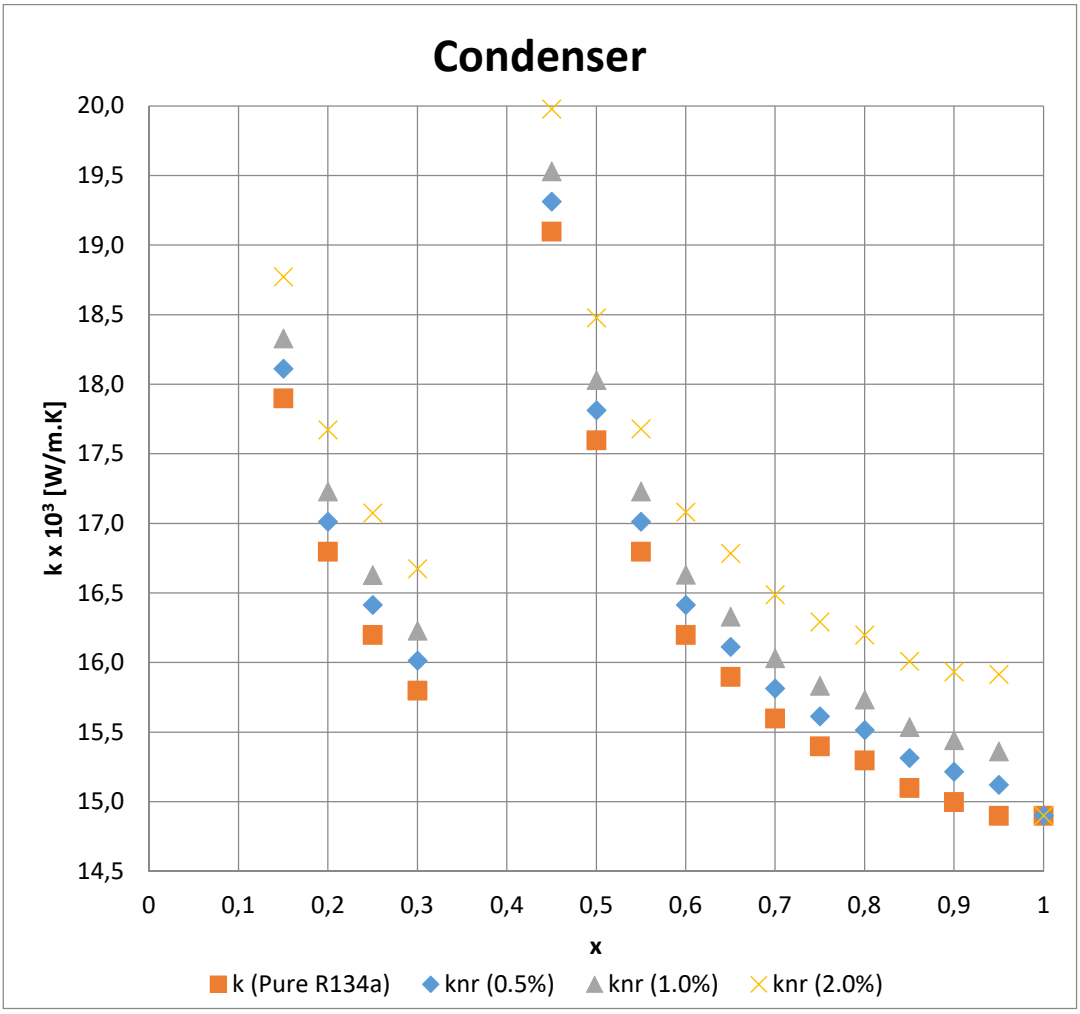

Figure 5.8. Conductivity change of Cu-R134a nanorefrigerant with quality for condenser for three mass fraction values (P_{sat}=883.24 kPa)

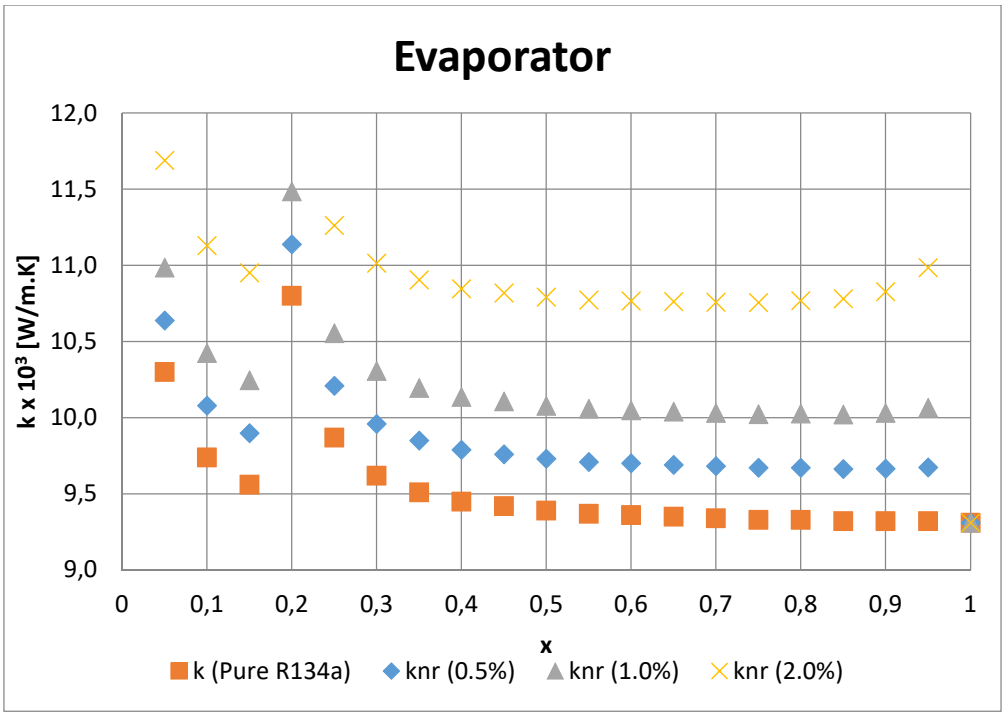

Figure 5.9. Conductivity change of Cu-R134a nanorefrigerant with quality for evaporator for three mass fraction values (P_{sat}=101.325 kPa)

The results in Table A.13-A.18 are presented in Figure 5.8 and Figure 5.9 for the condenser and evaporator, respectively. They indicate that The results given in Table A.19-A.24 are presented in Figure 5.10 and Figure 5.11 for condenser and evaporator, respectively. They reveal that viscosity increases with volume fraction, too, as expected. Among the three models used, the Einstein model predicts a lower increase than Batchelor and Lungren models, while this difference is not significant. Nanoparticles increase viscosity for the evaporator than for the condenser because of the similar condition in density and conductivity. The increase is much higher than conductivity, up to 45% for a 2% mass fraction. The single-phase refrigerant studies in literature, such as Habib et al. (2022) and Mahbubul et al. (2015), reported a 10.75% and 13.68% increase in viscosity. In contrast, Peng et al. (2008) observed a 20.8% increase in friction factor. The difference may occur again because of vapor's presence along the two-phase refrigerant flow. The vapor inclusion tends to increase the viscous behavior more than liquid.

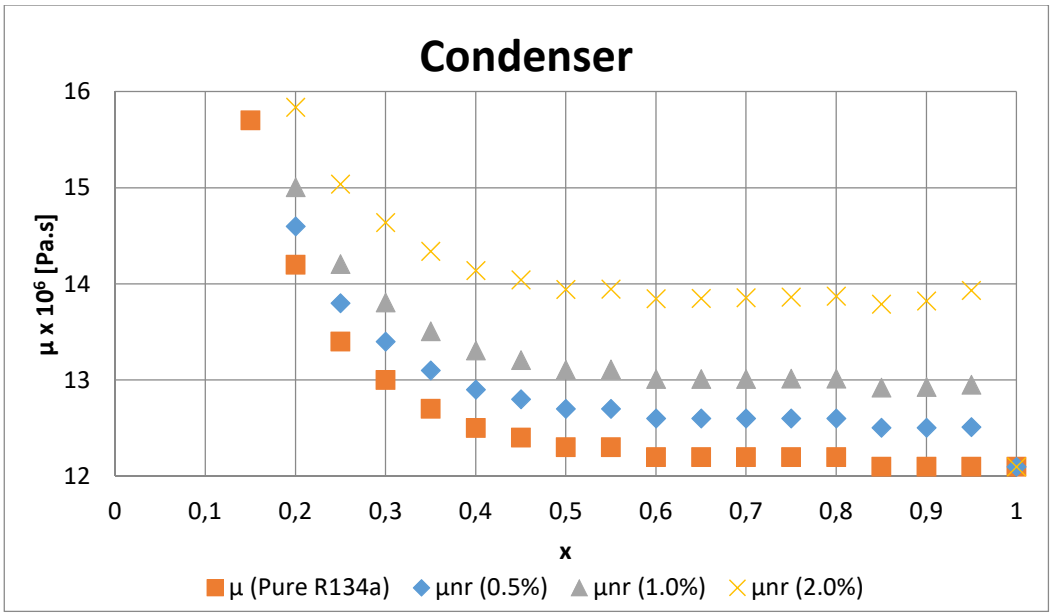

Figure 5.10. Viscosity change of Cu-R134a nanorefrigerant with quality for condenser for three mass fraction values (P_{sat}=883.24 kPa)

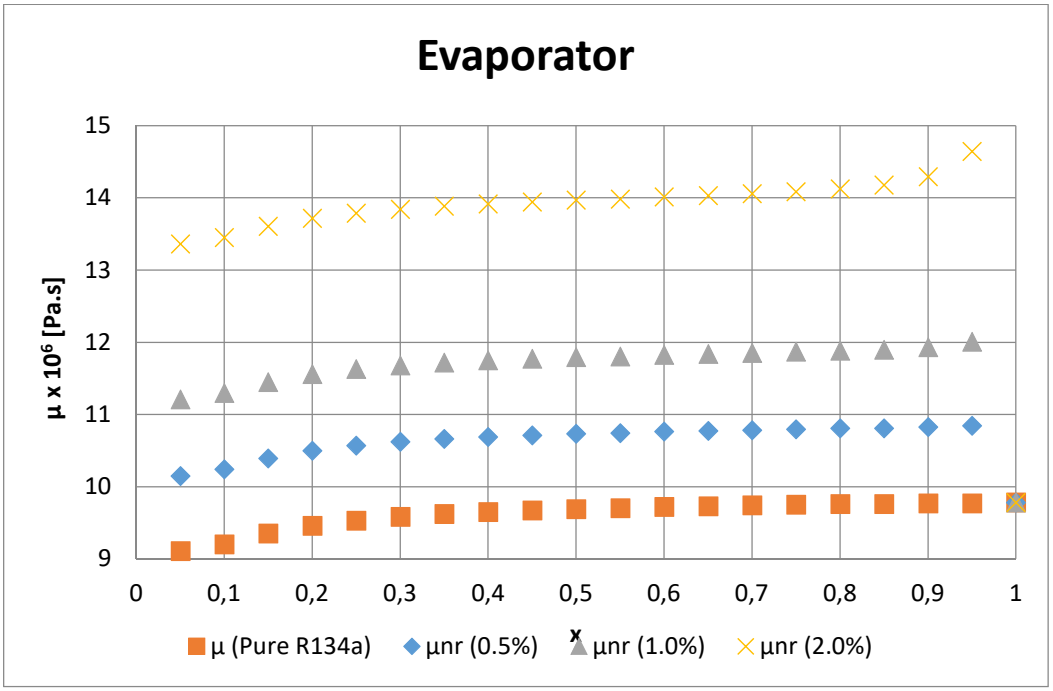

Figure 5.11. Viscosity change of Cu-R134a nanorefrigerant with quality for evaporator for three mass fraction values (P_{sat}=101.325 kPa)

5.2 Verification of the New Model

For the verification of the proposed model, there are two options:

- to use the existing correlations to determine the heat transfer coefficient with the thermophysical properties calculated by our model.
- to apply the model to the limited number of available experimental heat transfer studies.

The first alternative is to formulate the heat transfer coefficient as a function of thermophysical properties. Since the formulations available in the literature, mentioned in Section 3, are highly nonlinear, it is considered unsuitable for verification. The second alternative needs a numerical methodology to apply the existing model to the available experimental heat transfer studies. The method is selected as using ANN.

5.3 ANN

Artificial Neural Networks are computational models inspired by the structure and functioning of biological neural networks in the human brain. They are a subset of machine learning algorithms that can be used to learn patterns and relationships in data. ANNs consist of interconnected nodes, called artificial neurons or units, organized into layers [Haykin, 2009]. The formal definition of an ANN involves mathematical notation and concepts such as activation functions, weights, biases, and training algorithms. The specific details may vary depending on the type of neural networks, such as feedforward neural networks, recurrent neural networks, or convolutional neural networks [Bishop, 2006]. The overview of the components of an ANN is given by Bishop (2006) as the following:

Neurons: Neurons, also called units or nodes, are the basic building blocks of the network. They receive input signals, perform computations, and produce output signals.

Layers: Neurons are organized into layers, which can be input, hidden, or output layers. The input layer receives the initial data, the hidden layers process the information, and the output layer produces the final results.

Connections: Neurons are connected to each other via connections, which have associated weights. These weights determine the strength of the connection between neurons and are adjusted during the learning process.

Activation function: Each neuron applies an activation function to the weighted sum of its inputs. The activation function introduces non-linearity and allows the network to learn complex relationships in the data.

Training: The neural network is trained using a process called backpropagation. This involves presenting training examples to the network, comparing the network's output with the desired output, and updating the weights to minimize the difference between the two.

These are just the essential elements of ANNs. More advanced concepts include different types of layers (e.g., convolutional layers for image processing), regularization techniques, optimization algorithms, and architectures tailored for specific tasks [Bishop, 2006].

The layers, as mentioned earlier, are schematically shown in Figure 5.12. The sample system in Figure 5.12 is a 4-input, 2-output, 1-hidden layer, and 6-neuron system. All the input parameters have certain weights on the process of neurons for training

and testing. These weights depend on the algorithms used in the ANN system. There may be more than 1-hidden layer.

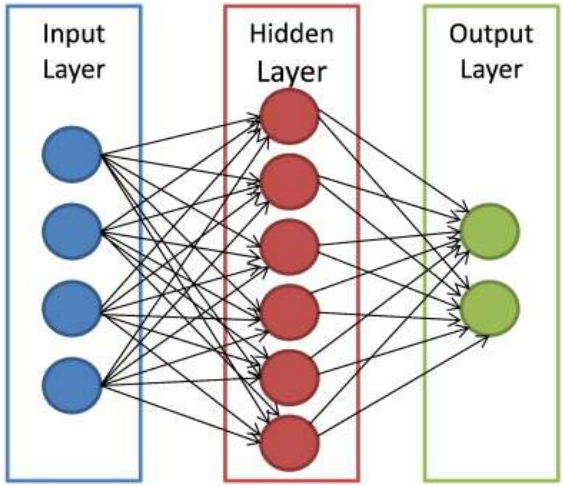

Figure 5.12 ANN layers

Having a data set with sufficient data points for approximation problems with several parameters or verifying a desired input/output system, ANN is a helpful tool to approximate a result and/or verify the system. The ANN works with the following steps.

- A major percentage of the data points, 70-90% recommended, with clearly defined input and output parameters are selected for the training of the model.
- Remaining data points are used for validation. The neurons learn for the data set, generalize a network and use these test data points to compare the outputs. The iteration continues until all the outputs are in the specified error range.
- For desired outputs with known input parameters, the results are calculated with the generated network.

5.4 Problems about Generalization using ANN

When the limited number of experimental studies in the literature about the heat transfer coefficient of nanorefrigerants with the two-phase flow of the refrigerant is investigated, there are problematic issues regarding the use of ANN analyses to verify the model. The reasons for these problems are:

- The deviations of the results: For different studies, the enhancement of the heat transfer and the increase in heat transfer coefficient varies from 1% to more than 100%. The potential reason for these variations is either the different flow conditions or different ways to calculate heat transfer coefficient or experimental errors, or any combination of these. In any case, it is difficult to generalize the model and not meant to cover the studies with such deviations.

- The limited number of data points for some of the studies: For the majority of the studies in the literature, there are limited and insufficient numbers of data points for covering the n-dimensional space with the input parameters to train the ANN model.

- Unspecified flow conditions and/or geometrical parameters: Most of the experimental studies do not present the study's flow conditions and geometrical parameters, such as heat flux, quality, mass flux, or wall, inlet, and exit temperatures.

- Different refrigerants and nanoparticles: Since the physics of the nanorefrigerant flow has yet to be discovered well, the effects of the different refrigerants and nanoparticles are not apparent, either. The thermal and flow interactions of the nanoparticles and refrigerants may depend on various parameters such as density, heat capacity, molecular weight,

chemical/radiative activity of the particles, and chemical/physical forces among refrigerant molecules and between the refrigerant and the nanoparticles.

- Overall cycle analysis instead of two-phase heat transfer regions: Some experimental studies focus on the overall heat transfer enhancement of the nanoparticle presence in the VCRC. The change in evaporator and condenser heat transfer rates is not examined.

5.5 Verification of the Model using ANN with a Reference Study

With the known generalization problems of ANN, the verification of the new approach is decided to be performed by selecting a reference study and using the limits of this study as boundary conditions for the n-dimensional (number of parameters) space to be created. These parameters are used to form the input layers of Figure 5.12. The limits of the ANN model are the extreme values of the input parameters because of the lack of extrapolation property of ANN.

The study for verifying the model is selected as the experimental work by Sun and Yang (2014). This research is about heat transfer characteristics in flow boiling of R141b nano-refrigerants in a horizontal tube. Many researchers studied with R141 b-based nano-refrigerants refrigerant in the literature as mentioned in Chapter 1 [Zhang et al., 2020], [Mahbubul et al., 2014], [Zhang et al., 2022], [Mahbubul et al., 2013-2], [Kumar et al., 2022]. Moreover, Refex Industries (2023) mentioned that R141b replaced R11 because of its environmental advantages, which are used in refrigeration and cleaning systems.

There are 12 figures presented in the study [Sun and Yang, 2014] about heat transfer coefficient results with respect to quality for different nanoparticles and mass flux values. The variable parameters in the selected work are three mass fraction values

(0.10%, 0.20%, 0.30%), four nanoparticles (Cu, Al, Al_2O_3, CuO), three mass flux values (120, 210, 330 kg/m2s), and six quality values (0.3, 0.4, 0.5, 0.6, 0.7, 0.8). All experiments are also performed for the pure refrigerant. Therefore; for the pure refrigerant, with three mass flux and six quality values, there are 18 data points; for nanorefrigerants, with four nanoparticles, three mass flux, three mass fraction, and six quality values, there are 216 data points. There are 234 data points. For example, the data are presented in Figure 5.13 for Cu nanoparticles with 120 kg/m^{2}s.

Since the output of the study is the heat transfer coefficient, it will be used as the output layer of Figure 5.6. The data from Figure 5.13 and the remaining 11 figures from the study [Sun and Yang, 2014] are captured by the "Get Data" software. The flow conditions, heat transfer coefficient, quality values, and nanoparticle mass fraction are gathered. These data points are presented in Appendix, Table B.1.

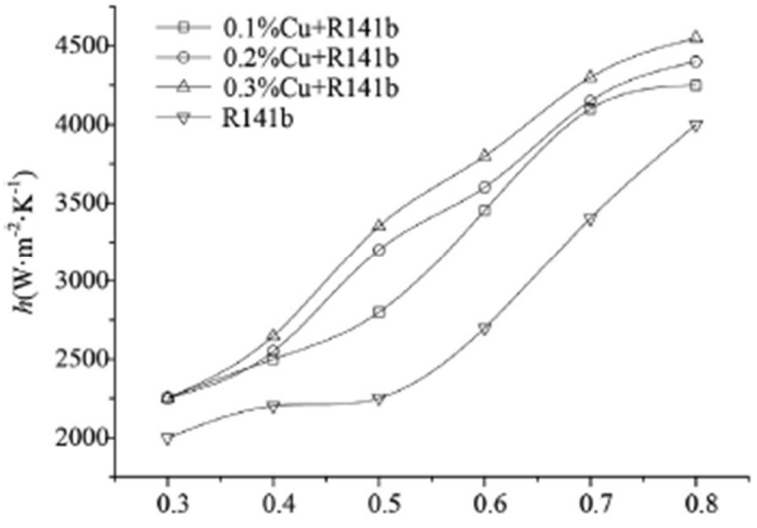

Figure 5.13 Heat transfer coefficients of Cu-R141b nanorefrigerant for G = 120 kg/m^{2}s [Sun and Yang, 2014]

For ANN analyses, 164 data points (70%) are selected for training, 35 data points (15%) are selected for testing, and 35 data points (15%) are selected for verification.

The data points used for training, testing, and verification are given in detail in Tables 5.3-5.6.

Table 5.3 Data point details used in ANN (Overall)

Overall	φ_m	Pure	Cu	Al	Al_2O_3	CuO	Total
G=120 kg/m^{2}s	0.00%	6	0	0	0	0	6
	0.10%	0	6	6	6	6	24
	0.20%	0	6	6	6	6	24
	0.30%	0	6	6	6	6	24
G=210 kg/m^{2}s	0.00%	6	0	0	0	0	6
	0.10%	0	6	6	6	6	24
	0.20%	0	6	6	6	6	24
	0.30%	0	6	6	6	6	24
G=330 kg/m^{2}s	0.00%	6	0	0	0	0	6
	0.10%	0	6	6	6	6	24
	0.20%	0	6	6	6	6	24
	0.30%	0	6	6	6	6	24
	TOTAL	18	54	54	54	54	234

Table 5.4 Data point details used in ANN (Training)

Training	φ_m	Pure	Cu	Al	Al_2O_3	CuO	Total
G=120 kg/m^{2}s	0.00%	4	0	0	0	0	4
	0.10%	0	4	4	5	4	17
	0.20%	0	4	4	4	4	16
	0.30%	0	4	4	5	4	17
G=210 kg/m^{2}s	0.00%	4	0	0	0	0	4
	0.10%	0	4	4	4	5	17
	0.20%	0	4	5	4	5	18
	0.30%	0	4	5	4	4	17
G=330 kg/m^{2}s	0.00%	4	0	0	0	0	4
	0.10%	0	5	4	4	4	17
	0.20%	0	4	4	4	4	16
	0.30%	0	5	4	4	4	17
	TOTAL	12	38	38	38	38	164

Table 5.5 Data point details used in ANN (Test)

Test	φ_m	Pure	Cu	Al	Al_2O_3	CuO	Total
G=120 kg/m^{2}s	0.00%	1	0	0	0	0	1
	0.10%	0	1	1	1	1	4
	0.20%	0	1	1	1	1	4
	0.30%	0	1	1	0	1	3
G=210 kg/m^{2}s	0.00%	1	0	0	0	0	1
	0.10%	0	1	1	1	0	3
	0.20%	0	1	1	1	1	4
	0.30%	0	1	0	1	1	3
G=330 kg/m^{2}s	0.00%	1	0	0	0	0	1
	0.10%	0	1	1	1	1	4
	0.20%	0	1	1	1	1	4
	0.30%	0	0	1	1	1	3
	TOTAL	3	8	8	8	8	35

Table 5.6 Data point details used in ANN (Verification)

Verification	φ_m	Pure	Cu	Al	Al_2O_3	CuO	Total
G=120 kg/m^{2}s	0.00%	1	0	0	0	0	1
	0.10%	0	1	1	0	1	3
	0.20%	0	1	1	1	1	4
	0.30%	0	1	1	1	1	4
G=210 kg/m^{2}s	0.00%	1	0	0	0	0	1
	0.10%	0	1	1	1	1	4
	0.20%	0	1	0	1	0	2
	0.30%	0	1	1	1	1	4
G=330 kg/m^{2}s	0.00%	1	0	0	0	0	1
	0.10%	0	0	1	1	1	3
	0.20%	0	1	1	1	1	4
	0.30%	0	1	1	1	1	4
	TOTAL	3	8	8	8	8	35

For ANN analyses, JustNN software is used. The input parameters are selected according to the reference paper. Since the same refrigerant with the same saturation

temperature is used for all experiments, the parameters covering the pure refrigerant type and conditions, such as refrigerant molecular weight, saturation pressure/temperature, and refrigerant Prandtl number, are not used. The parameters selected as input are presented in Table 5.7. The thermophysical properties of the nanorefrigerant for all 234 data points were calculated using the new model introduced at the beginning of Chapter 5.

For R141b, the constants to be used in the property calculation of Cu-R141b, Al-R141b, Al_2O_3-R141b, and CuO-R141b nanorefrigerants are determined. These constants are calculated according to Equations (67), and (68) using pure R141b two-phase properties and are used in nanorefrigerant property calculations by implementing them into Equations (70) and (71).

As it is presented for specific volume, the change in two-phase region with quality is linear, therefore the constants are "0". The constants for conductivity, and viscosity of R141b are presented in Table 5.8. For R141b, the conductivity is also linear, therefore the constants are "0" as in specific volume.

Table 5.7 Input Parameters used in ANN

Parameter		Unit
M_{np}	molecular weight of nanoparticle	kg/kmol
ρ_p	density of nanoparticle	kg/m^3
c_p	heat capacity of nanoparticle	kJ/kgK
k_p	conductivity of nanoparticle	W/mK
G	mass flux	kg/m^{2}s
x	quality	-
φ_m	mass fraction	-
ρ_{nr}	density of nanorefrigerant	kg/m^3
k_{nr}	conductivity of nanorefrigerant	W/mK
μ_{nr}	viscosity of nanorefrigerant	Pa.s

Nanofluid density, conductivity, and viscosity are determined using the mixture, Maxwell Garnett, and Batchelor models, respectively. The specific volume is determined for density, and the reciprocal is taken in the analysis. For all 234 data points, these three thermophysical properties are determined and used as input to ANN analyses. The input and output parameters for all data points are in the Appendix C in Table C.1.

Table 5.8 Constants for R141b

x	k	k_{linear}	Δk	μ	μ_{linear}	$\Delta\mu$
	[W/mK]			[Pa.s]		
0	0.089	0.089	0	3.772E-04	3.772E-04	0.00
0.1	0.081	0.081	0	7.682E-05	3.404E-04	-2.636E-04
0.2	0.073	0.073	0	4.276E-05	3.036E-04	-2.609E-04
0.3	0.065	0.065	0	2.963E-05	2.695E-04	-2.372E-04
0.4	0.057	0.057	0	2.267E-05	2.301E-04	-2.074E-04
0.5	0.05	0.05	0	1.836E-05	1.933E-04	-1.749E-04
0.6	0.042	0.042	0	1.542E-05	1.565E-04	-1.411E-04
0.7	0.034	0.034	0	1.330E-05	1.197E-04	-1.064E-04
0.8	0.026	0.026	0	1.169E-05	8.296E-05	-7.128E-05
0.9	0.018	0.018	0	1.042E-05	4.618E-05	-3.576E-05
1	0.01	0.01	0	9.407E-06	9.407E-06	0.00

The analyses are performed for different numbers of hidden layers and convergence criteria. One, two, and three hidden layers are studied, and 1-10% (with 1% increments) errors of verification data points are done; as a result, 30 analyses are examined. Figures 5.14, 5.15, and 5.16 give one example for each hidden layer configuration. The overall analysis report is presented in Figure 5.17 and Table 5.7.

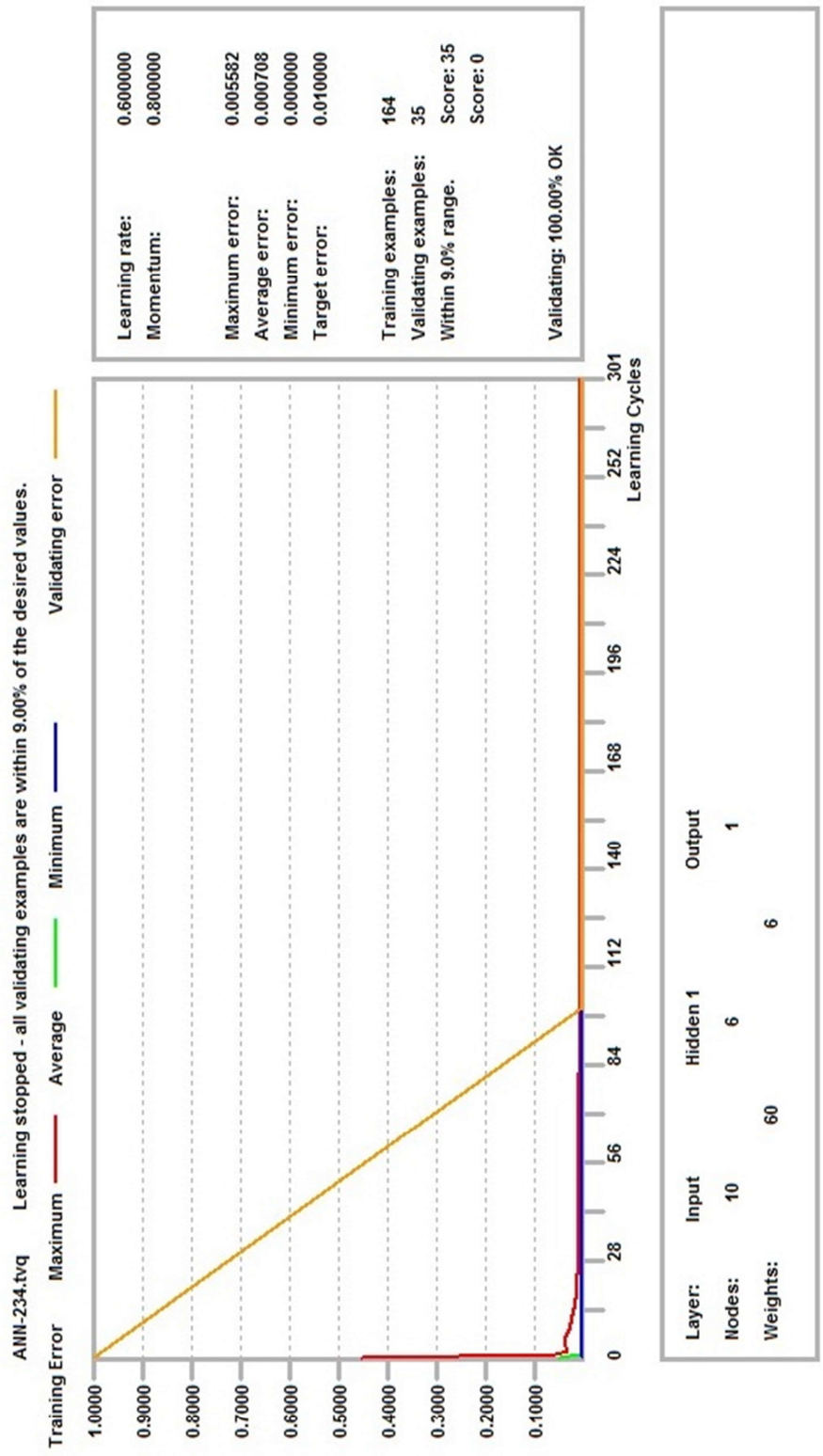

Figure 5.14 Error graph for ANN analysis of 1 hidden layer, Convergence criteria for error: 9%

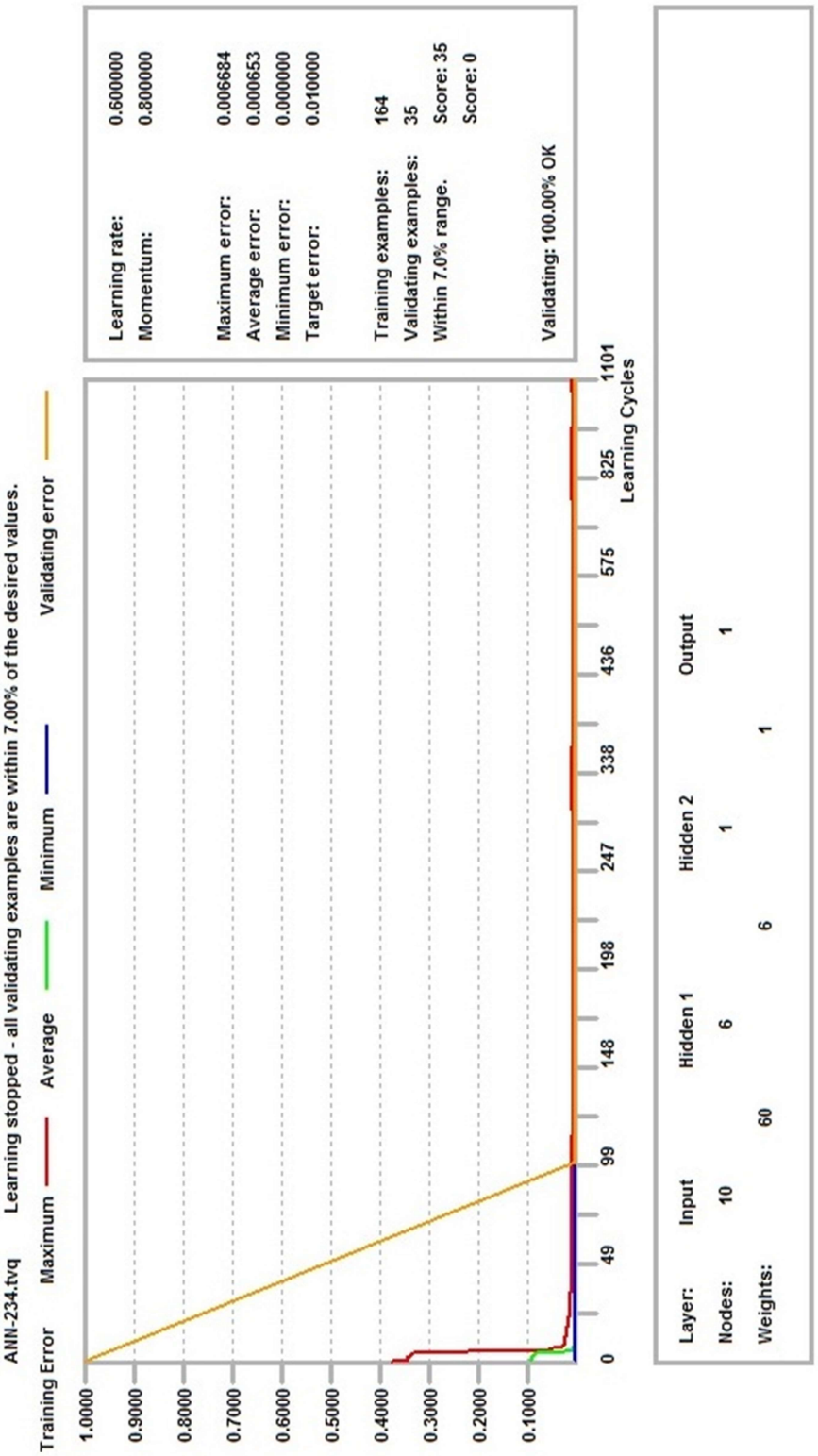

Figure 5.15 Error graph for ANN analysis of 2 hidden layers, Convergence criteria for error: 7%

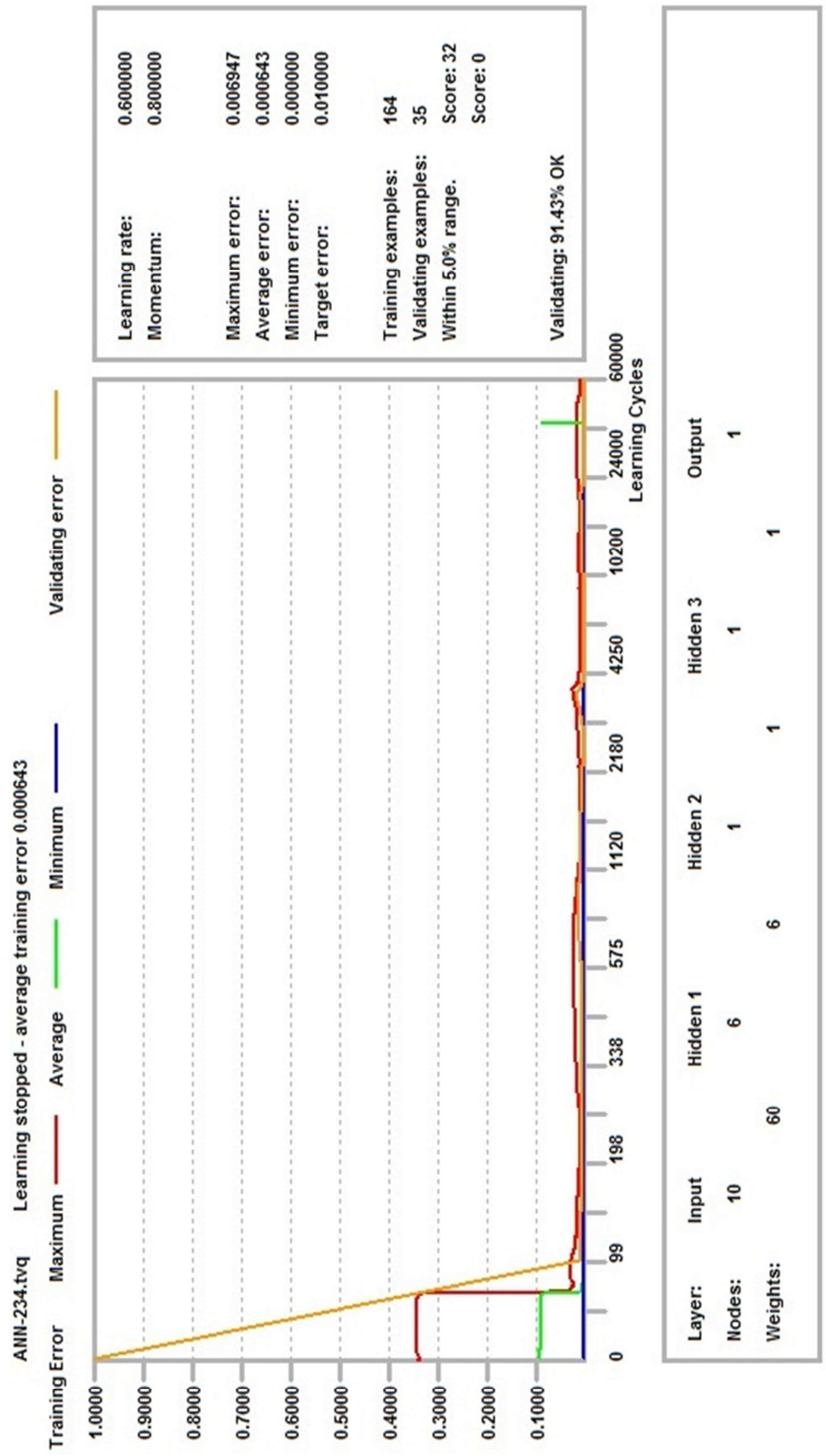

Figure 5.16 Error graph for ANN analysis of 3 hidden layers, Convergence criteria for error: 5%

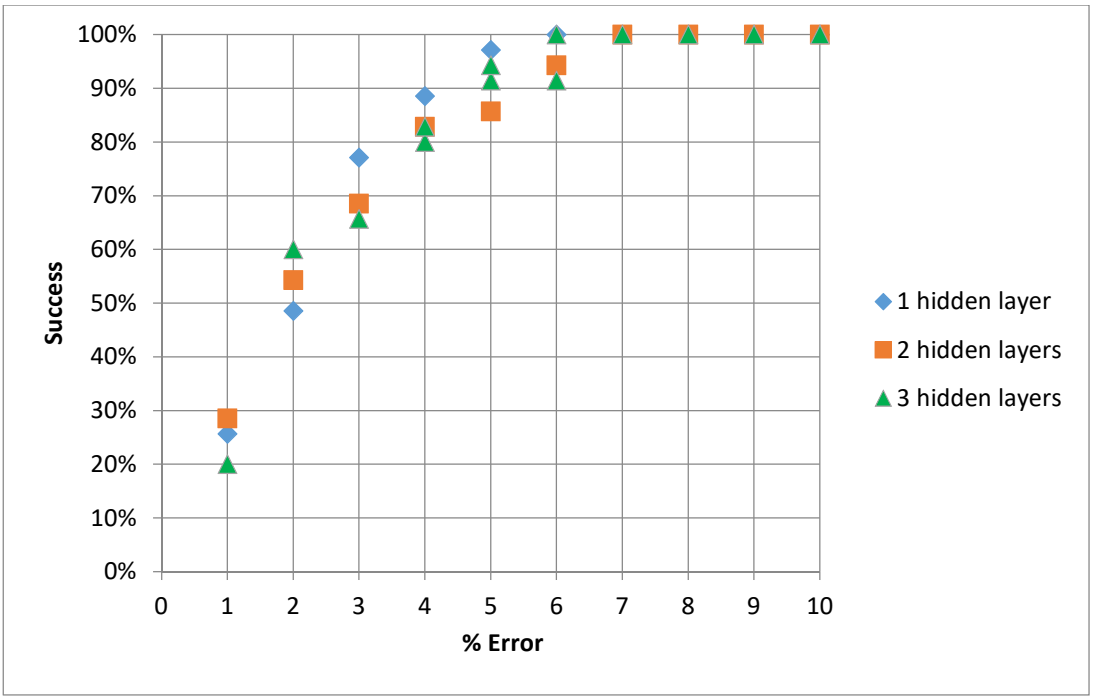

Figure 5.17 Success vs % Error graph for ANN analyses

As seen in Figure 5.17 and the yellow rows of Table 5.9, in some analyses, not all 35 verification data points are verified with ANN. The software is capable of 2,000,000 iterations, and when the convergence criterion for the % error value is low, some validation data points were not within the limits. For one hidden layer configuration, when the convergence is desired as 6% and more, all data points are found by ANN analyses with 100% success. For two hidden layers, 7% and more; for three hidden layers, same as one hidden layer, 6% and more, all data points are calculated. When the convergence % error is decreased, convergence success also decreases. This is because of the computation cycle limit. On the other hand, for a field of study with various controversial experimental results, a 6-7% error of analyses with 100% success for a vast data set used seems a satisfactory way to validate the theory. In addition, the analyses seem independent of the number of hidden layers, as presented in Figure 5.17.

Table 5.9 Overall ANN analyses data

				Hidden node weights			
Hidden	Error %	Verified	Success	1	2	3	Total Weights
1	1	9	25.71%	6	0	0	66
1	2	17	48.57%	6	0	0	66
1	3	27	77.14%	6	0	0	66
1	4	31	88.57%	6	0	0	66
1	5	34	97.14%	6	0	0	66
1	6	35	100.00%	6	0	0	66
1	7	35	100.00%	6	0	0	66
1	8	35	100.00%	6	0	0	66
1	9	35	100.00%	6	0	0	66
1	10	35	100.00%	6	0	0	66
2	1	10	28.57%	6	1	0	67
2	2	19	54.29%	6	1	0	67
2	3	24	68.57%	6	1	0	67
2	4	29	82.86%	6	1	0	67
2	5	30	85.71%	6	1	0	67
2	6	33	94.29%	6	1	0	67
2	7	35	100.00%	6	1	0	67
2	8	35	100.00%	6	1	0	67
2	9	35	100.00%	6	1	0	67
2	10	35	100.00%	6	1	0	67
3	1	7	20.00%	6	1	1	68
3	2	21	60.00%	6	1	1	68
3	3	23	65.71%	6	1	1	68
3	4	28	80.00%	6	1	1	68
3	4	29	82.86%	4	1	8	60
3	5	32	91.43%	6	1	1	68
3	5	33	94.29%	4	1	8	60
3	6	32	91.43%	6	1	1	68
3	6	35	100.00%	4	1	8	60
3	7	35	100.00%	6	1	1	68
3	8	35	100.00%	4	1	4	52
3	9	35	100.00%	6	1	1	68
3	10	35	100.00%	6	1	1	68

In 30 different analyses performed with ANN, it is aimed to verify the theory suggested as a thermophysical property determination model for two-phase nanorefrigerants. All validation data points converged within 6-7% error convergence criteria in three different hidden layer configurations. For a 1% error over 20%, for 2% error over 50%, for 3% error over 65%, for 4% error over 80%, and 5% error over 85%, success is observed. As mentioned in the previous sections, in the literature on two-phase nanorefrigerant flow studies, many controversial results are presented. Therefore 6 to 7% error is considered a satisfactory result to verify the current new model. A 6.5% error is accepted for the model.

5.6 Uncertainty of the New Approach

The error found in the previous section can be considered as the uncertainty of the ANN model for the heat transfer coefficient, which is ±6.5%. Moreover, there is an uncertainty analysis of the reference study [Sun and Yang, 2014]. The authors calculated the uncertainty of the heat transfer coefficient measurements with the uncertainty parameters of the equipment used in the experiments. It is reported as ±7.08% [Sun and Yang, 2014]. Since the ANN model has a ±6.5% error, the total uncertainty of the heat transfer coefficient is the summation of these two values to cover the uncertainty in extreme cases, which is ±13.58%.

CHAPTER 6

CASE STUDY: REMODELLING THE CYCLE WITH THE NEW APPROACH

To calculate the nanorefrigerant effect on the heat transfer performance, the ideal cycle modeled in Chapter 4 is remodeled here. The ANN model introduced in Chapter 5 to verify the new model proposed for determining thermophysical properties is used to calculate the heat transfer coefficient.

Since R141b was the refrigerant in the reference paper [Sun and Yang, 2014] used in ANN verification, the refrigerant used in the modeled ideal cycle must be changed to R141b. The reference study is performed at 1 atm (101.325 kPa) saturation pressure of R141b; the saturation temperature is 32.07ºC. Therefore the evaporator saturation temperature is 32.07ºC for the ANN model formed in Chapter 5 to be used in the heat transfer coefficient calculations of the evaporator. Pure refrigerant properties are gathered from Etermo (2009). Since the saturation temperature of the evaporator should be lower than the low-temperature reservoir temperature, the low-temperature reservoir is selected as 55ºC. The high-temperature reservoir is selected as 70ºC because the low and high-temperature reservoir temperature difference for the ideal R134a cycle formed in Chapter 4 was 4ºC and 20ºC, respectively. The temperature difference is aimed to be similar to the ideal R141b cycle. The condenser saturation temperature should be higher than the high-temperature reservoir temperature. Therefore, it is selected as 80ºC. The corresponding saturation pressure is 421.20 kPa.

The thermodynamic parameters for modeling the ideal R141b VCRC, which are used to determine the mass flow rate, the states, and the sizing of the evaporator and condenser, are presented in Table 6.1. The saturation pressure for the evaporator is

selected to maintain saturation pressure below 4ºC. The cooling rate, and power input, are determined to be in the range of a VCRC and COP to be 2, as in the first modeled cycle.

Table 6.1 Input thermodynamic parameters for Ideal R141b VCRC modeling

T_H	70	ºC
T_L	55	ºC
$\dot{W}$	50	W
$\dot{Q}_L$	100	W
P_1	101.325	kPa
$\dot{Q}_H$	150	W

The same procedure mentioned in Chapter 4 for modeling the evaporator and condenser is applied. Tables 6.2 and 6.3 give the final geometries of the evaporator and condenser.

Table 6.2 The geometry of the evaporator to be used in calculations

$A_{air,evap}$	1.5415	m^2
$L_{ref,evap}$	4.636	m
$d_{ref,evap}$	2	mm
$A_{ref,evap}$	0.0291	m^2

The cycle is formed with these parameters and the flow charts of the evaporator and condenser. The mass flow rate and the mass flux are evaluated as 0.605 g/s and 192.58 kg/m^2s, respectively. The mass flux should be between 120 and 330 kg/m^2s, the minimum and maximum values the ANN model covers. The states of the ideal R141b cycle are presented in Table 6.4.

Table 6.3 The geometry of the condenser to be used in calculations

$L_{ref,cond}$	7.5	m
$d_{ref,cond}$	2	mm
$A_{ref,cond}$	0.047	m^2
Width of condenser	4520	mm
Height of condenser	1400	mm
Distance between refrigerant tubes	80	mm
Wire # on each side of the tube	79	mm
$A_{air,cond}$	1.042	m^2

Table 6.4 The states of the R141b cycle

R141b	1	2	2'	3	4
P [kPa]	101.325	421.20	421.20	421.20	101.325
i [kJ/kg]	459.63	542.27	491.86	294.34	294.34
T [K]	305.22	374.70	353.15	353.15	305.22
x	1	-	1	0	0.26
s [kJ/kgK]	1.857	1.857	1.861	1.302	1.316

When modeling the ideal R141b cycle for the evaporator, the heat transfer coefficient is calculated from the ANN model formed in Chapter 5. The existing correlations are utilized for the condenser because the reference study for forming the ANN database was done only at the saturation pressure of the evaporator.

The heat transfer coefficient is calculated by the integrated sum of local heat transfer coefficients for the evaporator. For specified inlet (x_4) and exit (x_1) quality values of evaporator, the integrated sum is given as:

$$\bar{h} = \frac{1}{y_2 - y_1} \int_{y_1}^{y_2} h_y \, dy \tag{72}$$

Here $\bar{h}$ is the average heat transfer coefficient and h_y is the local heat transfer coefficient as a function of length, y.

The integral sum is converted to finite incremental summation and Eqn. (72) is written as:

$$\bar{h} = \frac{1}{y_2 - y_1} \sum_{y_1}^{y_2} h_y \, \Delta y \tag{73}$$

To calculate the local heat transfer coefficient as a function of evaporator length, it is necessary to determine the quality change along the evaporator since, with the ANN model, the heat transfer coefficient with respect to quality can be found.

The ANN model is formed for heat transfer coefficients with a quality range between 0.3 and 0.8 [Sun and Yang, 2014]. To calculate the integral sum of local heat transfer coefficient values, the heat transfer coefficient for quality 0.8-1.0 values are needed because the exit of the evaporator is always saturated vapor. Since ANN cannot extrapolate, it is performed by adding a trend line to the heat transfer coefficient values found from ANN, which are for quality values of 0.3-0.8.

After finding these values, extrapolating the h values for quality 0.8-1.0 and 0.1-0.3 is performed using a fourth-order polynomial, as shown in yellow in Figure 6.1. Second, third, fourth, and fifth-order polynomial fits are tried. Since the results found by correlations used in Chapter 4.1 converge similarly to the fourth-order polynomial fit, it is used for pure and nanorefrigerants.

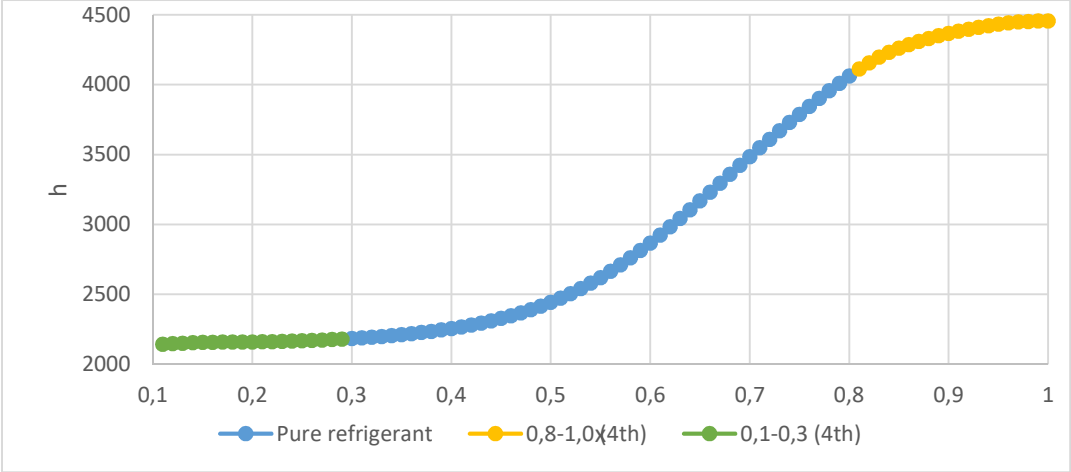

Figure 6.1 R141b heat transfer coefficient values by ANN with changing quality (polynomial fit for quality 0.8-1.0 and 0.1-0.3)

To calculate the evaporator quality values as a function of length, the following procedure is applied.

- The heat flux along evaporator flow is assumed constant, which is given as:

$$q^{"} = \frac{\dot{Q}_L}{A_{ref,evap}} = \frac{100}{0.0291} = 3433\ \frac{W}{m^2} \tag{74}$$

- For each 0.01 incremental h_x value, the corresponding wall temperature, T_w, is determined with equation (74):

$$T_{w_x} = \frac{q^{"}}{h_x} + T_{sat-evap} \tag{75}$$

  Here $T_{sat-evap}$ is the evaporator saturation temperature, which is 32.07°C.

- T_{w_x} for evaporator inlet $(x_4 = 0.26)$ and exit $(x_1 = 1.00)$ quality are calculated as 33.65°C and 32.84°C, respectively.
- Logarithmic temperature difference for refrigerant side in the evaporator is calculated with the following.

$$\Delta T_{LM,evap} = \frac{(T_{w_{x=0.26}} - T_{sat-evap}) - (T_{w_{x=1.00}} - T_{sat-evap})}{ln\frac{T_{w_{x=0.26}} - T_{sat-evap}}{T_{w_{x=1.00}} - T_{sat-evap}}} \quad (76)$$

It is calculated as 1.128°C.

- The average heat transfer coefficient is calculated by:

$$\bar{h} = \frac{q^{"}}{\Delta T_{LM,evap}} = \frac{3433}{1.128} = 3044.52 \frac{W}{m^2 K} \quad (77)$$

This value is used to validate the quality change along evaporator length.

- The evaporator refrigerant part is divided into subparts for each 0.1 quality increments: i.e., 0.3-0.4, 0.4-0.5, …, 0.9-1.0.
- The change in quality within this 0.1 increment is assumed linear along length.
- The average heat transfer coefficient for the 0.1 increment is calculated with the formula given below.

$$\bar{h}_{x_1 - x_2} = \frac{1}{x_2 - x_1} \sum_{x_1}^{x_2} h_x \, \Delta x \quad (78)$$

Since the linear assumption is made, the average heat transfer coefficient for the corresponding 0.1 increments is the finite incremental summation of the heat transfer coefficient within this region as a quality function. Δx is taken as 0.01 increments. h_x of each 0.01 quality value is determined using the ANN model.

- For pure R141b, $\bar{h}_{x_1 - x_2}$ values are calculated using equation (78) from 0.26 to 1.00 and presented in Table 6.5.

Table 6.5 Heat transfer coefficient values for 0.1 increments

$x_1 - x_2$	$\bar{h}_{x_1-x_2}$
[-]	[W/m²K]
0.26-0.30	2177.61
0.31-0.40	2218.55
0.41-0.50	2344.85
0.51-0.60	2654.11
0.61-0.70	3202.32
0.71-0.80	3811.97
0.81-0.90	4260.38
0.91-1.00	4429.78

- The length of each 0.1 increment quality portion is determined by trial and error to reach the overall heat transfer coefficient calculated from equation (76). The total length of evaporator is given in Table 6.2, which is 4.636 m, 4636 mm.

Table 6.6 The evaporator length portion for each 0.1 quality increments

$x_1 - x_2$	Δy
[-]	[mm]
0.26-0.30	383
0.31-0.40	747
0.41-0.50	717
0.51-0.60	677
0.61-0.70	627
0.71-0.80	568
0.81-0.90	498
0.91-1.00	418

- The evaporator length with respect to quality values is assumed to be the same as those for the pure refrigerant. For each nanorefrigerant case study presented in Section 6.1, equation (72) is used to calculate the heat transfer coefficient and follow this procedure. When the inlet quality value changes,

the lengths given in Table 6.6 are reformed by using pure refrigerant local heat transfer coefficient to determine the new length variation along the evaporator with respect to quality.

6.1 ANN Results for Modelled Cycles with the presence of Nanoparticles

For three different mass fractions (0.10%, 0.20%, and 0.30%) of Cu, Al, Al_2O_3, and CuO nanoparticles, the cycle is analyzed in terms of COP. The geometry, power input, mass flux, and saturation pressures of the cycle are assumed to be constant. Also, the exit of the evaporator is taken as saturated vapor as in the pure R141b cycle.

The heat transfer coefficient is altered with the presence of nanoparticles. With the increase in heat transfer coefficient, the cycle is rated in terms of evaporator heat transfer.

The procedure is done as follows:

- The heat transfer coefficient of the specified nanoparticle and mass fraction with inlet quality of (the inlet for the pure refrigerant cycle) is calculated with the ANN model, with the input parameters used as given in Table 5.5, using procedure given above and equation (73).
- With the calculated heat transfer coefficient, the heat transfer rate at the evaporator is determined by assuming the same wall temperature found by equaion (76) and the heat transfer area given in Table 6.2.
- The enthalpy of the evaporator inlet state is found by using Eqn. (24), where the exit enthalpy of the evaporator and mass flux is assumed to be the same as the pure refrigerant cycle.
- From the enthalpy, evaporator inlet quality is determined with the known saturation pressure value.

- For the evaporator quality (mean value of inlet and exit quality values), the heat transfer coefficient is calculated as in the first step by changing the inlet quality with the value found one step earlier.
- The iteration stops where the heat transfer coefficient for two consecutive analyses is the same.

For the local heat transfer coefficient of each mass fraction and nanorefrigerant calculations, Figure D.1-12 are used which are given in Appendix D.

A sample iteration is given in Table 6.7, for 0.10% mass fraction of Cu nanoparticles in Cu-R141b nanorefrigerant flow.

The inlet quality of the evaporator decreased to 0.196 from 0.26 with the presence of Cu nanoparticles. The exit state is saturated vapor, and the power input to the compressor is 50 W. The iteration is stopped when two consecutive average heat transfer coefficient values of the evaporator, $\bar{h}$, are the same. As the inlet quality decreases, the enthalpy at the inlet decreases. With the same mass flow rate and exit enthalpy (saturated vapor), the heat transfer rate increases from 100 W to 108.38 W, as given in the table.

Table 6.7 The analysis and iteration for Cu with 0.10% mass fraction

Nanorefrigerant	Cu-R141b
φ_m	0.10%
$x_{4-initial}$ [-]	0.26
$\bar{h}$ [W/m^{2}K]	3406

$\dot{Q}_L$	i_4	x_4	$\bar{h}$
[W]	[kJ/kg]	-	[W/m^{2}K]
112.21	274.16	0.17	3243.07
106.84	283.03	0.21	3311.12
109.08	279.33	0.19	3276.23
107.93	281.23	0.20	3293.45
108.50	280.29	0.195	3284.78
108.22	280.75	0.197	3288.23
108.33	280.57	0.196	3289.78
108.38	280.49	0.196	3289.78

The COP for this case and the increase in COP:

$$\eta_I = COP = \frac{\dot{Q}_L}{\dot{W}_{in}} = \frac{108.38}{50} = 2.1676 \tag{79}$$

$$\Delta COP = \frac{2.1676}{2} = 1.0838 = 8.38\% \tag{80}$$

These analyses are performed for all four nanoparticles and three mass fraction values. The results are tabulated in Table 6.8. Throughout all the analyses, the power input (50 W) and the exit of the evaporator (saturated vapor) are accepted as constant.

The analyses with nanorefrigerants with the remodeled ideal cycle show that the highest increase in COP occurs for Cu nanoparticles, up to 13.17% for 0.3% mass fraction. The second most increase is for Al, the third is for Al_2O_3, and the fourth is for CuO nanoparticles presence, which is very similar to Al_2O_3. The lowest increase is for a 0.1% mass fraction for CuO, a 4.15% increase in COP. In addition, for all four nanorefrigerants, the COP increases with increasing mass fraction values.

The evaporator sizing is performed for pure R141b, and the nanorefrigerant analyses are done for the same geometry and exit state of the evaporator, which is saturated vapor. The inlet quality for pure R141b is 0.26, and for the nanorefrigerants, it decreases to 0.16. The geometry of the evaporator needs to be checked in terms of low-quality capacity. Therefore, the analysis is redone for pure R141b for inlet quality to be lower than 0.16.

The heat transfer in evaporator side is calculated only for the refrigerant side for COP analysis. Therefore, the change in heat transfer coefficient is proportional to heat transfer and COP, and uncertainty of COP is the same as uncertainty of heat transfer coefficient, which is ±13.58%. The increase in COP turns out to be in the range of

uncertainity, the increase in COP is expected with nanoparticle presence but to increase the accuracy, the uncertainty should be decreased.

Table 6.8 The analysis and iteration for Cu with 0.10% mass fraction

Cu	$\dot{Q}_L$ [W]	x_4	COP	COP % increase
0.10%	108.38	0.196	2.168	8.38%
0.20%	111.13	0.175	2.223	11.13%
0.30%	113.17	0.160	2.263	13.17%

Al	$\dot{Q}_L$ [W]	x_4	COP	COP % increase
0.10%	106.30	0.211	2.126	6.30%
0.20%	110.03	0.183	2.201	10.03%
0.30%	112.96	0.162	2.259	12.96%

CuO	$\dot{Q}_L$ [W]	x_4	COP	COP % increase
0.10%	104.15	0.227	2.083	4.15%
0.20%	106.96	0.206	2.139	6.96%
0.30%	109.69	0.186	2.194	9.69%

Al_2O_3	$\dot{Q}_L$ [W]	x_4	COP	COP % increase
0.10%	105.15	0.220	2.103	5.15%
0.20%	107.90	0.199	2.158	7.90%
0.30%	110.46	0.180	2.209	10.46%

For the same mass flow rate, the cycle is rated again with condenser sub-cooling. The input parameters are presented in Table 6.9.

Table 6.9 Input parameters for Ideal R141b modeling with condenser sub-cooling

T_H	70	ºC
T_L	55	ºC
$\dot{W}$	50	W
$\dot{Q}_L$	120	W
P_1	101.325	kPa
$\dot{Q}_H$	170	W

The geometry for evaporator and condenser are also the same as Table 6.2 and Table 6.3. The states of the cycle are found and the inlet quality is determined as 0.11. Therefore, the cycle heat capacity is verified in terms of nanorefrigerant analysis. The states of the sub-cooled cycle is presented in Table 6.10.

Table 6.10 The states of the R141b cycle with condenser sub-cooling

R141b	1	2	2'	3	4
P [kPa]	101.325	421.20	421.20	421.20	101.325
i [kJ/kg]	459.63	542.27	491.8600	261.28	261.28
T [K]	305.22	374.70	353.15	353.15	305.22
x	1	-	1	-	0.11
s [kJ/kgK]	1.857	1.857	1.861	1.207	1.207

CHAPTER 7

DISCUSSION AND CONCLUSION

In recent decades, there has been a growing interest in utilizing nanorefrigerants to enhance heat transfer performance in various applications. Incorporating nanoparticles into working fluids has shown promising results in improving thermal conductivity and overall system efficiency. However, despite the increasing interest, there is a significant gap in the literature regarding studies on the thermophysical properties of two-phase nanorefrigerants.

While numerous investigations have focused on single-phase nanofluids, which exhibit enhanced thermal conductivity, the understanding of two-phase nanorefrigerants still needs to be improved. The complex behavior of nanorefrigerants in the vapor-liquid phase poses challenges in accurately predicting their thermophysical properties, such as heat transfer coefficients and saturation pressures. Nanorefrigerants exhibit enhanced heat transfer, but conventional heat transfer models designed for pure refrigerants are inadequate for capturing their behavior due to nanoparticle presence. Nonlinear behavior, phase change effects, enhanced heat transfer mechanisms, critical heat flux improvement, optimization, and efficiency, as well as experimental validation, underscore the importance of considering two-phase nanorefrigerant thermophysical properties to predict and optimize cooling systems accurately. Therefore, accurate nanorefrigerant two-phase conductivity and viscosity prediction may lead to a better understanding of these factors.

In the first modeled ideal cycle using R134a, the study incorporated a relatively high mass fraction (30%) of nanoparticles, specifically CuO. The existing correlations, which were derived for the single-phase flow of base fluid, for thermal conductivity

and viscosity, commonly used in the literature, were applied to estimate the thermophysical properties of the nanorefrigerant. However, the obtained results were incompatible with the findings reported in the existing literature. This discrepancy highlighted the limitations of the current approach and emphasized the need for a new methodology to accurately determine the thermophysical properties of nanorefrigerants with high nanoparticle concentrations. The observed inconsistencies underscored the complexity and unique behavior of nanorefrigerants in the two-phase region, necessitating an innovative approach for property determination to advance the understanding and optimization of nanorefrigerant systems.

The lack of comprehensive studies addressing the two-phase properties of nanorefrigerants motivated the current research. The objective was to develop a new approach to analyze the impact of nanorefrigerants on heat transfer performance in a refrigeration cycle, explicitly focusing on the evaporator. By investigating the behavior of nanorefrigerants in the two-phase region, a better understanding of their heat transfer characteristics could be achieved.

The new approach presented in this study aimed to investigate the thermophysical properties of nanorefrigerant. The approach drew inspiration from the analogy between nanorefrigerant flow and fluidized beds, where the dispersed nanoparticles behave similarly to fluidized particles. By considering the characteristics of fluidized beds, such as particle-to-particle and particle-to-fluid interactions (the interaction between nanoparticles and the gas phase of refrigerant is neglected as an analogy to the fluidized beds, a novel framework was developed for estimating the thermophysical properties of nanorefrigerants in the two-phase region.

However, it is essential to note the assumptions made in this approach. Firstly, it assumes that the nanoparticles are uniformly dispersed in the base refrigerant and that nanoparticles are not agglomerated or settling during flow. This assumption is

crucial for maintaining a stable dispersion and accurate property calculations. Additionally, the approach assumes that the interactions between the nanoparticles and the base refrigerant are independent of the nanoparticle concentration.

Furthermore, the proposed methodology introduces the concept of a "singular point," which represents a specific condition in the nanorefrigerant flow where the quality is one, which means the saturated vapor phase. The new approach does not cover the thermophysical property values at this specific point.

By incorporating these considerations, the new approach offers a promising avenue for accurately predicting the thermophysical properties of nanorefrigerants in the two-phase region, accounting for the unique behavior and interactions of nanoparticles.

The validation of the approach is done with the ANN tool. To accomplish this, the ideal cycle from a previous study was remodeled with R141b, the refrigerant used in the reference paper. One of the critical aspects of this approach was the utilization of ANN to determine the thermophysical properties required for the cycle analysis.

The ANN model is constructed using data from experimental studies that employed R141b as the refrigerant. The validation process involved comparing the ANN-predicted values with the reference data, ensuring that the model accurately captured the thermophysical properties of the refrigerant. It is important to note that the ANN model was trained explicitly for quality values between 0.3 and 0.8, limiting its extrapolation capability.

In the remodeled ideal cycle, the heat transfer coefficient for the evaporator was calculated using the ANN model. Existing correlations were employed for the condenser since the reference study used for ANN verification focused solely on the evaporator's saturation pressure. The heat transfer coefficient was determined

through an integrated sum of local heat transfer coefficients obtained by incrementally changing the inlet quality.

The analysis results demonstrated that the presence of nanoparticles in nanorefrigerants led to an increase in the heat transfer coefficient, subsequently affecting the cycle's COP. The COP values were calculated for different mass fractions of Cu, Al, Al_2O_3, and CuO nanoparticles. The highest increase in COP was observed for Cu nanoparticles, with a maximum enhancement of up to 13.17% for a 0.3% mass fraction. Al, Al_2O_3, and CuO nanoparticles also exhibited significant COP improvements.

Acknowledging that these analyses focused solely on the heat transfer coefficient, assuming constant power input is essential. Changes in pumping power and other factors were not considered. Nonetheless, the results indicate the potential benefits of utilizing nanorefrigerants in terms of improved COP and heat transfer performance.

In summary, the new approach incorporating nanorefrigerants and the ANN verification showcased the impact of nanoparticles on heat transfer and COP in the refrigeration cycle. The use of the ANN model provided an efficient means to determine the thermophysical properties required for the analysis. The results demonstrated notable enhancements in COP with the presence of different nanoparticles, emphasizing the potential of nanorefrigerants in enhancing heat transfer performance.

In terms of future work, several avenues can be explored to enhance the understanding and application of the proposed approach for thermophysical property determination of nanorefrigerants. One important direction is to conduct experimental studies to validate and refine the model. Experimental measurements of thermophysical properties, such as conductivity and viscosity, can provide

valuable data for comparison and calibration. These experiments can be performed under different operating conditions, including varying nanoparticle concentrations, temperatures, and pressures, to capture a wide range of nanorefrigerant behaviors.

Additionally, experimental investigations focused on heat transfer coefficient measurements in nanorefrigerant flows can further validate and improve the proposed approach's accuracy. The approach has 6.5% error in the present study; with more experimental results, ANN can be trained more to decrease the error. The model's performance can be evaluated by comparing the predicted heat transfer coefficients with experimental results, and adjustments or modifications can be made to enhance its predictive capabilities.

Moreover, to expand the applicability and reliability of the approach, incorporating more experimental data from the literature can significantly enhance the database for the validation of the ANN model. By incorporating a more comprehensive range of experimental conditions and nanorefrigerant compositions, the ANN model can be trained to capture a greater diversity of behaviors and provide more accurate predictions. The increase in accuracy would decrease uncertainty of the results, as well. In addition, these experiments should be made with more accurate measurements to decrease uncertainty. This can be achieved by collecting and integrating data from various experimental studies investigating nanorefrigerant properties and heat transfer performance.

By analyzing the trends and patterns observed in the expanded database, additional summation or multiplication constants can be introduced to account for different conditions or factors that may influence the thermophysical properties. These modifications can help improve the model's predictive accuracy and enhance its versatility in capturing the complexities of nanorefrigerant behavior.

On the other hand, the approach is based on the linear variation of the properties along the flow with quality change, and the deviation from linear variation is compensated by introducing a constant for incremental quality values. This can be altered by changing the linear approach by adding constants for nonlinear properties to polynomial, logarithmic, or power functions for the change of the specific property with respect to quality.

In conclusion, future research endeavors should focus on conducting experimental studies to validate and refine the proposed approach. These experiments can include measurements of thermophysical properties and heat transfer coefficients under various operating conditions. Additionally, integrating more experimental data from the literature into the ANN model can improve its performance and broaden its applicability. By combining experimental insights with the proposed approach, significant advancements can be made in understanding and utilizing nanorefrigerants for enhanced overall cycle performance.

REFERENCES

Abdel-Hadi, E.A., Taher, S.H., Torki, A.H.M., Hamad, S.S., 2011. Heat Transfer Analysis of Vapor Compression System Using Nano CuO-R134a, Int. Conf. on Advanced Materials Engineering, 15. 80-84.

Abed, H., Ali Fazilati, M., Toghraie, D., Pirmoradian, M., and Mehmandoust, B., 2022. Molecular dynamics study of the thermal behavior of ammonia refrigerant in the presence of copper nanoparticles at different volume ratios and initial temperatures. Journal of Molecular Modeling, 28(6), 157.

Agyenim, F., Eames, P., and Smyth, M., 2010. A review of materials, heat transfer and phase change problem formulation for latent heat thermal energy storage systems (LHTESS). Renewable and Sustainable Energy Reviews, 14(2), 615-628.

Alawi, O. A., Sidik, N. A. C., and Kherbeet, A. Sh., 2015. Measurements and correlations of frictional pressure drop of TiO_2/R123 flow boiling inside a horizontal smooth tube. International Communications in Heat and Mass Transfer, 61, 42-48.

Alawi, O. A., and Sidik, N. A. C., 2014. Influence of particle concentration and temperature on the thermophysical properties of CuO/R134a nanorefrigerant. International Communications in Heat and Mass Transfer, 58, 79–84.

Ali, N., Bahman, A. M., Aljuwayhel, N. F., Ebrahim, S. A., Mukherjee, S., and Alsayegh, A., 2021. Carbon-based nanofluids and their advances towards heat transfer applications—a review. Nanomaterials, 11(6), 1628.

ASTM International., 2016. ASTM E2585-16: Standard Test Method for Thermal Diffusivity by the Flash Method. West Conshohocken, PA: ASTM International.

ASTM International., 2018. ASTM D7896-18: Standard Test Method for Thermal Conductivity, Thermal Diffusivity, and Volumetric Heat Capacity of Engine Coolants and Related Fluids by Transient Hot Wire Liquid Thermal Conductivity Method. West Conshohocken, PA: ASTM International.

Awais, M., Ullah, N., Ahmad, J., Sikandar, F., Ehsan, M. M., Salehin, S., and Bhuiyan, A. A., 2021. Heat transfer and pressure drop performance of Nanofluid: A state-of-the-art review. International Journal of Thermofluids, 9, 100065.

Azmi, W. H., Sharif, M. Z., Yusof, T. M., Mamat, R., and Redhwan, A. A. M., 2017. Potential of nanorefrigerant and nanolubricant on energy saving in refrigeration system–A review. Renewable and Sustainable Energy Reviews, 69, 415-428.

Bartelt, K., Park, Y., Liu, L., Jacobi, A., 2008. Flow-Boiling of R-134a/POE/CuO Nanofluids in a Horizontal Tube, Int. Ref. and Air Conditioning Conference, paper 928.

Batchelor, G., 1977. The effect of Brownian motion on the bulk stress in a suspension of spherical particles, J. Fluid Mech., 83. 97–117.

Benam, B. P., Sadaghiani, A. K., Yağcı, V., Parlak, M., Sefiane, K., and Koşar, A., 2021. Review on high heat flux flow boiling of refrigerants and water for electronics cooling. International Journal of Heat and Mass Transfer, 180, 121787.

Bhat, M.W., Vyas, G., Jaffri, A.J., Dondapati, R.S., 2018. Investigation on the thermophysical properties of Al_2O_3, Cu and SiC based Nanorefrigerants. ICCMMEMS 2018, 27820–27827.

Bi, S., Guo, K., Liu, Z., Wu, J., 2011. Performance of a domestic refrigerator using TiO_2-R600a nanorefrigerant as working fluid, Energy Conversion and Management, 52. 733-737.

Bi, S., Shi, L., Zhang, L., 2008. Application of nanoparticles in domestic refrigerators, Applied Thermal Engineering, 28. 1834-1843.

Bishop, C. M. , 2006. Pattern Recognition and Machine Learning. Chapter 5: Neural Networks. Springer.

Bilen, K., Dağidir, K., Arcaklioğlu, E., 2022. The effect of nanorefrigerants on performance of the vapor compression refrigeration system: A comprehensive review. Energy Sources, Part A: Recovery, Utilization, and Environmental Effects, 44(2), 3178-3204. DOI: 10.1080/15567036.2022.2062071.

Björk, E., Palm, B., 2006. Performance of a domestic refrigerator under influence of varied expansion device capacity, refrigerant charge and ambient temperature, Int. Journal of Refrigeration, 29. 789-798.

Bobbo, S., Fedele, L., Fabrizio, M., Barison, S., Battiston, S., 2010. Influence of nanoparticles dispersion in POE oils on lubricity and R134a solubility. Int. J. Refrigeration 33, 1180-1186.

Brinkman, H.C., The viscosity of concentrated suspensions and solutions, J.Chem.Phys., 1952, 20, pp. 571.

Bruggeman, D.A.G., 1935. Berechnung verschiedener physikalischer konstanten vonheterogenen substanzen, I. Dielektrizitatskonstanten und leitfahigkeiten dermischkorper aus isotropen substanzen, Ann. Phys., Leipzig, 24. 636–679.

Buongiorno, J., 2006. Convective transport in nanofluids. Journal of Heat Transfer, 128(3), 240-250.

Cheng, L., Mewes, D., Luke, A., 2007. Boiling phenomena with surfactants and polymeric additives: a state-of-the-art review. Int. J. Heat Mass. Transfer 50, 2744-2771.

Cheng, L., 2009. Nanofluid heat transfer technologies. Recent Patents on Engineering, 3(1), 1-7.

Cheng, L. and Liu, L., 2013. Boiling and two-phase flow phenomena of refrigerant-based nanofluids: fundamentals, applications and challenges. International journal of refrigeration, 36(2), 421-446.

Choi, S.U.S., and Eastman, J.A., 1995. Enhancing thermal conductivity of fluids with nanoparticles. In Developments and Applications of Non-Newtonian Flows, pp. 99-105. ASME.

Chon, C. H., Kihm, K. D., Lee, S. P., and Choi, S. U., 2005. Empirical correlation finding the role of temperature and particle size for nanofluid (Al_2O_3) thermal conductivity enhancement. Applied Physics Letters, 87(15), 153107.

Cremaschi, L., 2012, November. A fundamental view of the flow boiling heat transfer characteristics of nano-refrigerants. In ASME International Mechanical Engineering Congress and Exposition (Vol. 45233, pp. 2779-2792). American Society of Mechanical Engineers.

Çengel, Y. A., and Boles, M. A. 2006. Thermodynamics An Engineering Approach, 5th Edition, McGraw-Hill, Boston.

Das, S. K., Putra, N., Thiesen, P., and Roetzel, W., 2003. Temperature dependence of thermal conductivity enhancement for nanofluids. Journal of Heat Transfer, 125(4), 567-574.

Dhindsa, G.S., Kundan, L., Singh, K., 2013. Experimental Investigation of Various Parameters on Thermal Conductivity of Al_2O_3 Based Nanorefrigerant, Int. J. Engineering Res. and Tech., 2. 3408-3417.

Duangthongsuk, W., and Wongwises, S., 2009. Heat transfer enhancement and pressure drop characteristics of TiO_2—water nanofluid in a double-tube counter flow heat exchanger. International Journal of Heat and Mass Transfer, 52(7-8), 2059-2067.

Duangthongsuk, W., and Wongwises, S., 2009-II. Measurement of temperature-dependent thermal conductivity and viscosity of TiO_2–R141b nanorefrigerants. Experimental Thermal and Fluid Science, 33(4), 706-714.

Einstein, A., 1906. Eine neue bestimmung der molekuldimensionen, Ann. Phys., 19. 289–306.

Ethermo, 2009. Thermodynamics & Transport Properties. Retrieved June 30, 2023, from http://www.ethermo.us/ShowDetail48.htm

Ewim, D.R.E., Shote, A.S., Onyiriuka, E.J., Adio, S.A., Bhattacharyya, S., Kaood, A., 2021. "Thermal Performance of Nano Refrigerants: A Short Review." Journal of Mechanical Engineering Research and Developments, 44(9), 89-115.

Fadhilah, S. A., Marhamah, R. S., and Izzat, A. H. M., 2014. Copper oxide nanoparticles for advanced refrigerant thermophysical properties: mathematical modeling. Journal of Nanoparticles, 2014.

Faizan, A., and Han, D., 2016. Thermophysical property and heat transfer analysis of R245fa/Al_2O_3 nanorefrigerant. The International Journal of Engineering and Science (IJES), 5(4), 45-53.

Fan, W. and Zhong, F., 2020. Effects of Macroparameters on the Thickness of an Interfacial Nanolayer of Al_2O_3– and TiO_2–Water-Based Nanofluids. ACS Omega, 5 (43), 27972-27977. https://doi.org/10.1021/acsomega.0c03452

Feroskhan, M., Venugopal, T., Almakayeel, N. M., Yunus Khan, T. M., Alghamdi, S., Almuflih, A. S., and Gobinath, N., 2022. Fundamentals, Thermophysical Properties, and Heat Transfer Characteristics of Nanorefrigerants: A Review. Journal of Nanomaterials, Volume 2022, Article ID 8618152. https://doi.org/10.1155/2022/8618152.

Fu, H.L. and Gao, L., 2012. Effect of interfacial nanolayer on thermophoresis in nanofluids, Int. Journal of Thermal Sciences, 61. 61-66.

Govindasamy, S., Kaliyannan, M., Sadhasivam, S., and Kadasari, R., 2022. Experimental analysis of domestic refrigeration system using nanorefrigerant [CeO2+ ZnO+ R134a]. Thermal Science, 26(2 Part A), 969-974.

Habib K., Ahmed M., Abdullah A.Q., Alawi O.A., Bakthavatchalam B., Hussein O.A., 2022. Metallic Oxides for Innovative Refrigerant Thermo-Physical Properties: Mathematical Models. Tikrit Journal of Engineering Sciences, 29(1), 1- 15. http://doi.org/10.25130/tjes.29.1.1.

Hai, T., Ali, M. A., Alizadeh, A.A., Chauhan, B.S., Almojil, S.F., Almohana, A.I., and Alali, A. F., 2023. Applying energy-exergy, environmental, sustainability, and exergoeconomic metrics and bi-objective optimization for assessment of an innovative tri-generation system. International Journal of Hydrogen Energy.

Halim, N. F. C., and Sidik, N. A. C., 2020. Nanorefrigerants: A Review on Thermophysical Properties and Their Heat Transfer Performance. Journal of Advanced Research in Applied Sciences and Engineering Technology, 20(1), 42-50.

Hamilton, R.L. and Crosser, O.K., 1962. Thermal conductivity of heterogeneous two-component systems, IandEC Fundam. 1. 182-191.

Haykin, S., 2009. Neural Networks and Learning Machines. Pearson Education.

He, Y., Jin, Y., Chen, H., Ding, Y., Cang, D., and Lu, H., 2007. Heat transfer and flow behavior of aqueous suspensions of TiO_2 nanoparticles (nanofluids) flowing upward through a vertical pipe. International Journal of Heat and Mass Transfer, 50(11-12), 2272-2281.

Helvaci, H. U., and Khan, Z. A., 2017. Heat transfer and entropy generation analysis of HFE 7000 based nanorefrigerants. International Journal of Heat and Mass Transfer, 104, 318-327.

Henderson, K., Park, Y., Liu, L., Jacobi, A.M., 2010. Flow-boiling heat transfer of R134a-based nanofluids in a horizontal tube, Int. J. Heat and Mass Transfer, 53. 944-951.

Hu, J., Liu, C., Liu, L., and Li, Q., 2018. Thermal energy storage of R1234yf, R1234ze, R134a and R32/MOF-74 nanofluids: a molecular simulation study. Materials, 11(7), 1164.

Incropera, F. P., DeWitt, D. P., 2002. Fundamentals of Heat and Mass Transfer, John Wiley and Sons, New York, 5th edition.

International Organization for Standardization., 2015. ISO 22007-2: Determination of thermal conductivity and thermal diffusivity - Part 2: Transient plane heat source (hot disc) method. Geneva, Switzerland: International Organization for Standardization.

Intergovernmental Panel on Climate Change (IPCC), 2013. Climate Change 2013: The Physical Science Basis. Contribution of Working Group I to the Fifth Assessment Report of the Intergovernmental Panel on Climate Change, Cambridge University Press.

Jang, S.P. and Choi, S.U.S., 2004. Role of Brownian motion in the enhanced thermal conductivity of nanofluids, Appl. Phys. Lett., 84. 4316–4318.

Javadi, F.S., Saidur, R., 2013. Energetic, economic and environmental impacts of using nanorefrigerant in domestic refrigerators in Malaysia, Energy Conversion and Management, 73. 335-339.

Jeffrey, D.J., 1973. Conduction through a random suspension of spheres, Proc. Roy.Soc. (Lond.), A335. 355–367.

Jiang, W., Ding, G., Peng, H., 2009. Measurement and model on thermal conductivities of carbon nanotube nanorefrigerants, Int. J. Thermal Sciences, 48. 1108-1115.

Jiang, W., Ding, G., Peng, H., Gao, Y., and Wang, K., 2009. Experimental and Model Research on Nanorefrigerant Thermal Conductivity. HVACandR Research, 15(3), 651-669.

Jixiang, W.A.N.G., Yunze, L.I., Xiangdong, L.I.U., Chaoqun, S.H.E.N., Zhang, H., and Xiong, K., 2021. Recent active thermal management technologies for the

development of energy-optimized aerospace vehicles in China. Chinese Journal of Aeronautics, 34(2), 1-27.

Kakaç, S. and Liu, H., 2002. Heat Exchangers: Selection, Rating, and Thermal Design, CRC, Florida.

Kakaç, S., and Pramuanjaroenkij, A., 2009. Review of convective heat transfer enhancement with nanofluids. International Journal of Heat and Mass Transfer, 52(13-14), 3187-3196.

Kandlikar, S. G., 1990. A General Correlation for Saturated Two-Phase Flow Boiling Heat Transfer Inside Horizontal and Vertical Tubes, Journal of Heat Transfer, Vol. 112. 219-228.

Kasaeian, A., Hosseini, S. M., Sheikhpour, M., Mahian, O., Yan, W. M., and Wongwises, S., 2018. Applications of eco-friendly refrigerants and nanorefrigerants: A review. Renewable and Sustainable Energy Reviews, 96, 91-99.

Keblinski, P., Phillpot, S. R., Choi, S. U. S., and Eastman, J. A., 2002. Mechanisms of heat flow in suspensions of nano-sized particles (nanofluids). International Journal of Heat and Mass Transfer, 45(4), 855-863.

Khanafer, K. and Vafai, K., 2011. A critical synthesis of thermophysical characteristics of nanofluids, Int. Journal of Heat and Mass Transfer, 54. 4410-4428.

Koo, J. and Kleinstreuer, C., 2004. A new thermal conductivity model for nanofluids, J.Nanopart. Res. 6, 6. 577–588.

Kumar, R., Singh, D. K., Chander, S., 2022. A critical review on the effect of nanorefrigerant and nanolubricant on the performance of heat transfer cycles. Heat and Mass Transfer, 58, 1507-1531. https://doi.org/10.1007/s00231-022-03194-2.

Kumar, A., Gupta, P. R., Tiwari, A. K., and Said, Z., 2022. Performance evaluation of small scale solar organic Rankine cycle using MWCNT + R141b nanorefrigerant. Energy Conversion and Management, 260, 115631.

Kundan, L., and Singh, K., 2021. Improved performance of a nanorefrigerant-based vapor compression refrigeration system: A new alternative. Journal of Power and Energy, 235(1), 106-123. DOI: 10.1177/0957650920904553.

Liu, Z. H., Xia, Y., and Zhang, Z. H., 2016. A review of the applications of nanofluids in solar energy. International Journal of Heat and Mass Transfer, 100, 606-619.

Lundgren, T., 1972. Slow flow through stationary random beds and suspensions of spheres, J. Fluid Mech., 51. 273–299.

Mahbubul, I.M., Saidur, R., Amalina, M.A., 2012. Investigation of viscosity of R123-TiO_2 Nanorefrigerant, Int. J. Mechanical and Materials Engineering, 7. 146-151.

Mahbubul, I.M., Saidur, R., Amalina, M.A., 2013. Heat transfer and pressure drop characteristics of Al_2O_3-R141b nanorefrigerant in horizontal smooth circular tube, 5th BSME Int. Conf. on Thermal Engineering, 56. 323-329.

Mahbubul, I.M., Saidur, R., Amalina, M.A., 2013. Thermal conductivity, viscosity and density of R141b refrigerant based nanofluid, 5th BSME Int. Conf. on Thermal Engineering, 56. 310-315.

Mahbubul, I.M., Khaleduzzaman, S.S., Saidur, R., Amalina, M.A., 2014. Rheological behavior of Al_2O_3/R141b nanorefrigerant. International Journal of Heat and Mass Transfer, 73, 118-123.

Mahbubul, I.M., Saadah, A., Saidur, R., Khairul, M.A., Kamyar, A., 2015. Thermal performance analysis of Al_2O_3/R-134a nanorefrigerant. International Journal of Heat and Mass Transfer, 85, 1034–1040.

Maheshwarya, P. B., Handab, C. C., and Nemadec, K. R., 2018. Effect of Shape on Thermophysical and Heat Transfer Properties of ZnO/R134a Nanorefrigerant. In Proceedings of the International Conference on Processing of Materials, Minerals and Energy (PMME 2016), 1635-1639.

Mahian, O., Kianifar, A., Kleinstreuer, C., Al-Nimr, M.A., Pop, I., Sahin, A.Z., Wongwises, S., 2013. A review of entropy generation in nanofluid flow, Int. Journal of Heat and Mass Transfer, 65. 514-532.

Maxwell Garnett, J.C., 1904. Colours in metal glasses and in metallic films, Philosophical Transactions of the Royal Society of London, A 203, 385–420.

Matlab Answers, 2021. https://www.mathworks.com/matlabcentral/answers/60753-ann-cannot-extrapolate-any-data-which-method-can-do, last viewed on July, 4, 2021.

Moghaddami, M., Mohammadzade, A., Esfehani, S.A.V., 2011. Second law analysis of nanofluid flow, Energy Conversion and Management, 52. 1397-1405.

Mondejar, M. E., Regidor, M., Krafczyk, J., Ihmels, C., Schmid, B., Kontogeorgis, G. M., and Haglind, F., 2021. An open-access database of the thermophysical properties of nanofluids. Journal of Molecular Liquids, 333, 115140.

Muroyama, K., Fan, L.S., 1985. Fundamentals of Gas-Liquid-Solid Fluidization, AlChe Journal, 31. 1-34.

Nair, V., Parekh, A. D., and Tailor, P. R., 2020. Performance analysis of Al_2O_3–R718 nanorefrigerant turbulent flow through a flooded chiller tube: a numerical investigation. Journal of the Brazilian Society of Mechanical

Sciences and Engineering, 42, 350. https://doi.org/10.1007/s40430-020-02429-9.

Nuclear Power, 2023. Flow Patterns-Two-phase Flow. Retrieved July 24, 2023, from https://www.nuclear-power.com/nuclear-engineering/fluid-dynamics/two-phase-fluid-flow/flow-patterns-two-phase-flow/

Patil, M. S., Kim, S. C., Seo, J. H., and Lee, M. Y., 2015. Review of the thermo-physical properties and performance characteristics of a refrigeration system using refrigerant-based nanofluids. Energies, 9(1), 22.

Peng, H., Ding, G., Jiang, W., Hu, H., Gao, Y., 2009-1. Heat transfer characteristics of refrigerant-based nanofluid flow boiling inside a horizontal smooth tube, Int. J. Refrigeration, 32. 1259-1270.

Peng, H., Ding, G., Jiang, W., Hu, H., Gao, Y., 2009-2. Measurement and correlation of frictional pressure drop of refrigerant-based nanofluid flow boiling inside a horizontal smooth tube, Int. J. Refrigeration, 32. 1756-1764.

Redhwan, A. A. M., Azmi, W. H., Sharif, M. Z., and Mamat, R., 2016. Development of nanorefrigerants for various types of refrigerant based: A comprehensive review on performance. International Communications in Heat and Mass Transfer, 76, 285-293.

Refex Industries, 2023. Ril Products R-141b. Retrieved July 24, 2023, from https://www.refex.co.in/r-141b.php

Saidur, R., Kazi, S. N., Hossain, M. S., Rahman, M. M., and Mohammed, H. A., 2011. A review on the performance of nanoparticles suspended with refrigerants and lubricating oils in refrigeration systems. Renewable and Sustainable Energy Reviews, 15(1), 310-323.

Saidur, R., Leong, K. Y., and Mohammed, H. A., 2011. A review on applications and challenges of nanofluids. Renewable and sustainable energy reviews, 15(3), 1646-1668.

Sanukrishna, S.S., Murukan, M., Jose, P.M., 2018. An overview of experimental studies on nanorefrigerants: Recent research, development and applications. International Journal of Refrigeration, 88, 552–577.

Sanukrishna, S.S., and Vishnu, A.S., 2017. Nanorefrigerants for energy efficient refrigeration systems. Journal of Mechanical Science and Technology 31. 3993-4001.

Shah, M.M., 1982. Chart Correlation for Saturated Boiling Heat Transfer: Equations and Further Study, ASHRAE Transactions, Vol.88, Part I. 185-196.

Sonawane, S., 2023. Investigation of turbulent heat transfer performance of aviation turbine fuel multi-wall carbon nanotube nanofluid. Advanced Powder Technology, 34(9), 104079.

Subramani, N., Prakash, M.J., 2011. Experimental studies on a vapour compression system using nanorefrigerants, Int. J. Engineering, Science and Technology, 3. 95-102.

Sun, B., Yang, D., 2014. Flow boiling heat transfer characteristics of nanorefrigerants in a horizontal tube, Int. J. of Refrigeration, 38. 206-214.

Tekin, B., Yazıcıoğlu, A.G., 2016. Thermophysical Properties of Two-Phase Refrigerant Based Nanofluids in a Refrigeration Cycle, ASME 2016 SHTC, HT2016-7192, July 10-14.

Trask, A., Hill, F., Reed, S., Rae, J, 2021. Neural Arithmetic Logic Units, preprint, viewed at https://arxiv.org/pdf/1808.00508.pdf, last viewed on July, 4, 2021.

Vamshi, J., Anand, K.M., Sharma, A., Kumar, A., Kumar, S., Kotia, A., Choudhary, R., 2022. A review on the utilization of nanoparticles in the refrigeration system as nanorefrigerant and nano-lubricant. Materials Today: Proceedings, 50, 782-788.

Verma, K. N., Dondapapti, R. S., Usurumarti, P. R., and Vyas, G., 2016, June. Feasibility studies on nano-refrigerants for cooling of micro-electronic devices. In 3rd International Conference on Electrical, Electronics, Engineering Trends, Communication, Optimization and Sciences (EEECOS 2016) (pp. 1-6). IET.

Wang, X., and Mujumdar, A. S., 2007. Heat transfer characteristics of nanofluids: A review. International Journal of Thermal Sciences, 46(1), 1-19.

Wang, K., Shiromoto K., Mizogami, T., 2007. Eexperiment study on the effect of nano-scaleparticle on condensation process. In: The 22nd International Congress of Refrigeration, 2007, Beijing, China, in CD-ROM, Paper number: ICR07-B1-1005.

Wang, X., and Mujumdar, A. S., 2008. A review on nanofluids: Part II: Experiments and applications. Brazilian Journal of Chemical Engineering, 25(4), 631-648.

Wang, X., Xu, X., and Choi, S. U., 1999. Thermal conductivity of nanoparticle-fluid mixture. Journal of Thermophysics and Heat Transfer, 13(4), 474-480.

Wen, D., and Ding, Y., 2004. Experimental investigation into convective heat transfer of nanofluids at the entrance region under laminar flow conditions. International Journal of Heat and Mass Transfer, 47(24), 5181-5188.

Xing, M., Zhang, H., and Zhang, C., 2022. An Update Review on Performance Enhancement of Refrigeration Systems Using Nano-Fluids. Journal of Thermal Science, 31(4), 1236-1251. https://doi.org/10.1007/s11630-022-1607-8.

Xiong, Y., Abd Alreda, B., Abosinnee, A. S., Mohammed, M. S., Yasin, Y., Hashim, F. S., ... and Toghraie, D., 2023. Investigating the Effect of Different Base

Fluids in Atomic and Thermal Behaviors of Different Nano-refrigerants Using Molecular Dynamics Simulation. International Journal of Refrigeration.

Xuan, Y., Li, Q., 2003. Investigation on convective heat transfer and flow features of nanofluids. Journal of Heat Transfer, 125(1), 151-155.

Xue, Q.Z., 2006. Model for the effective thermal conductivity of carbon nanotube composites, Nanotech. 17, 1655–1670.

Yang, G.Q., Du, B., Fan, L.S., 2007. Bubble formation and dynamics in gas–liquid–solid fluidization—A review, Chemical Engineering Science, 62. 2-27.

Yıldız, G., Ağbulut, Ü., and Gürel, A. E., 2021. A review of stability, thermophysical properties and impact of using nanofluids on the performance of refrigeration systems. International Journal of Refrigeration, 129, 342-364.

Yu, W., Xie, H., 2012. A review on nanofluids: Preparation, stability mechanisms, and applications. Journal of Nanomaterials, 2012, 435873.

Yu, W., Choi, S.U.S., 2003. The role of interfacial layers in the enhanced thermal of nanofluids: a renovated Maxwell model, J. Nanopart. Res. 5, 1-2, pp. 167–171.

Zhang, X., Ahmadi, G., 2005. Eulerian–Lagrangian simulations of liquid–gas–solid flows in three-phase slurry reactors, Chemical Engineering Science, 60. 5089-5104.

Zhang, J., Li, Y., Fan, L.S., 2000. Discrete phase simulation of gas–liquid–solid fluidization systems: single bubble rising behavior, Powder Technology, 113. 310-326.

Zhang, S., Yu, Y., Xu, Z., Huang, H., Liu, Z., Liu, C., Long, X., and Ge, Z., 2020. Measurement and modeling of the thermal conductivity of nanorefrigerants with low volume concentrations. Thermochimica Acta, 688, 178603.

Zhang, S., Li, Y., Xu, Z., Liu, C., Liu, Z., Ge, Z., and Ma, L., 2022. Experimental investigation and intelligent modeling of thermal conductivity of R141b based nanorefrigerants containing metallic oxide nanoparticles. Powder Technology, 395, 850-871.

Zhou, L. P., Wang, B. X., Peng, X. F., Du, X. Z., and Yang, Y. P., 2010. On the specific heat capacity of CuO nanofluid. Advances in mechanical engineering, 2, 172085.

APPENDICES

A. Condenser and Evaporator Properties

Table A.1 Constants for condenser properties

x	m_l	ϕ_m	ϕ	x	m_l	ϕ_m	ϕ
-	g /s	-	-	-	g /s	-	-
0	0.45	0.500%	0.093%	0.50	0.225	0.995%	0.186%
0.01	0.4455	0.505%	0.094%	0.55	0.2025	1.104%	0.206%
0.05	0.4275	0.526%	0.098%	0.60	0.18	1.241%	0.232%
0.10	0.405	0.555%	0.103%	0.65	0.1575	1.415%	0.265%
0.15	0.3825	0.588%	0.109%	0.70	0.135	1.647%	0.309%
0.20	0.36	0.624%	0.116%	0.75	0.1125	1.970%	0.371%
0.25	0.3375	0.666%	0.124%	0.80	0.09	2.451%	0.463%
0.30	0.315	0.713%	0.133%	0.85	0.0675	3.241%	0.616%
0.35	0.2925	0.767%	0.143%	0.90	0.045	4.785%	0.922%
0.40	0.27	0.831%	0.155%	0.95	0.0225	9.132%	1.827%
0.45	0.2475	0.905%	0.169%	1	0	100.000%	100.000%

Table A.2 Mass and volume fraction of condenser (1.0%)

x	m_l	ϕ_m	ϕ	x	m_l	ϕ_m	ϕ
-	g /s	-	-	-	g /s	-	-
0	0.45	1.000%	0.187%	0.50	0.225	1.980%	0.373%
0.01	0.4455	1.010%	0.189%	0.55	0.2025	2.195%	0.414%
0.05	0.4275	1.052%	0.196%	0.60	0.18	2.463%	0.465%
0.10	0.405	1.110%	0.207%	0.65	0.1575	2.805%	0.531%
0.15	0.3825	1.174%	0.220%	0.70	0.135	3.257%	0.619%
0.20	0.36	1.247%	0.233%	0.75	0.1125	3.883%	0.742%
0.25	0.3375	1.329%	0.249%	0.80	0.09	4.808%	0.926%
0.30	0.315	1.422%	0.266%	0.85	0.0675	6.309%	1.231%
0.35	0.2925	1.530%	0.287%	0.90	0.045	9.174%	1.836%
0.40	0.27	1.656%	0.311%	0.95	0.0225	16.807%	3.605%
0.45	0.2475	1.803%	0.339%	1	0	100.000%	100.000%

Table A.3 Mass and volume fraction of condenser (2.0%)

x	m_l	ϕ_m	ϕ	x	m_l	ϕ_m	ϕ
-	g /s	-	-	-	g /s	-	-
0	0.45	2.000%	0.376%	0.50	0.225	3.922%	0.750%
0.01	0.4455	2.020%	0.380%	0.55	0.2025	4.338%	0.833%
0.05	0.4275	2.103%	0.396%	0.60	0.18	4.854%	0.936%
0.10	0.405	2.217%	0.418%	0.65	0.1575	5.510%	1.068%
0.15	0.3825	2.345%	0.443%	0.70	0.135	6.369%	1.244%
0.20	0.36	2.488%	0.470%	0.75	0.1125	7.547%	1.489%
0.25	0.3375	2.649%	0.501%	0.80	0.09	9.259%	1.854%
0.30	0.315	2.833%	0.537%	0.85	0.0675	11.976%	2.457%
0.35	0.2925	3.044%	0.578%	0.90	0.045	16.949%	3.641%
0.40	0.27	3.289%	0.626%	0.95	0.0225	28.986%	7.025%
0.45	0.2475	3.578%	0.682%	1	0	100.000%	100.000%

Table A.4 Mass and volume fraction of evaporator (0.5%)

x	m_l	ϕ_m	ϕ	x	m_l	ϕ_m	ϕ
-	g /s	-	-	-	g /s	-	-
0	0.45	0.500%	0.110%	0.50	0.225	0.995%	0.219%
0.01	0.4455	0.505%	0.111%	0.55	0.2025	1.104%	0.243%
0.05	0.4275	0.526%	0.115%	0.60	0.18	1.241%	0.274%
0.10	0.405	0.555%	0.122%	0.65	0.1575	1.415%	0.313%
0.15	0.3825	0.588%	0.129%	0.70	0.135	1.647%	0.364%
0.20	0.36	0.624%	0.137%	0.75	0.1125	1.970%	0.437%
0.25	0.3375	0.666%	0.146%	0.80	0.09	2.451%	0.546%
0.30	0.315	0.713%	0.157%	0.85	0.0675	3.241%	0.726%
0.35	0.2925	0.767%	0.169%	0.90	0.045	4.785%	1.085%
0.40	0.27	0.831%	0.183%	0.95	0.0225	9.132%	2.147%
0.45	0.2475	0.905%	0.199%	1	0	100.000%	100.000%

Table A.5 Mass and volume fraction of evaporator (1.0%)

x	m_l	ϕ_m	ϕ	x	m_l	ϕ_m	ϕ
-	g /s	-	-	-	g /s	-	-
0	0.45	1.000%	0.220%	0.50	0.225	1.980%	0.439%
0.01	0.4455	1.010%	0.222%	0.55	0.2025	2.195%	0.488%
0.05	0.4275	1.052%	0.232%	0.60	0.18	2.463%	0.548%
0.10	0.405	1.110%	0.244%	0.65	0.1575	2.805%	0.626%
0.15	0.3825	1.174%	0.259%	0.70	0.135	3.257%	0.730%
0.20	0.36	1.247%	0.275%	0.75	0.1125	3.883%	0.875%
0.25	0.3375	1.329%	0.293%	0.80	0.09	4.808%	1.091%
0.30	0.315	1.422%	0.314%	0.85	0.0675	6.309%	1.449%
0.35	0.2925	1.530%	0.338%	0.90	0.045	9.174%	2.158%
0.40	0.27	1.656%	0.366%	0.95	0.0225	16.807%	4.225%
0.45	0.2475	1.803%	0.399%	1	0	100.000%	100.000%

Table A.6 Mass and volume fraction of evaporator (2.0%)

x	m_l	ϕ_m	ϕ	x	m_l	ϕ_m	ϕ
-	g /s	-	-	-	g /s	-	-
0	0.45	2.000%	0.444%	0.50	0.225	3.922%	0.883%
0.01	0.4455	2.020%	0.448%	0.55	0.2025	4.338%	0.981%
0.05	0.4275	2.103%	0.467%	0.60	0.18	4.854%	1.102%
0.10	0.405	2.217%	0.493%	0.65	0.1575	5.510%	1.257%
0.15	0.3825	2.345%	0.522%	0.70	0.135	6.369%	1.464%
0.20	0.36	2.488%	0.554%	0.75	0.1125	7.547%	1.751%
0.25	0.3375	2.649%	0.591%	0.80	0.09	9.259%	2.180%
0.30	0.315	2.833%	0.633%	0.85	0.0675	11.976%	2.885%
0.35	0.2925	3.044%	0.681%	0.90	0.045	16.949%	4.266%
0.40	0.27	3.289%	0.737%	0.95	0.0225	28.986%	8.183%
0.45	0.2475	3.578%	0.804%	1	0	100.000%	100.000%

Table A.7 Specific volume of refrigerant and nanorefrigerant for condenser (0.5%)

x	v	v_{nr}	% change	x	v	v_{nr}	% change
-	kg/m^3	kg/m^3		-	kg/m^3	kg/m^3	
0	8.547E-04	8.512E-04	-0.41%	0.50	1.195E-02	1.130E-02	-5.40%
0.01	1.079E-03	1.073E-03	-0.51%	0.55	1.305E-02	1.229E-02	-5.87%
0.05	1.965E-03	1.946E-03	-0.93%	0.60	1.416E-02	1.327E-02	-6.34%
0.10	3.077E-03	3.032E-03	-1.45%	0.65	1.527E-02	1.423E-02	-6.80%
0.15	4.184E-03	4.102E-03	-1.96%	0.70	1.639E-02	1.520E-02	-7.26%
0.20	5.291E-03	5.160E-03	-2.47%	0.75	1.748E-02	1.614E-02	-7.70%
0.25	6.410E-03	6.219E-03	-2.98%	0.80	1.859E-02	1.707E-02	-8.14%
0.30	7.519E-03	7.258E-03	-3.47%	0.85	1.972E-02	1.803E-02	-8.59%
0.35	8.621E-03	8.279E-03	-3.96%	0.90	2.083E-02	1.896E-02	-9.00%
0.40	9.709E-03	9.278E-03	-4.44%	0.95	2.193E-02	1.988E-02	-9.35%
0.45	1.083E-02	1.030E-02	-4.93%	1	2.304E-02	2.304E-02	0.00%

Table A.8 Specific volume of refrigerant and nanorefrigerant for condenser (1.0%)

x	v	v_{nr}	% change	x	v	v_{nr}	% change
-	kg/m^3	kg/m^3		-	kg/m^3	kg/m^3	
0	8.547E-04	8.477E-04	-0.81%	0.50	1.195E-02	1.072E-02	-10.28%
0.01	1.079E-03	1.068E-03	-1.03%	0.55	1.305E-02	1.160E-02	-11.13%
0.05	1.965E-03	1.928E-03	-1.85%	0.60	1.416E-02	1.247E-02	-11.95%
0.10	3.077E-03	2.989E-03	-2.87%	0.65	1.527E-02	1.332E-02	-12.76%
0.15	4.184E-03	4.022E-03	-3.87%	0.70	1.639E-02	1.417E-02	-13.56%
0.20	5.291E-03	5.035E-03	-4.84%	0.75	1.748E-02	1.498E-02	-14.32%
0.25	6.410E-03	6.038E-03	-5.80%	0.80	1.859E-02	1.579E-02	-15.06%
0.30	7.519E-03	7.012E-03	-6.74%	0.85	1.972E-02	1.661E-02	-15.80%
0.35	8.621E-03	7.962E-03	-7.65%	0.90	2.083E-02	1.741E-02	-16.45%
0.40	9.709E-03	8.881E-03	-8.53%	0.95	2.193E-02	1.822E-02	-16.91%
0.45	1.083E-02	9.814E-03	-9.42%	1	2.304E-02	2.304E-02	0.00%

Table A.9 Specific volume of refrigerant and nanorefrigerant for condenser (2.0%)

x	v	v_{nr}	% change	x	v	v_{nr}	% change
-	kg/m^3	kg/m^3		-	kg/m^3	kg/m^3	
0	8.547E-04	8.408E-04	-1.63%	0.50	1.195E-02	9.708E-03	-18.75%
0.01	1.079E-03	1.057E-03	-2.05%	0.55	1.305E-02	1.043E-02	-20.12%
0.05	1.965E-03	1.893E-03	-3.67%	0.60	1.416E-02	1.113E-02	-21.45%
0.10	3.077E-03	2.904E-03	-5.63%	0.65	1.527E-02	1.180E-02	-22.71%
0.15	4.184E-03	3.870E-03	-7.50%	0.70	1.639E-02	1.247E-02	-23.95%
0.20	5.291E-03	4.799E-03	-9.29%	0.75	1.748E-02	1.309E-02	-25.10%
0.25	6.410E-03	5.703E-03	-11.04%	0.80	1.859E-02	1.372E-02	-26.20%
0.30	7.519E-03	6.564E-03	-12.70%	0.85	1.972E-02	1.435E-02	-27.24%
0.35	8.621E-03	7.389E-03	-14.29%	0.90	2.083E-02	1.498E-02	-28.09%
0.40	9.709E-03	8.174E-03	-15.81%	0.95	2.193E-02	1.570E-02	-28.40%
0.45	1.083E-02	8.959E-03	-17.31%	1	2.304E-02	2.304E-02	0.00%

Table A.10 Specific volume of refrigerant and nanorefrigerant for evaporator (0.5%)

x	v	v_{nr}	% change	x	v	v_{nr}	% change
-	kg/m^3	kg/m^3		-	kg/m^3	kg/m^3	
0	7.246E-04	7.218E-04	-0.39%	0.50	9.524E-02	6.286E-02	-34.00%
0.01	2.618E-03	2.581E-03	-1.40%	0.55	1.049E-01	6.695E-02	-36.20%
0.05	1.020E-02	9.670E-03	-5.24%	0.60	1.144E-01	7.069E-02	-38.21%
0.10	1.969E-02	1.779E-02	-9.63%	0.65	1.239E-01	7.422E-02	-40.10%
0.15	2.915E-02	2.518E-02	-13.63%	0.70	1.333E-01	7.752E-02	-41.86%
0.20	3.861E-02	3.194E-02	-17.29%	0.75	1.429E-01	8.067E-02	-43.53%
0.25	4.808E-02	3.815E-02	-20.65%	0.80	1.522E-01	8.361E-02	-45.07%
0.30	5.747E-02	4.384E-02	-23.72%	0.85	1.618E-01	8.650E-02	-46.54%
0.35	6.711E-02	4.923E-02	-26.64%	0.90	1.712E-01	8.927E-02	-47.86%
0.40	7.634E-02	5.402E-02	-29.23%	0.95	1.808E-01	9.230E-02	-48.96%
0.45	8.621E-02	5.879E-02	-31.80%	1	1.901E-01	1.901E-01	0.00%

Table A.11 Specific volume of refrigerant and nanorefrigerant for evaporator (1.0%)

x	v	v_{nr}	% change	x	v	v_{nr}	% change
-	kg/m^3	kg/m^3		-	kg/m^3	kg/m^3	
0	7.246E-04	7.190E-04	-0.78%	0.50	9.524E-02	4.684E-02	-50.81%
0.01	2.618E-03	2.545E-03	-2.77%	0.55	1.049E-01	4.909E-02	-53.22%
0.05	1.020E-02	9.185E-03	-9.98%	0.60	1.144E-01	5.108E-02	-55.35%
0.10	1.969E-02	1.622E-02	-17.62%	0.65	1.239E-01	5.292E-02	-57.30%
0.15	2.915E-02	2.214E-02	-24.06%	0.70	1.333E-01	5.460E-02	-59.05%
0.20	3.861E-02	2.720E-02	-29.55%	0.75	1.429E-01	5.618E-02	-60.67%
0.25	4.808E-02	3.158E-02	-34.31%	0.80	1.522E-01	5.765E-02	-62.13%
0.30	5.747E-02	3.538E-02	-38.43%	0.85	1.618E-01	5.911E-02	-63.47%
0.35	6.711E-02	3.882E-02	-42.16%	0.90	1.712E-01	6.060E-02	-64.61%
0.40	7.634E-02	4.174E-02	-45.32%	0.95	1.808E-01	6.264E-02	-65.36%
0.45	8.621E-02	4.454E-02	-48.33%	1	1.901E-01	1.901E-01	0.00%

Table A.12 Specific volume of refrigerant and nanorefrigerant for evaporator (2.0%)

x	v	v_{nr}	% change	x	v	v_{nr}	% change
-	kg/m^3	kg/m^3		-	kg/m^3	kg/m^3	
0	7.246E-04	7.133E-04	-1.56%	0.50	9.524E-02	3.094E-02	-67.51%
0.01	2.618E-03	2.476E-03	-5.43%	0.55	1.049E-01	3.192E-02	-69.58%
0.05	1.020E-02	8.340E-03	-18.27%	0.60	1.144E-01	3.277E-02	-71.35%
0.10	1.969E-02	1.375E-02	-30.13%	0.65	1.239E-01	3.355E-02	-72.93%
0.15	2.915E-02	1.779E-02	-38.97%	0.70	1.333E-01	3.426E-02	-74.31%
0.20	3.861E-02	2.092E-02	-45.81%	0.75	1.429E-01	3.493E-02	-75.55%
0.25	4.808E-02	2.343E-02	-51.27%	0.80	1.522E-01	3.558E-02	-76.62%
0.30	5.747E-02	2.546E-02	-55.70%	0.85	1.618E-01	3.629E-02	-77.58%
0.35	6.711E-02	2.720E-02	-59.47%	0.90	1.712E-01	3.715E-02	-78.30%
0.40	7.634E-02	2.861E-02	-62.52%	0.95	1.808E-01	3.885E-02	-78.52%
0.45	8.621E-02	2.991E-02	-65.31%	1	1.901E-01	1.901E-01	0.00%

Table A.13 Conductivity of refrigerant and nanorefrigerant for condenser (0.5%)

		Maxwell Garnett		Bruggeman		Jeffrey		
x	k	k_{nr}	%change	k_{nr}	%change	k_{nr}	%change	%change
-	W/mK	W/mK		W/mK		W/mK		Average
0	7.69E-02	0.07711	0.27714	0.07711	0.27764	0.07711	0.27722	0.27733
0.01	5.14E-02	0.05161	0.41463	0.05161	0.41539	0.05161	0.41476	0.41493
0.05	2.65E-02	0.02671	0.80422	0.02671	0.80577	0.02671	0.80448	0.80482
0.10	2.02E-02	0.02041	1.05504	0.02041	1.05719	0.02041	1.05541	1.05588
0.15	1.79E-02	0.01811	1.19060	0.01811	1.19317	0.01811	1.19104	1.19160
0.20	1.68E-02	0.01701	1.26855	0.01701	1.27147	0.01701	1.26905	1.26969
0.25	1.62E-02	0.01641	1.31554	0.01641	1.31876	0.01641	1.31609	1.31680
0.30	1.58E-02	0.01601	1.34884	0.01601	1.35238	0.01601	1.34945	1.35022
0.35	4.56E-02	0.04581	0.46736	0.04581	0.46868	0.04581	0.46759	0.46788
0.40	2.25E-02	0.02271	0.94718	0.02271	0.95009	0.02271	0.94768	0.94832
0.45	1.91E-02	0.01931	1.11579	0.01931	1.11953	0.01931	1.11643	1.11725
0.50	1.76E-02	0.01781	1.21089	0.01781	1.21535	0.01781	1.21165	1.21263
0.55	1.68E-02	0.01701	1.26855	0.01701	1.27374	0.01701	1.26943	1.27057
0.60	1.62E-02	0.01641	1.31553	0.01641	1.32159	0.01641	1.31656	1.31789
0.65	1.59E-02	0.01611	1.34034	0.01611	1.34741	0.01611	1.34154	1.34310
0.70	1.56E-02	0.01581	1.36612	0.01581	1.37452	0.01581	1.36754	1.36939
0.75	1.54E-02	0.01561	1.38385	0.01561	1.39408	0.01561	1.38558	1.38784
0.80	1.53E-02	0.01551	1.39289	0.01552	1.40578	0.01551	1.39505	1.39791
0.85	1.51E-02	0.01531	1.41132	0.01532	1.42879	0.01531	1.41422	1.41811
0.90	1.50E-02	0.01521	1.42070	0.01522	1.44724	0.01521	1.42501	1.43098
0.95	1.49E-02	0.01511	1.43014	0.01512	1.48459	0.01511	1.43843	1.45105
1	1.49E-02	0.01490	0.00000	0.01490	0.00000	0.01490	0.00000	0.00000

Table A.14 Conductivity of refrigerant and nanorefrigerant for condenser (1.0%)

		Maxwell Garnett		Bruggeman		Jeffrey		
x	k	k_{nr}	%change	k_{nr}	%change	k_{nr}	%change	%change
-	W/mK	W/mK		W/mK		W/mK		Average
0	7.69E-02	0.07733	0.55707	0.07733	0.55913	0.07733	0.55742	0.55787
0.01	5.14E-02	0.05183	0.83343	0.05183	0.83655	0.05183	0.83397	0.83465
0.05	2.65E-02	0.02693	1.61654	0.02693	1.62284	0.02693	1.61762	1.61900
0.10	2.02E-02	0.02063	2.12071	0.02063	2.12944	0.02063	2.12220	2.12412
0.15	1.79E-02	0.01833	2.39320	0.01833	2.40363	0.01833	2.39498	2.39727
0.20	1.68E-02	0.01723	2.54990	0.01723	2.56171	0.01723	2.55191	2.55451
0.25	1.62E-02	0.01663	2.64434	0.01663	2.65740	0.01663	2.64656	2.64943
0.30	1.58E-02	0.01623	2.71128	0.01623	2.72564	0.01623	2.71372	2.71688
0.35	4.56E-02	0.04603	0.93943	0.04603	0.94479	0.04603	0.94034	0.94152
0.40	2.25E-02	0.02293	1.90391	0.02293	1.91569	0.02293	1.90591	1.90850
0.45	1.91E-02	0.01953	2.24283	0.01953	2.25797	0.01953	2.24539	2.24873
0.50	1.76E-02	0.01803	2.43397	0.01803	2.45205	0.01803	2.43702	2.44102
0.55	1.68E-02	0.01723	2.54987	0.01723	2.57093	0.01723	2.55341	2.55807
0.60	1.62E-02	0.01663	2.64430	0.01663	2.66890	0.01663	2.64842	2.65387
0.65	1.59E-02	0.01633	2.69418	0.01633	2.72286	0.01633	2.69896	2.70533
0.70	1.56E-02	0.01603	2.74597	0.01603	2.78014	0.01603	2.75164	2.75925
0.75	1.54E-02	0.01583	2.78161	0.01583	2.82325	0.01583	2.78846	2.79777
0.80	1.53E-02	0.01573	2.79975	0.01574	2.85233	0.01573	2.80829	2.82013
0.85	1.51E-02	0.01553	2.83677	0.01554	2.90825	0.01553	2.84813	2.86438
0.90	1.50E-02	0.01543	2.85556	0.01544	2.96484	0.01543	2.87218	2.89753
0.95	1.49E-02	0.01533	2.87435	0.01536	3.10297	0.01533	2.90478	2.96070
1	1.49E-02	0.01490	0.00000	0.01490	0.00000	0.01490	0.00000	0.00000

Table A.15 Conductivity of refrigerant and nanorefrigerant for condenser (2.0%)

		Maxwell Garnett		Bruggeman		Jeffrey		
x	k	k_{nr}	%change	k_{nr}	%change	k_{nr}	%change	%change
-	W/mK	W/mK		W/mK		W/mK		Average
0	7.69E-02	0.07777	1.12549	0.07777	1.13394	0.07777	1.12691	1.12878
0.01	5.14E-02	0.05227	1.68385	0.05227	1.69662	0.05227	1.68601	1.68883
0.05	2.65E-02	0.02737	3.26603	0.02737	3.29185	0.02737	3.27038	3.27609
0.10	2.02E-02	0.02107	4.28464	0.02107	4.32040	0.02107	4.29066	4.29857
0.15	1.79E-02	0.01877	4.83517	0.01877	4.87793	0.01877	4.84235	4.85182
0.20	1.68E-02	0.01767	5.15175	0.01767	5.20018	0.01767	5.15987	5.17060
0.25	1.62E-02	0.01707	5.34255	0.01707	5.39615	0.01707	5.35151	5.36340
0.30	1.58E-02	0.01667	5.47779	0.01667	5.53671	0.01667	5.48762	5.50071
0.35	4.56E-02	0.04647	1.89800	0.04648	1.92001	0.04647	1.90166	1.90655
0.40	2.25E-02	0.02337	3.84660	0.02338	3.89496	0.02337	3.85462	3.86539
0.45	1.91E-02	0.01997	4.53132	0.01998	4.59353	0.01997	4.54159	4.55548
0.50	1.76E-02	0.01847	4.91748	0.01848	4.99186	0.01847	4.92971	4.94635
0.55	1.68E-02	0.01767	5.15162	0.01768	5.23833	0.01767	5.16579	5.18525
0.60	1.62E-02	0.01707	5.34238	0.01708	5.44376	0.01707	5.35883	5.38166
0.65	1.59E-02	0.01677	5.44313	0.01678	5.56149	0.01677	5.46216	5.48893
0.70	1.56E-02	0.01647	5.54774	0.01649	5.68898	0.01647	5.57016	5.60229
0.75	1.54E-02	0.01627	5.61968	0.01629	5.79224	0.01627	5.64660	5.68618
0.80	1.53E-02	0.01617	5.65627	0.01620	5.87502	0.01617	5.68950	5.74026
0.85	1.51E-02	0.01597	5.73093	0.01601	6.03026	0.01597	5.77442	5.84521
0.90	1.50E-02	0.01587	5.76863	0.01593	6.23250	0.01587	5.83021	5.94378
0.95	1.49E-02	0.01577	5.80582	0.01592	6.81968	0.01578	5.90712	6.17754
1	1.49E-02	0.01490	0.00000	0.01490	0.00000	0.01490	0.00000	0.00000

Table A.16 Conductivity of refrigerant and nanorefrigerant for evaporator (0.5%)

		Maxwell Garnett		Bruggeman		Jeffrey		
x	k	k_{nr}	%change	k_{nr}	%change	k_{nr}	%change	%change
-	W/mK	W/mK		W/mK		W/mK		Average
0	1.04E-01	0.10434	0.32607	0.10434	0.32678	0.10434	0.32619	0.32635
0.01	1.70E-02	0.01734	1.99479	0.01734	1.99914	0.01734	1.99554	1.99649
0.05	1.03E-02	0.01064	3.29238	0.01064	3.29986	0.01064	3.29366	3.29530
0.10	9.74E-03	0.01008	3.48167	0.01008	3.49002	0.01008	3.48311	3.48493
0.15	9.56E-03	0.00990	3.54722	0.00990	3.55623	0.00990	3.54877	3.55074
0.20	1.08E-02	0.01114	3.13995	0.01114	3.14842	0.01114	3.14140	3.14326
0.25	9.87E-03	0.01021	3.43580	0.01021	3.44570	0.01021	3.43750	3.43967
0.30	9.62E-03	0.00996	3.52509	0.00996	3.53596	0.00996	3.52696	3.52934
0.35	9.51E-03	0.00985	3.56586	0.00985	3.57771	0.00985	3.56789	3.57049
0.40	9.45E-03	0.00979	3.58849	0.00979	3.60142	0.00979	3.59071	3.59354
0.45	9.42E-03	0.00976	3.59992	0.00976	3.61406	0.00976	3.60234	3.60544
0.50	9.39E-03	0.00973	3.61141	0.00973	3.62703	0.00973	3.61408	3.61751
0.55	9.37E-03	0.00971	3.61911	0.00971	3.63651	0.00971	3.62208	3.62590
0.60	9.36E-03	0.00970	3.62297	0.00970	3.64257	0.00970	3.62631	3.63062
0.65	9.35E-03	0.00969	3.62683	0.00969	3.64928	0.00969	3.63064	3.63558
0.70	9.34E-03	0.00968	3.63069	0.00968	3.65694	0.00968	3.63514	3.64092
0.75	9.33E-03	0.00967	3.63456	0.00967	3.66613	0.00967	3.63988	3.64686
0.80	9.33E-03	0.00967	3.63452	0.00967	3.67407	0.00967	3.64114	3.64991
0.85	9.32E-03	0.00966	3.63836	0.00966	3.69134	0.00966	3.64711	3.65893
0.90	9.32E-03	0.00966	3.63823	0.00967	3.71827	0.00966	3.65112	3.66921
0.95	9.32E-03	0.00966	3.63786	0.00967	3.80144	0.00966	3.66226	3.70052
1	9.31E-03	0.00931	0.00000	0.00931	0.00000	0.00931	0.00000	0.00000

Table A.17 Conductivity of refrigerant and nanorefrigerant for evaporator (1.0%)

		Maxwell Garnett		Bruggeman		Jeffrey		
x	k	k_{nr}	%change	k_{nr}	%change	k_{nr}	%change	%change
-	W/mK	W/mK		W/mK		W/mK		Average
0	1.04E-01	0.10468	0.65543	0.10468	0.65828	0.10468	0.65592	0.65654
0.01	1.70E-02	0.01768	4.00969	0.01768	4.02730	0.01768	4.01270	4.01657
0.05	1.03E-02	0.01098	6.61794	0.01098	6.64823	0.01098	6.62311	6.62976
0.10	9.74E-03	0.01042	6.99843	0.01042	7.03224	0.01042	7.00420	7.01162
0.15	9.56E-03	0.01024	7.13019	0.01025	7.16668	0.01024	7.13641	7.14442
0.20	1.08E-02	0.01148	6.31152	0.01149	6.34586	0.01148	6.31737	6.32492
0.25	9.87E-03	0.01055	6.90622	0.01056	6.94630	0.01055	6.91304	6.92185
0.30	9.62E-03	0.01030	7.08568	0.01031	7.12976	0.01030	7.09317	7.10287
0.35	9.51E-03	0.01019	7.16762	0.01020	7.21566	0.01019	7.17577	7.18635
0.40	9.45E-03	0.01013	7.21311	0.01014	7.26552	0.01013	7.22198	7.23354
0.45	9.42E-03	0.01010	7.23606	0.01011	7.29345	0.01010	7.24575	7.25842
0.50	9.39E-03	0.01007	7.25915	0.01008	7.32253	0.01007	7.26982	7.28383
0.55	9.37E-03	0.01005	7.27461	0.01006	7.34525	0.01005	7.28647	7.30211
0.60	9.36E-03	0.01004	7.28234	0.01005	7.36199	0.01004	7.29565	7.31333
0.65	9.35E-03	0.01003	7.29007	0.01004	7.38134	0.01003	7.30525	7.32555
0.70	9.34E-03	0.01002	7.29781	0.01003	7.40461	0.01002	7.31544	7.33929
0.75	9.33E-03	0.01001	7.30553	0.01002	7.43420	0.01001	7.32655	7.35543
0.80	9.33E-03	0.01001	7.30538	0.01003	7.46691	0.01001	7.33137	7.36789
0.85	9.32E-03	0.01000	7.31296	0.01002	7.53013	0.01000	7.34704	7.39671
0.90	9.32E-03	0.01000	7.31245	0.01003	7.64299	0.01001	7.36172	7.43906
0.95	9.32E-03	0.01000	7.31094	0.01007	8.00248	0.01001	7.39895	7.57079
1	9.31E-03	0.00931	0.00000	0.00931	0.00000	0.00931	0.00000	0.00000

Table A.18 Conductivity of refrigerant and nanorefrigerant for evaporator (2.0%)

		Maxwell Garnett		Bruggeman		Jeffrey		
x	k	k_{nr}	%change	k_{nr}	%change	k_{nr}	%change	%change
-	W/mK	W/mK		W/mK		W/mK		Average
0	1.04E-01	0.10538	1.32421	0.10539	1.33589	0.10538	1.32618	1.32876
0.01	1.70E-02	0.01838	8.10105	0.01839	8.17323	0.01838	8.11320	8.12916
0.05	1.03E-02	0.01168	13.37063	0.01169	13.49484	0.01168	13.39152	13.41900
0.10	9.74E-03	0.01112	14.13934	0.01113	14.27806	0.01112	14.16262	14.19334
0.15	9.56E-03	0.01094	14.40553	0.01095	14.55525	0.01094	14.43060	14.46379
0.20	1.08E-02	0.01218	12.75152	0.01219	12.89242	0.01218	12.77506	12.80634
0.25	9.87E-03	0.01125	13.95298	0.01126	14.11756	0.01125	13.98041	14.01698
0.30	9.62E-03	0.01100	14.31553	0.01101	14.49659	0.01100	14.34562	14.38591
0.35	9.51E-03	0.01089	14.48104	0.01091	14.67848	0.01089	14.51375	14.55776
0.40	9.45E-03	0.01083	14.57291	0.01085	14.78839	0.01083	14.60846	14.65659
0.45	9.42E-03	0.01080	14.61923	0.01082	14.85536	0.01080	14.65801	14.71086
0.50	9.39E-03	0.01077	14.66582	0.01079	14.92681	0.01077	14.70845	14.76703
0.55	9.37E-03	0.01075	14.69699	0.01077	14.98816	0.01075	14.74422	14.80979
0.60	9.36E-03	0.01074	14.71252	0.01077	15.04123	0.01074	14.76538	14.83971
0.65	9.35E-03	0.01073	14.72803	0.01076	15.10528	0.01073	14.78804	14.87378
0.70	9.34E-03	0.01072	14.74351	0.01076	15.18594	0.01072	14.81285	14.91410
0.75	9.33E-03	0.01071	14.75890	0.01076	15.29351	0.01071	14.84098	14.96446
0.80	9.33E-03	0.01071	14.75828	0.01077	15.43250	0.01072	14.85861	15.01646
0.85	9.32E-03	0.01070	14.77308	0.01078	15.68656	0.01071	14.90206	15.12057
0.90	9.32E-03	0.01070	14.77101	0.01083	16.18379	0.01071	14.95022	15.30167
0.95	9.32E-03	0.01070	14.76481	0.01099	17.88005	0.01072	15.04602	15.89696
1	9.31E-03	0.00931	0.00000	0.00931	0.00000	0.00931	0.00000	0.00000

Table A.19 Viscosity of refrigerant and nanorefrigerant for condenser (0.5%)

		Einstein		Batchelor		Lungren		
x	μ	μ_{nr}	%change	μ_{nr}	%change	μ_{nr}	%change	%change
-	Pa.s	Pa.s		Pa.s		Pa.s		Average
0	1.72E-04	1.72E-04	0.23235	1.72E-04	0.23289	1.72E-04	0.23290	0.23271
0.01	9.08E-05	9.12E-05	0.44014	9.12E-05	0.44116	9.12E-05	0.44117	0.44083
0.05	3.16E-05	3.20E-05	1.26465	3.20E-05	1.26772	3.20E-05	1.26776	1.26671
0.10	1.94E-05	1.98E-05	2.05984	1.98E-05	2.06512	1.98E-05	2.06517	2.06338
0.15	1.57E-05	1.61E-05	2.54513	1.61E-05	2.55203	1.61E-05	2.55210	2.54975
0.20	1.42E-05	1.46E-05	2.81379	1.46E-05	2.82189	1.46E-05	2.82198	2.81922
0.25	1.34E-05	1.38E-05	2.98154	1.38E-05	2.99070	1.38E-05	2.99081	2.98768
0.30	1.30E-05	1.34E-05	3.07301	1.34E-05	3.08313	1.34E-05	3.08324	3.07979
0.35	1.27E-05	1.31E-05	3.14528	1.31E-05	3.15643	1.31E-05	3.15656	3.15276
0.40	1.25E-05	1.29E-05	3.19522	1.29E-05	3.20749	1.29E-05	3.20764	3.20345
0.45	1.24E-05	1.28E-05	3.22054	1.28E-05	3.23403	1.28E-05	3.23419	3.22959
0.50	1.23E-05	1.27E-05	3.24617	1.27E-05	3.26112	1.27E-05	3.26132	3.25620
0.55	1.23E-05	1.27E-05	3.24550	1.27E-05	3.26211	1.27E-05	3.26233	3.25665
0.60	1.22E-05	1.26E-05	3.27126	1.26E-05	3.29009	1.26E-05	3.29035	3.28390
0.65	1.22E-05	1.26E-05	3.27018	1.26E-05	3.29168	1.26E-05	3.29200	3.28462
0.70	1.22E-05	1.26E-05	3.26873	1.26E-05	3.29379	1.26E-05	3.29419	3.28557
0.75	1.22E-05	1.26E-05	3.26672	1.26E-05	3.29675	1.26E-05	3.29728	3.28691
0.80	1.22E-05	1.26E-05	3.26369	1.26E-05	3.30116	1.26E-05	3.30191	3.28892
0.85	1.21E-05	1.25E-05	3.28559	1.25E-05	3.33582	1.25E-05	3.33701	3.31947
0.90	1.21E-05	1.25E-05	3.27550	1.25E-05	3.35037	1.25E-05	3.35275	3.32621
0.95	1.21E-05	1.25E-05	3.24558	1.25E-05	3.39261	1.25E-05	3.40088	3.34636
1	1.21E-05	1.21E-05	0.00000	1.21E-05	0.00000	1.21E-05	0.00000	0.00000

Table A.20 Viscosity of refrigerant and nanorefrigerant for condenser (1.0%)

		Einstein		Batchelor		Lungren		
x	μ	μ_{nr}	%change	μ_{nr}	%change	μ_{nr}	%change	%change
-	Pa.s	Pa.s		Pa.s		Pa.s		Average
0	1.72E-04	1.73E-04	0.46662	1.73E-04	0.46878	1.73E-04	0.46881	0.46807
0.01	9.08E-05	9.16E-05	0.88389	9.16E-05	0.88802	9.16E-05	0.88807	0.88666
0.05	3.16E-05	3.24E-05	2.53957	3.24E-05	2.55195	3.24E-05	2.55211	2.54788
0.10	1.94E-05	2.02E-05	4.13617	2.02E-05	4.15744	2.02E-05	4.15773	4.15045
0.15	1.57E-05	1.65E-05	5.11032	1.65E-05	5.13814	1.65E-05	5.13852	5.12899
0.20	1.42E-05	1.50E-05	5.64937	1.50E-05	5.68204	1.50E-05	5.68250	5.67130
0.25	1.34E-05	1.42E-05	5.98571	1.42E-05	6.02263	1.42E-05	6.02316	6.01050
0.30	1.30E-05	1.38E-05	6.16879	1.38E-05	6.20955	1.38E-05	6.21015	6.19617
0.35	1.27E-05	1.35E-05	6.31322	1.35E-05	6.35813	1.35E-05	6.35882	6.34339
0.40	1.25E-05	1.33E-05	6.41270	1.33E-05	6.46211	1.33E-05	6.46289	6.44590
0.45	1.24E-05	1.32E-05	6.46259	1.32E-05	6.51689	1.32E-05	6.51780	6.49909
0.50	1.23E-05	1.31E-05	6.51292	1.31E-05	6.57310	1.31E-05	6.57416	6.55339
0.55	1.23E-05	1.31E-05	6.51022	1.31E-05	6.57704	1.31E-05	6.57828	6.55518
0.60	1.22E-05	1.30E-05	6.56019	1.30E-05	6.63590	1.30E-05	6.63741	6.61117
0.65	1.22E-05	1.30E-05	6.55584	1.30E-05	6.64224	1.30E-05	6.64411	6.61406
0.70	1.22E-05	1.30E-05	6.55003	1.30E-05	6.65066	1.30E-05	6.65307	6.61792
0.75	1.22E-05	1.30E-05	6.54193	1.30E-05	6.66238	1.30E-05	6.66565	6.62332
0.80	1.22E-05	1.30E-05	6.52981	1.30E-05	6.67982	1.30E-05	6.68461	6.63141
0.85	1.21E-05	1.29E-05	6.56351	1.29E-05	6.76393	1.29E-05	6.77197	6.69980
0.90	1.21E-05	1.29E-05	6.52335	1.29E-05	6.82032	1.29E-05	6.83711	6.72692
0.95	1.21E-05	1.29E-05	6.40576	1.29E-05	6.97848	1.30E-05	7.04028	6.80817
1	1.21E-05	1.21E-05	0.00000	1.21E-05	0.00000	1.21E-05	0.00000	0.00000

Table A.21 Viscosity of refrigerant and nanorefrigerant for condenser (2.0%)

		Einstein		Batchelor		Lungren		
x	μ	μ_{nr}	%change	μ_{nr}	%change	μ_{nr}	%change	%change
-	Pa.s	Pa.s		Pa.s		Pa.s		Average
0	1.72E-04	1.74E-04	0.94097	1.74E-04	0.94975	1.74E-04	0.94991	0.94688
0.01	9.08E-05	9.24E-05	1.78238	9.24E-05	1.79919	9.24E-05	1.79949	1.79369
0.05	3.16E-05	3.32E-05	5.12071	3.32E-05	5.17102	3.32E-05	5.17193	5.15455
0.10	1.94E-05	2.10E-05	8.33912	2.10E-05	8.42557	2.10E-05	8.42719	8.39729
0.15	1.57E-05	1.73E-05	10.30185	1.73E-05	10.41491	1.73E-05	10.41710	10.37795
0.20	1.42E-05	1.58E-05	11.38693	1.58E-05	11.51967	1.58E-05	11.52233	11.47631
0.25	1.34E-05	1.50E-05	12.06297	1.50E-05	12.21291	1.50E-05	12.21604	12.16397
0.30	1.30E-05	1.46E-05	12.42968	1.46E-05	12.59517	1.46E-05	12.59877	12.54121
0.35	1.27E-05	1.43E-05	12.71805	1.43E-05	12.90032	1.43E-05	12.90448	12.84095
0.40	1.25E-05	1.41E-05	12.91532	1.41E-05	13.11574	1.41E-05	13.12057	13.05054
0.45	1.24E-05	1.40E-05	13.01207	1.40E-05	13.23223	1.40E-05	13.23785	13.16072
0.50	1.23E-05	1.39E-05	13.10892	1.39E-05	13.35273	1.39E-05	13.35939	13.27368
0.55	1.23E-05	1.39E-05	13.09800	1.39E-05	13.36845	1.39E-05	13.37643	13.28096
0.60	1.22E-05	1.38E-05	13.19163	1.38E-05	13.49775	1.38E-05	13.50760	13.39899
0.65	1.22E-05	1.38E-05	13.17402	1.38E-05	13.52293	1.39E-05	13.53539	13.41078
0.70	1.22E-05	1.38E-05	13.15062	1.39E-05	13.55623	1.39E-05	13.57262	13.42649
0.75	1.22E-05	1.38E-05	13.11799	1.39E-05	13.60231	1.39E-05	13.62509	13.44846
0.80	1.22E-05	1.38E-05	13.06935	1.39E-05	13.67027	1.39E-05	13.70456	13.48139
0.85	1.21E-05	1.37E-05	13.09642	1.38E-05	13.89438	1.38E-05	13.95346	13.64809
0.90	1.21E-05	1.37E-05	12.93749	1.38E-05	14.10556	1.38E-05	14.23288	13.75864
0.95	1.21E-05	1.36E-05	12.48304	1.39E-05	14.65794	1.39E-05	15.14259	14.09452
1	1.21E-05	1.21E-05	0.00000	1.21E-05	0.00000	1.21E-05	0.00000	0.00000

Table A.22 Viscosity of refrigerant and nanorefrigerant for evaporator (0.5%)

		Einstein		Batchelor		Lungren		
x	μ	μ_{nr}	%change	μ_{nr}	%change	μ_{nr}	%change	%change
-	Pa.s	Pa.s		Pa.s		Pa.s		Average
0	3.79E-04	3.80E-04	0.27401	3.80E-04	0.27476	3.80E-04	0.27477	0.27451
0.01	1.93E-05	2.03E-05	5.38084	2.03E-05	5.39561	2.03E-05	5.39577	5.39074
0.05	9.11E-06	1.01E-05	11.39904	1.02E-05	11.43166	1.02E-05	11.43202	11.42091
0.10	9.20E-06	1.02E-05	11.28681	1.02E-05	11.32089	1.02E-05	11.32127	11.30966
0.15	9.35E-06	1.04E-05	11.10494	1.04E-05	11.14045	1.04E-05	11.14085	11.12875
0.20	9.46E-06	1.05E-05	10.97493	1.05E-05	11.01221	1.05E-05	11.01264	10.99993
0.25	9.53E-06	1.06E-05	10.89332	1.06E-05	10.93279	1.06E-05	10.93325	10.91979
0.30	9.58E-06	1.06E-05	10.83534	1.06E-05	10.87739	1.06E-05	10.87790	10.86354
0.35	9.62E-06	1.07E-05	10.78898	1.07E-05	10.83408	1.07E-05	10.83463	10.81923
0.40	9.65E-06	1.07E-05	10.75393	1.07E-05	10.80262	1.07E-05	10.80323	10.78659
0.45	9.67E-06	1.07E-05	10.72991	1.07E-05	10.78289	1.07E-05	10.78359	10.76546
0.50	9.69E-06	1.07E-05	10.70563	1.07E-05	10.76377	1.07E-05	10.76456	10.74465
0.55	9.70E-06	1.07E-05	10.69199	1.07E-05	10.75649	1.07E-05	10.75741	10.73530
0.60	9.72E-06	1.08E-05	10.66675	1.08E-05	10.73912	1.08E-05	10.74021	10.71536
0.65	9.73E-06	1.08E-05	10.65163	1.08E-05	10.73418	1.08E-05	10.73550	10.70710
0.70	9.74E-06	1.08E-05	10.63515	1.08E-05	10.73127	1.08E-05	10.73293	10.69978
0.75	9.75E-06	1.08E-05	10.61651	1.08E-05	10.73156	1.08E-05	10.73377	10.69394
0.80	9.76E-06	1.08E-05	10.59405	1.08E-05	10.73741	1.08E-05	10.74056	10.69068
0.85	9.76E-06	1.08E-05	10.57482	1.08E-05	10.76527	1.08E-05	10.77035	10.70348
0.90	9.77E-06	1.08E-05	10.52578	1.08E-05	10.80910	1.08E-05	10.81935	10.71807
0.95	9.77E-06	1.08E-05	10.41276	1.08E-05	10.96730	1.08E-05	11.00348	10.79451
1	9.78E-06	9.78E-06	0.00000	9.78E-06	0.00000	9.78E-06	0.00000	0.00000

Table A.23 Viscosity of refrigerant and nanorefrigerant for evaporator (1.0%)

		Einstein		Batchelor		Lungren		
x	μ	μ_{nr}	%change	μ_{nr}	%change	μ_{nr}	%change	%change
-	Pa.s	Pa.s		Pa.s		Pa.s		Average
0	3.79E-04	3.81E-04	0.55019	3.81E-04	0.55319	3.81E-04	0.55323	0.55220
0.01	1.93E-05	2.14E-05	10.80394	2.14E-05	10.86350	2.14E-05	10.86432	10.84392
0.05	9.11E-06	1.12E-05	22.88656	1.12E-05	23.01803	1.12E-05	23.01986	22.97482
0.10	9.20E-06	1.13E-05	22.65975	1.13E-05	22.79714	1.13E-05	22.79910	22.75200
0.15	9.35E-06	1.14E-05	22.29302	1.14E-05	22.43611	1.14E-05	22.43820	22.38911
0.20	9.46E-06	1.15E-05	22.03024	1.16E-05	22.18045	1.16E-05	22.18271	22.13113
0.25	9.53E-06	1.16E-05	21.86441	1.16E-05	22.02341	1.16E-05	22.02587	21.97123
0.30	9.58E-06	1.17E-05	21.74574	1.17E-05	21.91513	1.17E-05	21.91785	21.85958
0.35	9.62E-06	1.17E-05	21.65009	1.17E-05	21.83167	1.17E-05	21.83469	21.77215
0.40	9.65E-06	1.17E-05	21.57671	1.18E-05	21.77269	1.18E-05	21.77610	21.70850
0.45	9.67E-06	1.18E-05	21.52491	1.18E-05	21.73813	1.18E-05	21.74202	21.66835
0.50	9.69E-06	1.18E-05	21.47191	1.18E-05	21.70578	1.18E-05	21.71028	21.62932
0.55	9.70E-06	1.18E-05	21.43931	1.18E-05	21.69864	1.18E-05	21.70396	21.61397
0.60	9.72E-06	1.18E-05	21.38216	1.18E-05	21.67296	1.18E-05	21.67937	21.57816
0.65	9.73E-06	1.18E-05	21.34347	1.18E-05	21.67494	1.18E-05	21.68293	21.56711
0.70	9.74E-06	1.18E-05	21.29932	1.19E-05	21.68484	1.19E-05	21.69517	21.55978
0.75	9.75E-06	1.18E-05	21.24647	1.19E-05	21.70726	1.19E-05	21.72136	21.55836
0.80	9.76E-06	1.18E-05	21.17839	1.19E-05	21.75129	1.19E-05	21.77210	21.56726
0.85	9.76E-06	1.18E-05	21.10167	1.19E-05	21.86001	1.19E-05	21.89486	21.61885
0.90	9.77E-06	1.18E-05	20.92844	1.19E-05	22.04849	1.19E-05	22.12192	21.69962
0.95	9.77E-06	1.18E-05	20.48634	1.20E-05	22.63281	1.20E-05	22.90566	22.00827
1	9.78E-06	9.78E-06	0.00000	9.78E-06	0.00000	9.78E-06	0.00000	0.00000

Table A.24 Viscosity of refrigerant and nanorefrigerant for evaporator (2.0%)

		Einstein		Batchelor		Lungren		
x	μ	μ_{nr}	%change	μ_{nr}	%change	μ_{nr}	%change	%change
-	Pa.s	Pa.s		Pa.s		Pa.s		Average
0	3.79E-04	3.83E-04	1.10911	3.83E-04	1.12131	3.83E-04	1.12155	1.11732
0.01	1.93E-05	2.35E-05	21.77897	2.36E-05	22.02100	2.36E-05	22.02572	21.94190
0.05	9.11E-06	1.33E-05	46.13116	1.34E-05	46.66530	1.34E-05	46.67597	46.49081
0.10	9.20E-06	1.34E-05	45.66803	1.35E-05	46.22604	1.35E-05	46.23756	46.04388
0.15	9.35E-06	1.36E-05	44.92237	1.36E-05	45.50339	1.36E-05	45.51581	45.31386
0.20	9.46E-06	1.37E-05	44.38555	1.37E-05	44.99531	1.37E-05	45.00885	44.79657
0.25	9.53E-06	1.37E-05	44.04326	1.38E-05	44.68841	1.38E-05	44.70336	44.47835
0.30	9.58E-06	1.38E-05	43.79491	1.38E-05	44.48196	1.38E-05	44.49863	44.25850
0.35	9.62E-06	1.38E-05	43.59160	1.39E-05	44.32771	1.39E-05	44.34649	44.08860
0.40	9.65E-06	1.38E-05	43.43144	1.39E-05	44.22551	1.39E-05	44.24694	43.96796
0.45	9.67E-06	1.39E-05	43.31259	1.39E-05	44.17589	1.39E-05	44.20070	43.89639
0.50	9.69E-06	1.39E-05	43.18848	1.40E-05	44.13463	1.40E-05	44.16380	43.82897
0.55	9.70E-06	1.39E-05	43.10165	1.40E-05	44.14979	1.40E-05	44.18479	43.81208
0.60	9.72E-06	1.39E-05	42.96031	1.40E-05	44.13416	1.40E-05	44.17714	43.75720
0.65	9.73E-06	1.39E-05	42.84871	1.40E-05	44.18467	1.40E-05	44.23914	43.75751
0.70	9.74E-06	1.39E-05	42.71522	1.41E-05	44.26573	1.41E-05	44.33760	43.77285
0.75	9.75E-06	1.39E-05	42.54686	1.41E-05	44.39473	1.41E-05	44.49492	43.81217
0.80	9.76E-06	1.39E-05	42.31799	1.41E-05	44.60539	1.41E-05	44.75672	43.89337
0.85	9.76E-06	1.39E-05	42.01276	1.42E-05	45.01879	1.42E-05	45.27859	44.10338
0.90	9.77E-06	1.38E-05	41.37293	1.42E-05	45.75017	1.43E-05	46.31226	44.47845
0.95	9.77E-06	1.36E-05	39.68014	1.44E-05	47.73287	1.46E-05	49.88563	45.76621
1	9.78E-06	9.78E-06	0.00000	9.78E-06	0.00000	9.78E-06	0.00000	0.00000

B. ANN Reference Paper Data Set

Table B.1 Reference paper data set (R141b) [Sun and Yang, 2014]

#	d [mm]	L[mm]	P[atm]	Np	G	φ_m	x	h[W/m^{2}K]
1	10	1400	1	-	120	0.00%	0.30	2003.87
2	10	1400	1	-	120	0.00%	0.40	2201.58
3	10	1400	1	-	120	0.00%	0.50	2247.97
4	10	1400	1	-	120	0.00%	0.60	2699.56
5	10	1400	1	-	120	0.00%	0.70	3402.56
6	10	1400	1	-	120	0.00%	0.80	4003.05
7	10	1400	1	Cu	120	0.10%	0.30	2248.37
8	10	1400	1	Cu	120	0.10%	0.40	2492.67
9	10	1400	1	Cu	120	0.10%	0.50	2805.37
10	10	1400	1	Cu	120	0.10%	0.60	3460.10
11	10	1400	1	Cu	120	0.10%	0.70	4105.05
12	10	1400	1	Cu	120	0.10%	0.80	4251.63
13	10	1400	1	Cu	120	0.20%	0.30	2267.92
14	10	1400	1	Cu	120	0.20%	0.40	2551.30
15	10	1400	1	Cu	120	0.20%	0.50	3206.03
16	10	1400	1	Cu	120	0.20%	0.60	3606.68
17	10	1400	1	Cu	120	0.20%	0.70	4153.91
18	10	1400	1	Cu	120	0.20%	0.80	4407.98
19	10	1400	1	Cu	120	0.30%	0.30	2277.69
20	10	1400	1	Cu	120	0.30%	0.40	2639.25
21	10	1400	1	Cu	120	0.30%	0.50	3362.38
22	10	1400	1	Cu	120	0.30%	0.60	3802.12
23	10	1400	1	Cu	120	0.30%	0.70	4300.49
24	10	1400	1	Cu	120	0.30%	0.80	4554.56
25	10	1400	1	Al	120	0.10%	0.30	2199.51
26	10	1400	1	Al	120	0.10%	0.40	2414.50
27	10	1400	1	Al	120	0.10%	0.50	2707.65
28	10	1400	1	Al	120	0.10%	0.60	3147.39
29	10	1400	1	Al	120	0.10%	0.70	3792.35
30	10	1400	1	Al	120	0.10%	0.80	4193.00

Table B.1 Reference paper data set (R141b) [Sun and Yang, 2014] (continued)

#	d [mm]	L[mm]	P[atm]	Np	G	φm	x	h[W/m2K]
31	10	1400	1	Al	120	0.20%	0.30	2238.60
32	10	1400	1	Al	120	0.20%	0.40	2473.13
33	10	1400	1	Al	120	0.20%	0.50	3088.76
34	10	1400	1	Al	120	0.20%	0.60	3479.64
35	10	1400	1	Al	120	0.20%	0.70	4007.33
36	10	1400	1	Al	120	0.20%	0.80	4339.58
37	10	1400	1	Al	120	0.30%	0.30	2258.14
38	10	1400	1	Al	120	0.30%	0.40	2619.71
39	10	1400	1	Al	120	0.30%	0.50	3323.29
40	10	1400	1	Al	120	0.30%	0.60	3645.77
41	10	1400	1	Al	120	0.30%	0.70	4105.05
42	10	1400	1	Al	120	0.30%	0.80	4437.30
43	10	1400	1	Al_2O_3	120	0.10%	0.30	2198.05
44	10	1400	1	Al_2O_3	120	0.10%	0.40	2402.60
45	10	1400	1	Al_2O_3	120	0.10%	0.50	2607.14
46	10	1400	1	Al_2O_3	120	0.10%	0.60	3006.49
47	10	1400	1	Al_2O_3	120	0.10%	0.70	3649.35
48	10	1400	1	Al_2O_3	120	0.10%	0.80	4165.58
49	10	1400	1	Al_2O_3	120	0.20%	0.30	2227.27
50	10	1400	1	Al_2O_3	120	0.20%	0.40	2470.78
51	10	1400	1	Al_2O_3	120	0.20%	0.50	2889.61
52	10	1400	1	Al_2O_3	120	0.20%	0.60	3240.26
53	10	1400	1	Al_2O_3	120	0.20%	0.70	3853.90
54	10	1400	1	Al_2O_3	120	0.20%	0.80	4321.43
55	10	1400	1	Al_2O_3	120	0.30%	0.30	2246.75
56	10	1400	1	Al_2O_3	120	0.30%	0.40	2626.62
57	10	1400	1	Al_2O_3	120	0.30%	0.50	3152.60
58	10	1400	1	Al_2O_3	120	0.30%	0.60	3405.84
59	10	1400	1	Al_2O_3	120	0.30%	0.70	3980.52
60	10	1400	1	Al_2O_3	120	0.30%	0.80	4409.09
61	10	1400	1	CuO	120	0.10%	0.30	2199.51
62	10	1400	1	CuO	120	0.10%	0.40	2394.95
63	10	1400	1	CuO	120	0.10%	0.50	2551.30
64	10	1400	1	CuO	120	0.10%	0.60	2854.23
65	10	1400	1	CuO	120	0.10%	0.70	3499.19

Table B.1 Reference paper data set (R141b) [Sun and Yang, 2014] (continued)

#	d [mm]	L[mm]	P[atm]	Np	G	φm	x	h[W/m2K]
66	10	1400	1	CuO	120	0.10%	0.80	4153.91
67	10	1400	1	CuO	120	0.20%	0.30	2228.83
68	10	1400	1	CuO	120	0.20%	0.40	2453.58
69	10	1400	1	CuO	120	0.20%	0.50	2649.02
70	10	1400	1	CuO	120	0.20%	0.60	3245.11
71	10	1400	1	CuO	120	0.20%	0.70	3606.68
72	10	1400	1	CuO	120	0.20%	0.80	4007.33
73	10	1400	1	CuO	120	0.30%	0.30	2258.14
74	10	1400	1	CuO	120	0.30%	0.40	2600.16
75	10	1400	1	CuO	120	0.30%	0.50	2805.37
76	10	1400	1	CuO	120	0.30%	0.60	3391.69
77	10	1400	1	CuO	120	0.30%	0.70	3841.21
78	10	1400	1	CuO	120	0.30%	0.80	4456.84
79	10	1400	1	-	210	0.00%	0.30	2167.10
80	10	1400	1	-	210	0.00%	0.40	2402.35
81	10	1400	1	-	210	0.00%	0.50	2602.21
82	10	1400	1	-	210	0.00%	0.60	2898.75
83	10	1400	1	-	210	0.00%	0.70	3654.67
84	10	1400	1	-	210	0.00%	0.80	4144.72
85	10	1400	1	Cu	210	0.10%	0.30	2256.88
86	10	1400	1	Cu	210	0.10%	0.40	2605.50
87	10	1400	1	Cu	210	0.10%	0.50	2944.95
88	10	1400	1	Cu	210	0.10%	0.60	3577.98
89	10	1400	1	Cu	210	0.10%	0.70	4183.49
90	10	1400	1	Cu	210	0.10%	0.80	4302.75
91	10	1400	1	Cu	210	0.20%	0.30	2284.40
92	10	1400	1	Cu	210	0.20%	0.40	2752.29
93	10	1400	1	Cu	210	0.20%	0.50	3321.10
94	10	1400	1	Cu	210	0.20%	0.60	3697.25
95	10	1400	1	Cu	210	0.20%	0.70	4229.36
96	10	1400	1	Cu	210	0.20%	0.80	4568.81
97	10	1400	1	Cu	210	0.30%	0.30	2302.75
98	10	1400	1	Cu	210	0.30%	0.40	2807.34
99	10	1400	1	Cu	210	0.30%	0.50	3449.54
100	10	1400	1	Cu	210	0.30%	0.60	3944.95

Table B.1 Reference paper data set (R141b) [Sun and Yang, 2014] (continued)

#	d [mm]	L[mm]	P[atm]	Np	G	φm	x	h[W/m2K]
101	10	1400	1	Cu	210	0.30%	0.70	4477.06
102	10	1400	1	Cu	210	0.30%	0.80	4706.42
103	10	1400	1	Al	210	0.10%	0.30	2246.95
104	10	1400	1	Al	210	0.10%	0.40	2521.34
105	10	1400	1	Al	210	0.10%	0.50	2905.49
106	10	1400	1	Al	210	0.10%	0.60	3399.39
107	10	1400	1	Al	210	0.10%	0.70	4012.20
108	10	1400	1	Al	210	0.10%	0.80	4222.56
109	10	1400	1	Al	210	0.20%	0.30	2265.24
110	10	1400	1	Al	210	0.20%	0.40	2576.22
111	10	1400	1	Al	210	0.20%	0.50	3125.00
112	10	1400	1	Al	210	0.20%	0.60	3582.32
113	10	1400	1	Al	210	0.20%	0.70	4121.95
114	10	1400	1	Al	210	0.20%	0.80	4396.34
115	10	1400	1	Al	210	0.30%	0.30	2283.54
116	10	1400	1	Al	210	0.30%	0.40	2713.41
117	10	1400	1	Al	210	0.30%	0.50	3408.54
118	10	1400	1	Al	210	0.30%	0.60	3801.83
119	10	1400	1	Al	210	0.30%	0.70	4304.88
120	10	1400	1	Al	210	0.30%	0.80	4588.41
121	10	1400	1	Al_2O_3	210	0.10%	0.30	2211.54
122	10	1400	1	Al_2O_3	210	0.10%	0.40	2431.54
123	10	1400	1	Al_2O_3	210	0.10%	0.50	2786.92
124	10	1400	1	Al_2O_3	210	0.10%	0.60	3269.23
125	10	1400	1	Al_2O_3	210	0.10%	0.70	3810.77
126	10	1400	1	Al_2O_3	210	0.10%	0.80	4183.08
127	10	1400	1	Al_2O_3	210	0.20%	0.30	2236.92
128	10	1400	1	Al_2O_3	210	0.20%	0.40	2499.23
129	10	1400	1	Al_2O_3	210	0.20%	0.50	3006.92
130	10	1400	1	Al_2O_3	210	0.20%	0.60	3396.15
131	10	1400	1	Al_2O_3	210	0.20%	0.70	3996.92
132	10	1400	1	Al_2O_3	210	0.20%	0.80	4343.85
133	10	1400	1	Al_2O_3	210	0.30%	0.30	2262.31
134	10	1400	1	Al_2O_3	210	0.30%	0.40	2660.00
135	10	1400	1	Al_2O_3	210	0.30%	0.50	3277.69

Table B.1 Reference paper data set (R141b) [Sun and Yang, 2014] (continued)

#	d [mm]	L[mm]	P[atm]	Np	G	φm	x	h[W/m2K]
136	10	1400	1	Al_2O_3	210	0.30%	0.60	3582.31
137	10	1400	1	Al_2O_3	210	0.30%	0.70	4174.62
138	10	1400	1	Al_2O_3	210	0.30%	0.80	4521.54
139	10	1400	1	CuO	210	0.10%	0.30	2244.63
140	10	1400	1	CuO	210	0.10%	0.40	2497.70
141	10	1400	1	CuO	210	0.10%	0.50	2759.20
142	10	1400	1	CuO	210	0.10%	0.60	3096.63
143	10	1400	1	CuO	210	0.10%	0.70	3737.73
144	10	1400	1	CuO	210	0.10%	0.80	4193.25
145	10	1400	1	CuO	210	0.20%	0.30	2253.07
146	10	1400	1	CuO	210	0.20%	0.40	2506.13
147	10	1400	1	CuO	210	0.20%	0.50	2851.99
148	10	1400	1	CuO	210	0.20%	0.60	3206.29
149	10	1400	1	CuO	210	0.20%	0.70	3889.57
150	10	1400	1	CuO	210	0.20%	0.80	4252.30
151	10	1400	1	CuO	210	0.30%	0.30	2261.50
152	10	1400	1	CuO	210	0.30%	0.40	2590.49
153	10	1400	1	CuO	210	0.30%	0.50	3088.19
154	10	1400	1	CuO	210	0.30%	0.60	3501.53
155	10	1400	1	CuO	210	0.30%	0.70	3914.88
156	10	1400	1	CuO	210	0.30%	0.80	4496.93
157	10	1400	1	-	330	0.00%	0.30	1998.57
158	10	1400	1	-	330	0.00%	0.40	2490.43
159	10	1400	1	-	330	0.00%	0.50	2746.95
160	10	1400	1	-	330	0.00%	0.60	3101.30
161	10	1400	1	-	330	0.00%	0.70	3648.70
162	10	1400	1	-	330	0.00%	0.80	4299.23
163	10	1400	1	Cu	330	0.10%	0.30	2300.49
164	10	1400	1	Cu	330	0.10%	0.40	2628.66
165	10	1400	1	Cu	330	0.10%	0.50	2978.01
166	10	1400	1	Cu	330	0.10%	0.60	3623.78
167	10	1400	1	Cu	330	0.10%	0.70	4227.20
168	10	1400	1	Cu	330	0.10%	0.80	4481.27
169	10	1400	1	Cu	330	0.20%	0.30	2459.28
170	10	1400	1	Cu	330	0.20%	0.40	2787.46

Table B.1 Reference paper data set (R141b) [Sun and Yang, 2014] (continued)

#	d [mm]	L[mm]	P[atm]	Np	G	φm	x	h[W/m2K]
171	10	1400	1	Cu	330	0.20%	0.50	3369.71
172	10	1400	1	Cu	330	0.20%	0.60	3793.16
173	10	1400	1	Cu	330	0.20%	0.70	4354.23
174	10	1400	1	Cu	330	0.20%	0.80	4661.24
175	10	1400	1	Cu	330	0.30%	0.30	2554.56
176	10	1400	1	Cu	330	0.30%	0.40	2935.67
177	10	1400	1	Cu	330	0.30%	0.50	3507.33
178	10	1400	1	Cu	330	0.30%	0.60	4004.89
179	10	1400	1	Cu	330	0.30%	0.70	4565.96
180	10	1400	1	Cu	330	0.30%	0.80	4693.00
181	10	1400	1	Al	330	0.10%	0.30	2279.32
182	10	1400	1	Al	330	0.10%	0.40	2618.08
183	10	1400	1	Al	330	0.10%	0.50	2935.67
184	10	1400	1	Al	330	0.10%	0.60	3507.33
185	10	1400	1	Al	330	0.10%	0.70	4089.58
186	10	1400	1	Al	330	0.10%	0.80	4428.34
187	10	1400	1	Al	330	0.20%	0.30	2416.94
188	10	1400	1	Al	330	0.20%	0.40	2755.70
189	10	1400	1	Al	330	0.20%	0.50	3189.74
190	10	1400	1	Al	330	0.20%	0.60	3655.54
191	10	1400	1	Al	330	0.20%	0.70	4206.03
192	10	1400	1	Al	330	0.20%	0.80	4523.62
193	10	1400	1	Al	330	0.30%	0.30	2533.39
194	10	1400	1	Al	330	0.30%	0.40	2882.74
195	10	1400	1	Al	330	0.30%	0.50	3464.98
196	10	1400	1	Al	330	0.30%	0.60	3846.09
197	10	1400	1	Al	330	0.30%	0.70	4438.93
198	10	1400	1	Al	330	0.30%	0.80	4661.24
199	10	1400	1	Al_2O_3	330	0.10%	0.30	2247.56
200	10	1400	1	Al_2O_3	330	0.10%	0.40	2596.91
201	10	1400	1	Al_2O_3	330	0.10%	0.50	3062.70
202	10	1400	1	Al_2O_3	330	0.10%	0.60	3316.78
203	10	1400	1	Al_2O_3	330	0.10%	0.70	3888.44
204	10	1400	1	Al_2O_3	330	0.10%	0.80	4396.58
205	10	1400	1	Al_2O_3	330	0.20%	0.30	2279.32

Table B.1 Reference paper data set (R141b) [Sun and Yang, 2014] (continued)

#	d [mm]	L[mm]	P[atm]	Np	G	φm	x	h[W/m2K]
206	10	1400	1	Al_2O_3	330	0.20%	0.40	2618.08
207	10	1400	1	Al_2O_3	330	0.20%	0.50	3136.81
208	10	1400	1	Al_2O_3	330	0.20%	0.60	3528.50
209	10	1400	1	Al_2O_3	330	0.20%	0.70	4100.16
210	10	1400	1	Al_2O_3	330	0.20%	0.80	4513.03
211	10	1400	1	Al_2O_3	330	0.30%	0.30	2438.11
212	10	1400	1	Al_2O_3	330	0.30%	0.40	2872.15
213	10	1400	1	Al_2O_3	330	0.30%	0.50	3401.47
214	10	1400	1	Al_2O_3	330	0.30%	0.60	3666.12
215	10	1400	1	Al_2O_3	330	0.30%	0.70	4290.72
216	10	1400	1	Al_2O_3	330	0.30%	0.80	4597.72
217	10	1400	1	CuO	330	0.10%	0.30	2098.21
218	10	1400	1	CuO	330	0.10%	0.40	2594.16
219	10	1400	1	CuO	330	0.10%	0.50	2900.16
220	10	1400	1	CuO	330	0.10%	0.60	3248.38
221	10	1400	1	CuO	330	0.10%	0.70	3786.53
222	10	1400	1	CuO	330	0.10%	0.80	4387.99
223	10	1400	1	CuO	330	0.20%	0.30	2414.77
224	10	1400	1	CuO	330	0.20%	0.40	2752.44
225	10	1400	1	CuO	330	0.20%	0.50	3100.65
226	10	1400	1	CuO	330	0.20%	0.60	3301.14
227	10	1400	1	CuO	330	0.20%	0.70	3839.29
228	10	1400	1	CuO	330	0.20%	0.80	4482.95
229	10	1400	1	CuO	330	0.30%	0.30	2509.74
230	10	1400	1	CuO	330	0.30%	0.40	2857.95
231	10	1400	1	CuO	330	0.30%	0.50	3142.86
232	10	1400	1	CuO	330	0.30%	0.60	3501.62
233	10	1400	1	CuO	330	0.30%	0.70	3997.56
234	10	1400	1	CuO	330	0.30%	0.80	4641.23

C. ANN Input and Output Parameters

Table C.1 ANN input and output parameters for 234 data points

		I:0	I:1	I:2	I:3	I:4	I:5	I:6	I:7	I:8	I:9	O:10
#	-	M_{np}	ρ_p	c_p	k_p	G	x	ϕ_m	ρ_{nr}	k_{nr}	μ_{nr}	h
-	-	[gr/mol]	[kg/m^3]	[J/kgK]	[W/m.K]	[kg/m^{2}s]	-	-	[kg/m^3]	[W/m.K]	[Pa.s]	[W/m^{2}K]
0	T	-	-	-	-	120	0.3	0.00%	16.0490	0.0652	2.96E-05	2003.87
1	T	-	-	-	-	120	0.4	0.00%	12.0760	0.0573	2.26E-05	2201.58
2	T	-	-	-	-	120	0.5	0.00%	9.6800	0.0495	1.83E-05	2247.97
3	T	-	-	-	-	120	0.6	0.00%	8.0780	0.0417	1.54E-05	2699.56
4	T	64	8960	390	401	120	0.3	0.10%	17.5543	0.0652	2.97E-05	2248.37
5	V	-	-	-	-	120	0.7	0.00%	6.9300	0.0339	1.32E-05	3402.56
6	Q	-	-	-	-	120	0.8	0.00%	6.0680	0.0260	1.16E-05	4003.05
7	T	64	8960	390	401	120	0.5	0.10%	11.7873	0.0496	1.84E-05	2805.37
8	T	64	8960	390	401	120	0.6	0.10%	10.7119	0.0417	1.55E-05	3460.10
9	T	64	8960	390	401	120	0.8	0.10%	11.3340	0.0261	1.18E-05	4251.63
10	T	64	8960	390	401	120	0.3	0.20%	19.0590	0.0652	2.98E-05	2267.92
11	T	64	8960	390	401	120	0.4	0.20%	15.5875	0.0574	2.29E-05	2551.30
12	V	64	8960	390	401	120	0.4	0.10%	13.8321	0.0574	2.27E-05	2492.67
13	Q	64	8960	390	401	120	0.7	0.10%	10.4415	0.0339	1.34E-05	4105.05
14	T	64	8960	390	401	120	0.5	0.20%	13.8934	0.0496	1.86E-05	3206.03
15	T	64	8960	390	401	120	0.7	0.20%	13.9497	0.0339	1.35E-05	4153.91
16	T	64	8960	390	401	120	0.4	0.30%	17.3420	0.0575	2.30E-05	2639.25
17	T	64	8960	390	401	120	0.6	0.30%	15.9743	0.0418	1.58E-05	3802.12
18	T	64	8960	390	401	120	0.7	0.30%	17.4548	0.0340	1.36E-05	4300.49
19	V	64	8960	390	401	120	0.6	0.20%	13.3440	0.0418	1.56E-05	3606.68
20	Q	64	8960	390	401	120	0.8	0.20%	16.5928	0.0261	1.19E-05	4407.98
21	T	64	8960	390	401	120	0.8	0.30%	21.8445	0.0261	1.20E-05	4554.56
22	T	27	2700	900	237	120	0.3	0.10%	17.0037	0.0653	3.00E-05	2199.51
23	T	27	2700	900	237	120	0.5	0.10%	11.0163	0.0496	1.87E-05	2707.65
24	T	27	2700	900	237	120	0.6	0.10%	9.7480	0.0418	1.58E-05	3147.39
25	T	27	2700	900	237	120	0.8	0.10%	9.4042	0.0261	1.21E-05	4193.00
26	V	64	8960	390	401	120	0.3	0.30%	20.5631	0.0653	3.00E-05	2277.69
27	Q	64	8960	390	401	120	0.5	0.30%	15.9983	0.0496	1.87E-05	3362.38
28	T	27	2700	900	237	120	0.4	0.20%	14.3018	0.0576	2.35E-05	2473.13
29	T	27	2700	900	237	120	0.5	0.20%	12.3502	0.0498	1.92E-05	3088.76
30	T	27	2700	900	237	120	0.6	0.20%	11.4142	0.0419	1.62E-05	3479.64

Table C.1 ANN input and output parameters for 234 data points (continued)

		I:0	I:1	I:2	I:3	I:4	I:5	I:6	I:7	I:8	I:9	O:10
31	T	27	2700	900	237	120	0.7	0.20%	11.3749	0.0341	1.41E-05	4007.33
32	T	27	2700	900	237	120	0.3	0.30%	18.9095	0.0655	3.09E-05	2258.14
33	V	27	2700	900	237	120	0.7	0.10%	9.1558	0.0340	1.37E-05	3792.35
34	Q	27	2700	900	237	120	0.4	0.10%	13.1897	0.0575	2.30E-05	2414.50
35	T	27	2700	900	237	120	0.4	0.30%	15.4122	0.0577	2.39E-05	2619.71
36	T	27	2700	900	237	120	0.7	0.30%	13.5874	0.0342	1.45E-05	4105.05
37	T	27	2700	900	237	120	0.8	0.30%	16.0316	0.0264	1.29E-05	4437.30
38	T	102	3890	772	30	120	0.3	0.10%	17.2447	0.0653	2.99E-05	2198.05
39	T	102	3890	772	30	120	0.4	0.10%	13.4709	0.0574	2.29E-05	2402.60
40	V	27	2700	900	237	120	0.8	0.20%	12.7254	0.0263	1.25E-05	4339.58
41	Q	27	2700	900	237	120	0.3	0.20%	17.9572	0.0654	3.04E-05	2238.60
42	T	102	3890	772	30	120	0.5	0.10%	11.3537	0.0496	1.86E-05	2607.14
43	T	102	3890	772	30	120	0.7	0.10%	9.7184	0.0339	1.35E-05	3649.35
44	T	102	3890	772	30	120	0.8	0.10%	10.2484	0.0261	1.19E-05	4165.58
45	T	102	3890	772	30	120	0.3	0.20%	18.4394	0.0653	3.02E-05	2227.27
46	T	102	3890	772	30	120	0.5	0.20%	13.0254	0.0497	1.89E-05	2889.61
47	V	27	2700	900	237	120	0.5	0.30%	13.6816	0.0499	1.96E-05	3323.29
48	Q	27	2700	900	237	120	0.6	0.30%	13.0766	0.0420	1.67E-05	3645.77
49	T	102	3890	772	30	120	0.6	0.20%	12.2584	0.0419	1.60E-05	3240.26
50	T	102	3890	772	30	120	0.7	0.20%	12.5010	0.0340	1.38E-05	3853.90
51	T	102	3890	772	30	120	0.3	0.30%	19.6330	0.0654	3.05E-05	2246.75
52	T	102	3890	772	30	120	0.4	0.30%	16.2564	0.0576	2.35E-05	2626.62
53	T	102	3890	772	30	120	0.5	0.30%	14.6949	0.0498	1.92E-05	3152.60
54	V	102	3890	772	30	120	0.6	0.10%	10.1698	0.0418	1.57E-05	3006.49
55	Q	102	3890	772	30	120	0.4	0.20%	14.8644	0.0575	2.32E-05	2470.78
56	T	102	3890	772	30	120	0.6	0.30%	14.3437	0.0419	1.63E-05	3405.84
57	T	102	3890	772	30	120	0.8	0.30%	18.5701	0.0263	1.25E-05	4409.09
58	T	80	6320	528	32.9	120	0.3	0.10%	17.4551	0.0652	2.98E-05	2199.51
59	T	80	6320	528	32.9	120	0.5	0.10%	11.6483	0.0496	1.85E-05	2551.30
60	T	80	6320	528	32.9	120	0.6	0.10%	10.5381	0.0417	1.56E-05	2854.23
61	V	102	3890	772	30	120	0.8	0.20%	14.4158	0.0262	1.22E-05	4321.43
62	Q	102	3890	772	30	120	0.7	0.30%	15.2778	0.0341	1.41E-05	3980.52
63	T	80	6320	528	32.9	120	0.8	0.10%	10.9859	0.0261	1.18E-05	4153.91
64	T	80	6320	528	32.9	120	0.3	0.20%	18.8604	0.0653	2.99E-05	2228.83
65	T	80	6320	528	32.9	120	0.4	0.20%	15.3556	0.0574	2.30E-05	2453.58

Table C.1 ANN input and output parameters for 234 data points (continued)

		I:0	I:1	I:2	I:3	I:4	I:5	I:6	I:7	I:8	I:9	O:10
66	T	80	6320	528	32.9	120	0.7	0.20%	13.4850	0.0340	1.36E-05	3606.68
67	T	80	6320	528	32.9	120	0.8	0.20%	15.8942	0.0261	1.20E-05	4207.33
68	V	80	6320	528	32.9	120	0.4	0.10%	13.7163	0.0574	2.28E-05	2394.95
69	Q	80	6320	528	32.9	120	0.7	0.10%	10.2096	0.0339	1.34E-05	3499.19
70	T	80	6320	528	32.9	120	0.4	0.30%	16.9939	0.0575	2.32E-05	2600.16
71	T	80	6320	528	32.9	120	0.5	0.30%	15.5803	0.0497	1.89E-05	2805.37
72	T	80	6320	528	32.9	120	0.6	0.30%	15.4512	0.0418	1.59E-05	3391.69
73	T	80	6320	528	32.9	120	0.7	0.30%	16.7562	0.0340	1.38E-05	3841.21
74	T	-	-	-	-	210	0.3	0.00%	16.0490	0.0652	2.96E-05	2167.10
75	V	80	6320	528	32.9	120	0.6	0.20%	12.9959	0.0418	1.57E-05	3245.11
76	Q	80	6320	528	32.9	120	0.5	0.20%	13.6150	0.0496	1.87E-05	2649.02
77	T	-	-	-	-	210	0.5	0.00%	9.6800	0.0495	1.83E-05	2602.21
78	T	-	-	-	-	210	0.7	0.00%	6.9300	0.0339	1.32E-05	3654.67
79	T	-	-	-	-	210	0.8	0.00%	6.0680	0.0260	1.16E-05	4144.72
80	T	64	8960	390	401	210	0.3	0.10%	17.5543	0.0652	2.97E-05	2256.88
81	T	64	8960	390	401	210	0.4	0.10%	13.8321	0.0574	2.27E-05	2605.50
82	V	80	6320	528	32.9	120	0.8	0.30%	20.7932	0.0262	1.22E-05	4456.84
83	Q	80	6320	528	32.9	120	0.3	0.30%	20.2649	0.0653	3.01E-05	2258.14
84	T	64	8960	390	401	210	0.5	0.10%	11.7873	0.0496	1.84E-05	2944.95
85	T	64	8960	390	401	210	0.8	0.10%	11.3340	0.0261	1.18E-05	4302.75
86	T	64	8960	390	401	210	0.4	0.20%	15.5875	0.0574	2.29E-05	2752.29
87	T	64	8960	390	401	210	0.5	0.20%	13.8934	0.0496	1.86E-05	3321.10
88	T	64	8960	390	401	210	0.6	0.20%	13.3440	0.0418	1.56E-05	3697.25
89	V	-	-	-	-	210	0.4	0.00%	12.0760	0.0573	2.26E-05	2402.35
90	Q	-	-	-	-	210	0.6	0.00%	8.0780	0.0417	1.54E-05	2898.75
91	T	64	8960	390	401	210	0.7	0.20%	13.9497	0.0339	1.35E-05	4229.36
92	T	64	8960	390	401	210	0.3	0.30%	20.5631	0.0653	3.00E-05	2302.75
93	T	64	8960	390	401	210	0.6	0.30%	15.9743	0.0418	1.58E-05	3944.95
94	T	64	8960	390	401	210	0.7	0.30%	17.4548	0.0340	1.36E-05	4477.06
95	T	64	8960	390	401	210	0.8	0.30%	21.8445	0.0261	1.20E-05	4706.42
96	V	64	8960	390	401	210	0.6	0.10%	10.7119	0.0417	1.55E-05	3577.98
97	Q	64	8960	390	401	210	0.7	0.10%	10.4415	0.0339	1.34E-05	4183.49
98	T	27	2700	900	237	210	0.3	0.10%	17.0037	0.0653	3.00E-05	2246.95
99	T	27	2700	900	237	210	0.5	0.10%	11.0163	0.0496	1.87E-05	2905.49
100	T	27	2700	900	237	210	0.7	0.10%	9.1558	0.0340	1.37E-05	4012.20

Table C.1 ANN input and output parameters for 234 data points (continued)

		I:0	I:1	I:2	I:3	I:4	I:5	I:6	I:7	I:8	I:9	O:10
101	T	27	2700	900	237	210	0.8	0.10%	9.4042	0.0261	1.21E-05	4222.56
102	T	27	2700	900	237	210	0.3	0.20%	17.9572	0.0654	3.04E-05	2265.24
103	V	64	8960	390	401	210	0.8	0.20%	16.5928	0.0261	1.19E-05	4568.81
104	Q	64	8960	390	401	210	0.3	0.20%	19.0590	0.0652	2.98E-05	2284.40
105	T	27	2700	900	237	210	0.4	0.20%	14.3018	0.0576	2.35E-05	2576.22
106	T	27	2700	900	237	210	0.5	0.20%	12.3502	0.0498	1.92E-05	3125.00
107	T	27	2700	900	237	210	0.6	0.20%	11.4142	0.0419	1.62E-05	3582.32
108	T	27	2700	900	237	210	0.8	0.20%	12.7254	0.0263	1.25E-05	4396.34
109	T	27	2700	900	237	210	0.3	0.30%	18.9095	0.0655	3.09E-05	2283.54
110	V	64	8960	390	401	210	0.4	0.30%	17.3420	0.0575	2.30E-05	2807.34
111	Q	64	8960	390	401	210	0.5	0.30%	15.9983	0.0496	1.87E-05	3449.54
112	T	27	2700	900	237	210	0.4	0.30%	15.4122	0.0577	2.39E-05	2713.41
113	T	27	2700	900	237	210	0.5	0.30%	13.6816	0.0499	1.96E-05	3408.54
114	T	27	2700	900	237	210	0.6	0.30%	13.0766	0.0420	1.67E-05	3801.83
115	T	27	2700	900	237	210	0.7	0.30%	13.5874	0.0342	1.45E-05	4304.88
116	T	102	3890	772	30	210	0.4	0.10%	13.4709	0.0574	2.29E-05	2431.54
117	V	27	2700	900	237	210	0.4	0.10%	13.1897	0.0575	2.30E-05	2521.34
118	Q	27	2700	900	237	210	0.6	0.10%	9.7480	0.0418	1.58E-05	3399.39
119	T	102	3890	772	30	210	0.5	0.10%	11.3537	0.0496	1.86E-05	2786.92
120	T	102	3890	772	30	210	0.7	0.10%	9.7184	0.0339	1.35E-05	3810.77
121	T	102	3890	772	30	210	0.8	0.10%	10.2484	0.0261	1.19E-05	4183.08
122	T	102	3890	772	30	210	0.3	0.20%	18.4394	0.0653	3.02E-05	2236.92
123	T	102	3890	772	30	210	0.4	0.20%	14.8644	0.0575	2.32E-05	2499.23
124	V	27	2700	900	237	210	0.7	0.20%	11.3749	0.0341	1.41E-05	4121.95
125	Q	27	2700	900	237	210	0.8	0.30%	16.0316	0.0264	1.29E-05	4588.41
126	T	102	3890	772	30	210	0.5	0.20%	13.0254	0.0497	1.89E-05	3006.92
127	T	102	3890	772	30	210	0.6	0.20%	12.2584	0.0419	1.60E-05	3396.15
128	T	102	3890	772	30	210	0.3	0.30%	19.6330	0.0654	3.05E-05	2262.31
129	T	102	3890	772	30	210	0.6	0.30%	14.3437	0.0419	1.63E-05	3582.31
130	T	102	3890	772	30	210	0.7	0.30%	15.2778	0.0341	1.41E-05	4174.62
131	V	102	3890	772	30	210	0.3	0.10%	17.2447	0.0653	2.99E-05	2211.54
132	Q	102	3890	772	30	210	0.6	0.10%	10.1698	0.0418	1.57E-05	3269.23
133	T	102	3890	772	30	210	0.8	0.30%	18.5701	0.0263	1.25E-05	4521.54
134	T	80	6320	528	32.9	210	0.3	0.10%	17.4551	0.0652	2.98E-05	2244.63
135	T	80	6320	528	32.9	210	0.4	0.10%	13.7163	0.0574	2.28E-05	2497.70

Table C.1 ANN input and output parameters for 234 data points (continued)

		I:0	I:1	I:2	I:3	I:4	I:5	I:6	I:7	I:8	I:9	O:10
136	T	80	6320	528	32.9	210	0.5	0.10%	11.6483	0.0496	1.85E-05	2759.20
137	T	80	6320	528	32.9	210	0.7	0.10%	10.2096	0.0339	1.34E-05	3737.73
138	V	102	3890	772	30	210	0.7	0.20%	12.5010	0.0340	1.38E-05	3996.92
139	Q	102	3890	772	30	210	0.8	0.20%	14.4158	0.0262	1.22E-05	4343.85
140	T	80	6320	528	32.9	210	0.8	0.10%	10.9859	0.0261	1.18E-05	4193.25
141	T	80	6320	528	32.9	210	0.4	0.20%	15.3556	0.0574	2.30E-05	2506.13
142	T	80	6320	528	32.9	210	0.5	0.20%	13.6150	0.0496	1.87E-05	2851.99
143	T	80	6320	528	32.9	210	0.6	0.20%	12.9959	0.0418	1.57E-05	3206.29
144	T	80	6320	528	32.9	210	0.7	0.20%	13.4850	0.0340	1.36E-05	3889.57
145	V	102	3890	772	30	210	0.5	0.30%	14.6949	0.0498	1.92E-05	3277.69
146	Q	102	3890	772	30	210	0.4	0.30%	16.2564	0.0576	2.35E-05	2660.00
147	T	80	6320	528	32.9	210	0.8	0.20%	15.8942	0.0261	1.20E-05	4252.30
148	T	80	6320	528	32.9	210	0.3	0.30%	20.2649	0.0653	3.01E-05	2261.50
149	T	80	6320	528	32.9	210	0.5	0.30%	15.5803	0.0497	1.89E-05	3088.19
150	T	80	6320	528	32.9	210	0.6	0.30%	15.4512	0.0418	1.59E-05	3501.53
151	T	80	6320	528	32.9	210	0.8	0.30%	20.7932	0.0262	1.22E-05	4496.93
152	V	80	6320	528	32.9	210	0.3	0.20%	18.8604	0.0653	2.99E-05	2253.07
153	Q	80	6320	528	32.9	210	0.6	0.10%	10.5381	0.0417	1.56E-05	3096.63
154	T	-	-	-	-	330	0.4	0.00%	12.0760	0.0573	2.26E-05	2490.43
155	T	-	-	-	-	330	0.6	0.00%	8.0780	0.0417	1.54E-05	3101.30
156	T	-	-	-	-	330	0.7	0.00%	6.9300	0.0339	1.32E-05	3648.70
157	T	-	-	-	-	330	0.8	0.00%	6.0680	0.0260	1.16E-05	4299.23
158	T	64	8960	390	401	330	0.3	0.10%	17.5543	0.0652	2.97E-05	2300.49
159	V	80	6320	528	32.9	210	0.7	0.30%	16.7562	0.0340	1.38E-05	3914.88
160	Q	80	6320	528	32.9	210	0.4	0.30%	16.9939	0.0575	2.32E-05	2590.49
161	T	64	8960	390	401	330	0.4	0.10%	13.8321	0.0574	2.27E-05	2628.66
162	T	64	8960	390	401	330	0.6	0.10%	10.7119	0.0417	1.55E-05	3623.78
163	T	64	8960	390	401	330	0.7	0.10%	10.4415	0.0339	1.34E-05	4227.20
164	T	64	8960	390	401	330	0.8	0.10%	11.3340	0.0261	1.18E-05	4481.27
165	T	64	8960	390	401	330	0.3	0.20%	19.0590	0.0652	2.98E-05	2459.28
166	V	-	-	-	-	330	0.5	0.00%	9.6800	0.0495	1.83E-05	2746.95
167	Q	-	-	-	-	330	0.3	0.00%	16.0490	0.0652	2.96E-05	1998.57
168	T	64	8960	390	401	330	0.5	0.20%	13.8934	0.0496	1.86E-05	3369.71
169	T	64	8960	390	401	330	0.6	0.20%	13.3440	0.0418	1.56E-05	3793.16
170	T	64	8960	390	401	330	0.8	0.20%	16.5928	0.0261	1.19E-05	4661.24

Table C.1 ANN input and output parameters for 234 data points (continued)

		I:0	I:1	I:2	I:3	I:4	I:5	I:6	I:7	I:8	I:9	O:10
171	T	64	8960	390	401	330	0.3	0.30%	20.5631	0.0653	3.00E-05	2554.56
172	V	64	8960	390	401	330	0.5	0.10%	11.7873	0.0496	1.84E-05	2978.01
173	Q	64	8960	390	401	330	0.4	0.20%	15.5875	0.0574	2.29E-05	2787.46
174	T	64	8960	390	401	330	0.4	0.30%	17.3420	0.0575	2.30E-05	2935.67
175	T	64	8960	390	401	330	0.5	0.30%	15.9983	0.0496	1.87E-05	3507.33
176	T	64	8960	390	401	330	0.7	0.30%	17.4548	0.0340	1.36E-05	4565.96
177	T	64	8960	390	401	330	0.8	0.30%	21.8445	0.0261	1.20E-05	4693.00
178	V	64	8960	390	401	330	0.7	0.20%	13.9497	0.0339	1.35E-05	4354.23
179	Q	64	8960	390	401	330	0.6	0.30%	15.9743	0.0418	1.58E-05	4004.89
180	T	27	2700	900	237	330	0.4	0.10%	13.1897	0.0575	2.30E-05	2618.08
181	T	27	2700	900	237	330	0.5	0.10%	11.0163	0.0496	1.87E-05	2935.67
182	T	27	2700	900	237	330	0.6	0.10%	9.7480	0.0418	1.58E-05	3507.33
183	T	27	2700	900	237	330	0.8	0.10%	9.4042	0.0261	1.21E-05	4428.34
184	V	27	2700	900	237	330	0.3	0.10%	17.0037	0.0653	3.00E-05	2279.32
185	Q	27	2700	900	237	330	0.7	0.10%	9.1558	0.0340	1.37E-05	4089.58
186	T	27	2700	900	237	330	0.3	0.20%	17.9572	0.0654	3.04E-05	2416.94
187	T	27	2700	900	237	330	0.4	0.20%	14.3018	0.0576	2.35E-05	2755.70
188	T	27	2700	900	237	330	0.6	0.20%	11.4142	0.0419	1.62E-05	3655.54
189	T	27	2700	900	237	330	0.7	0.20%	11.3749	0.0341	1.41E-05	4206.03
190	V	27	2700	900	237	330	0.5	0.20%	12.3502	0.0498	1.92E-05	3189.74
191	Q	27	2700	900	237	330	0.8	0.20%	12.7254	0.0263	1.25E-05	4523.62
192	T	27	2700	900	237	330	0.3	0.30%	18.9095	0.0655	3.09E-05	2533.39
193	T	27	2700	900	237	330	0.5	0.30%	13.6816	0.0499	1.96E-05	3464.98
194	T	27	2700	900	237	330	0.7	0.30%	13.5874	0.0342	1.45E-05	4438.93
195	T	27	2700	900	237	330	0.8	0.30%	16.0316	0.0264	1.29E-05	4661.24
196	V	27	2700	900	237	330	0.4	0.30%	15.4122	0.0577	2.39E-05	2882.74
197	Q	27	2700	900	237	330	0.6	0.30%	13.0766	0.0420	1.67E-05	3846.09
198	T	102	3890	772	30	330	0.3	0.10%	17.2447	0.0653	2.99E-05	2247.56
199	T	102	3890	772	30	330	0.4	0.10%	13.4709	0.0574	2.29E-05	2596.91
200	T	102	3890	772	30	330	0.6	0.10%	10.1698	0.0418	1.57E-05	3316.78
201	T	102	3890	772	30	330	0.7	0.10%	9.7184	0.0339	1.35E-05	3888.44
202	V	102	3890	772	30	330	0.8	0.10%	10.2484	0.0261	1.19E-05	4396.58
203	Q	102	3890	772	30	330	0.5	0.10%	11.3537	0.0496	1.86E-05	3062.70
204	T	102	3890	772	30	330	0.4	0.20%	14.8644	0.0575	2.32E-05	2618.08
205	T	102	3890	772	30	330	0.5	0.20%	13.0254	0.0497	1.89E-05	3136.81

Table C.1 ANN input and output parameters for 234 data points (continued)

		I:0	I:1	I:2	I:3	I:4	I:5	I:6	I:7	I:8	I:9	O:10
206	T	102	3890	772	30	330	0.7	0.20%	12.5010	0.0340	1.38E-05	4100.16
207	T	102	3890	772	30	330	0.8	0.20%	14.4158	0.0262	1.22E-05	4513.03
208	V	102	3890	772	30	330	0.6	0.20%	12.2584	0.0419	1.60E-05	3528.50
209	Q	102	3890	772	30	330	0.3	0.20%	18.4394	0.0653	3.02E-05	2279.32
210	T	102	3890	772	30	330	0.3	0.30%	19.6330	0.0654	3.05E-05	2438.11
211	T	102	3890	772	30	330	0.5	0.30%	14.6949	0.0498	1.92E-05	3401.47
212	T	102	3890	772	30	330	0.6	0.30%	14.3437	0.0419	1.63E-05	3666.12
213	T	102	3890	772	30	330	0.8	0.30%	18.5701	0.0263	1.25E-05	4597.72
214	V	102	3890	772	30	330	0.7	0.30%	15.2778	0.0341	1.41E-05	4290.72
215	Q	102	3890	772	30	330	0.4	0.30%	16.2564	0.0576	2.35E-05	2872.15
216	T	80	6320	528	32.9	330	0.3	0.10%	17.4551	0.0652	2.98E-05	2098.21
217	T	80	6320	528	32.9	330	0.5	0.10%	11.6483	0.0496	1.85E-05	2900.16
218	T	80	6320	528	32.9	330	0.7	0.10%	10.2096	0.0339	1.34E-05	3786.53
219	T	80	6320	528	32.9	330	0.8	0.10%	10.9859	0.0261	1.18E-05	4387.99
220	V	80	6320	528	32.9	330	0.6	0.10%	10.5381	0.0417	1.56E-05	3248.38
221	Q	80	6320	528	32.9	330	0.4	0.10%	13.7163	0.0574	2.28E-05	2594.16
222	T	80	6320	528	32.9	330	0.4	0.20%	15.3556	0.0574	2.30E-05	2752.44
223	T	80	6320	528	32.9	330	0.5	0.20%	13.6150	0.0496	1.87E-05	3100.65
224	T	80	6320	528	32.9	330	0.6	0.20%	12.9959	0.0418	1.57E-05	3301.14
225	T	80	6320	528	32.9	330	0.8	0.20%	15.8942	0.0261	1.20E-05	4482.95
226	V	80	6320	528	32.9	330	0.3	0.20%	18.8604	0.0653	2.99E-05	2414.77
227	Q	80	6320	528	32.9	330	0.7	0.20%	13.4850	0.0340	1.36E-05	3839.29
228	T	80	6320	528	32.9	330	0.3	0.30%	20.2649	0.0653	3.01E-05	2509.74
229	T	80	6320	528	32.9	330	0.4	0.30%	16.9939	0.0575	2.32E-05	2857.95
230	T	80	6320	528	32.9	330	0.6	0.30%	15.4512	0.0418	1.59E-05	3501.62
231	T	80	6320	528	32.9	330	0.7	0.30%	16.7562	0.0340	1.38E-05	3997.56
232	V	80	6320	528	32.9	330	0.8	0.30%	20.7932	0.0262	1.22E-05	4641.23
233	Q	80	6320	528	32.9	330	0.5	0.30%	15.5803	0.0497	1.89E-05	3142.86

D. Nanorefrigerant Heat Transfer Coefficient with respect to Quality Change with 4th order Polynomial Fitting for 0.1-0.3 and 0.8-1.0 (P_{sat}=101.325 kPa)

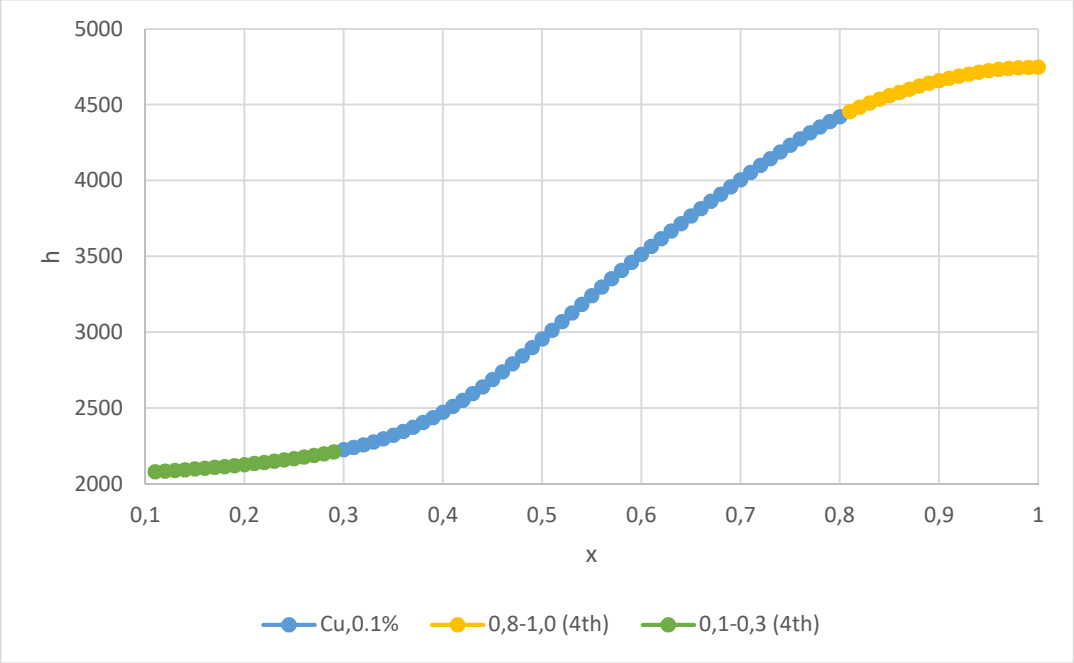

Figure D.1 0.1% mass fraction of R141b-Cu

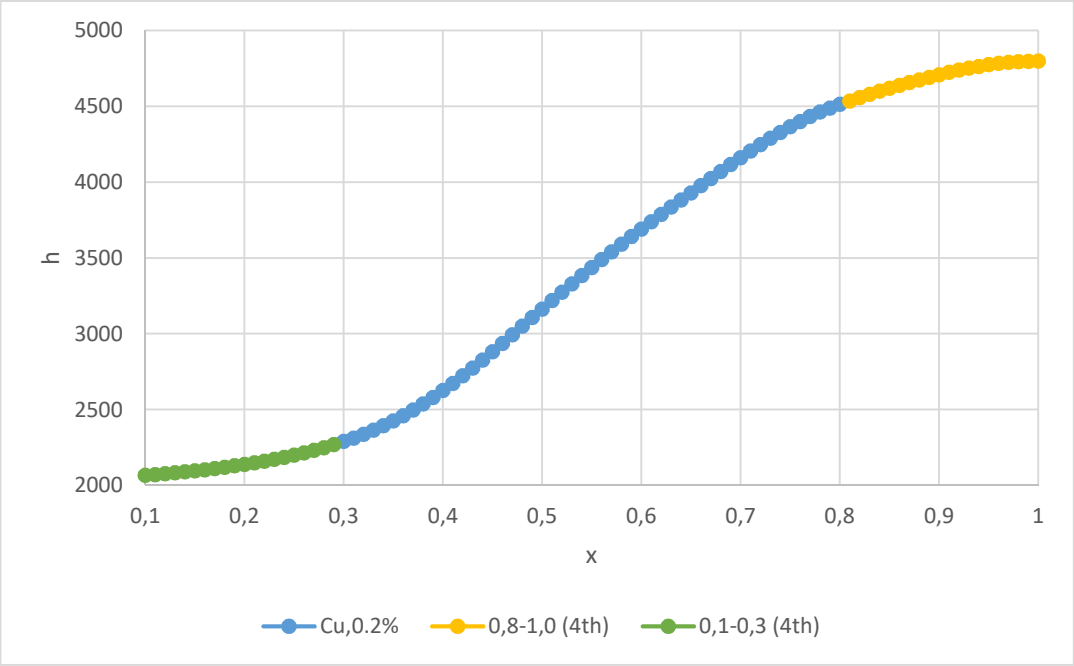

Figure D.2 0.2% mass fraction of R141b-Cu

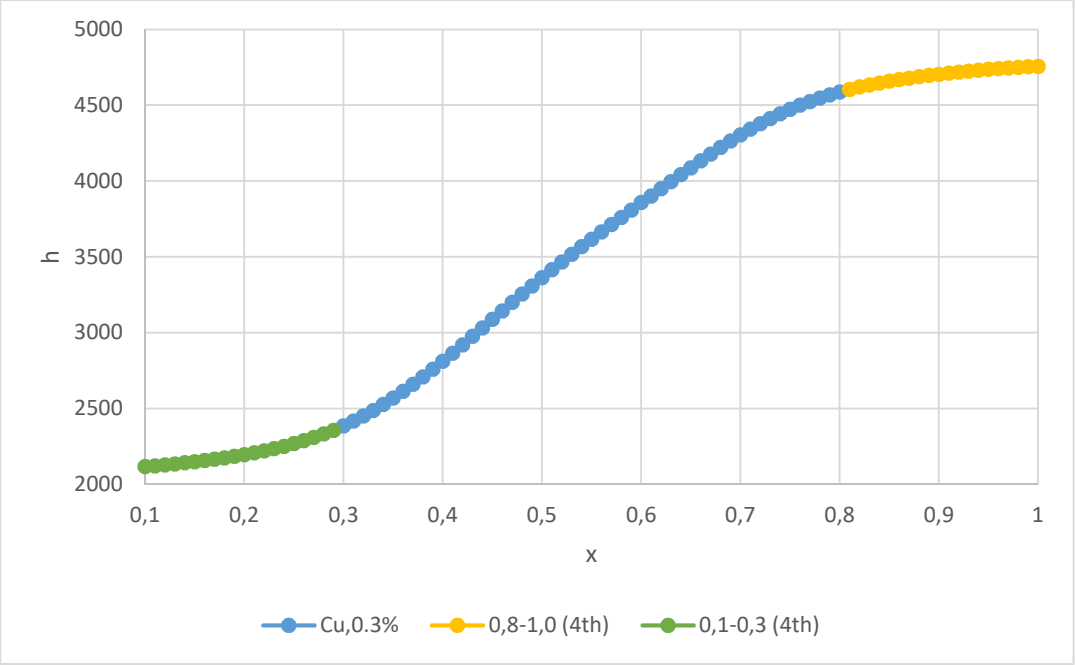

Figure D.3 0.3% mass fraction of R141b-Cu

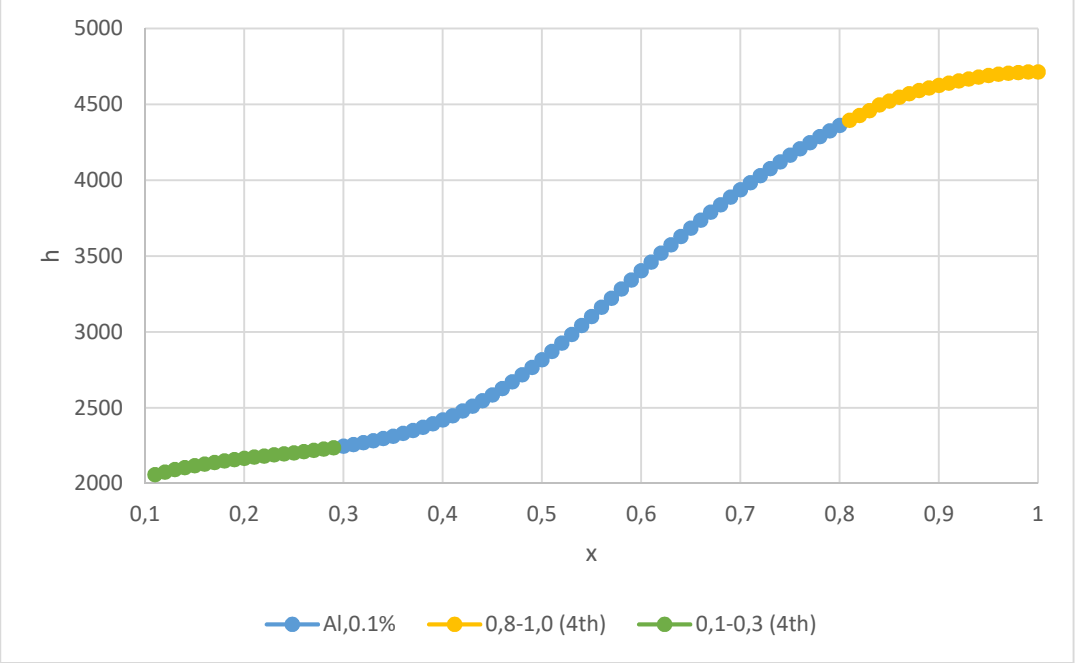

Figure D.4 0.1% mass fraction of R141b-Al

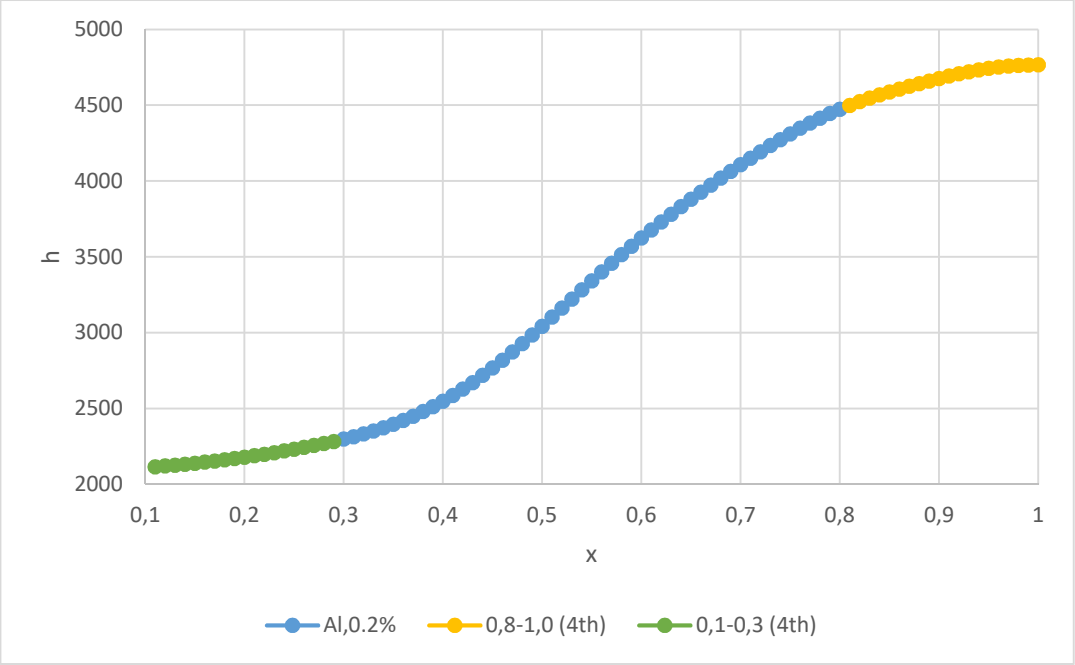

Figure D.5 0.2% mass fraction of R141b-Al

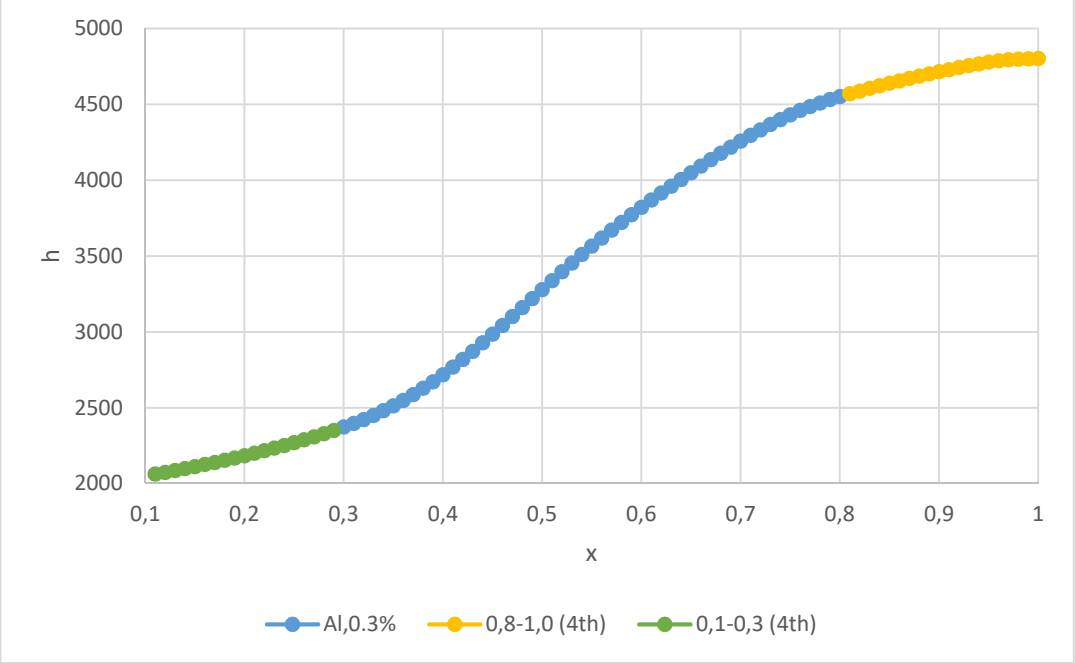

Figure D.6 0.3% mass fraction of R141b-Al

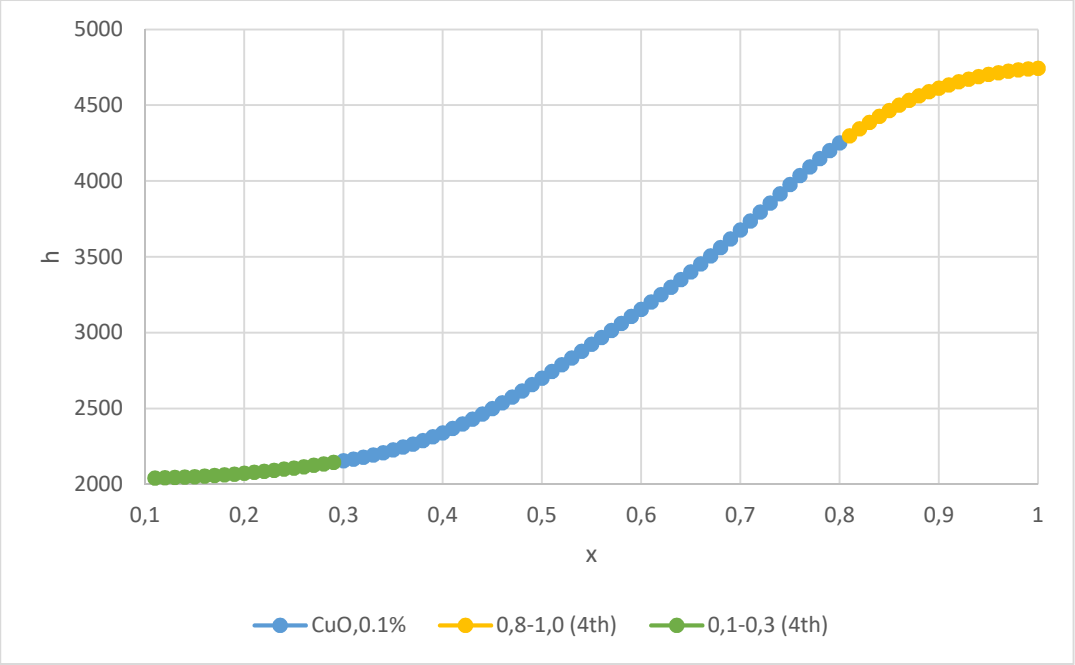

Figure D.7 0.1% mass fraction of R141b-CuO

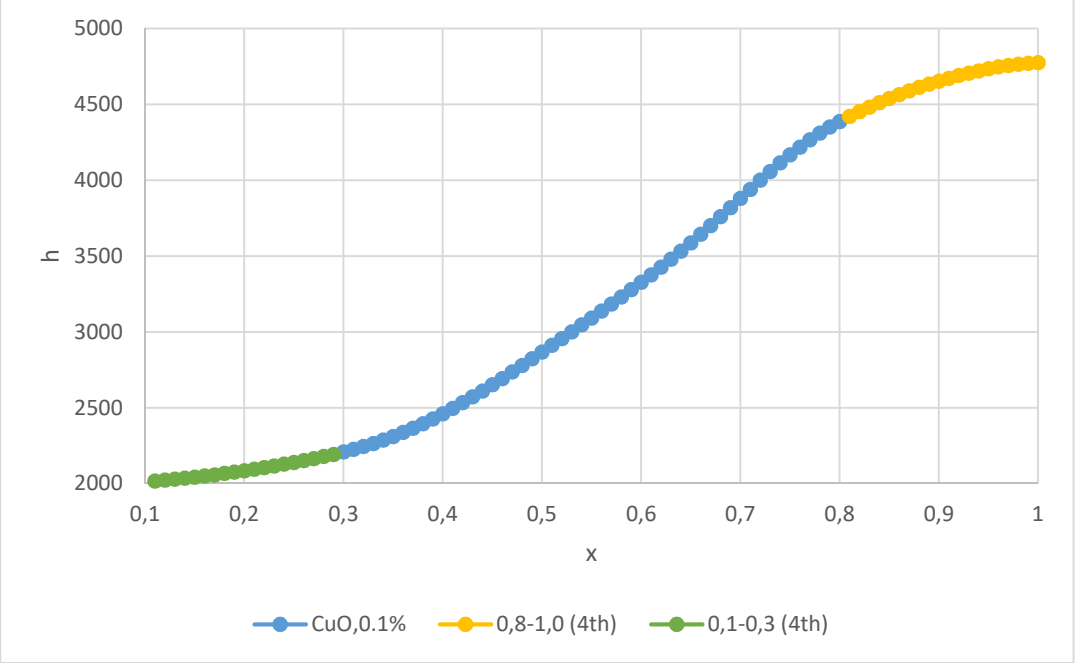

Figure D.8 0.2% mass fraction of R141b-CuO

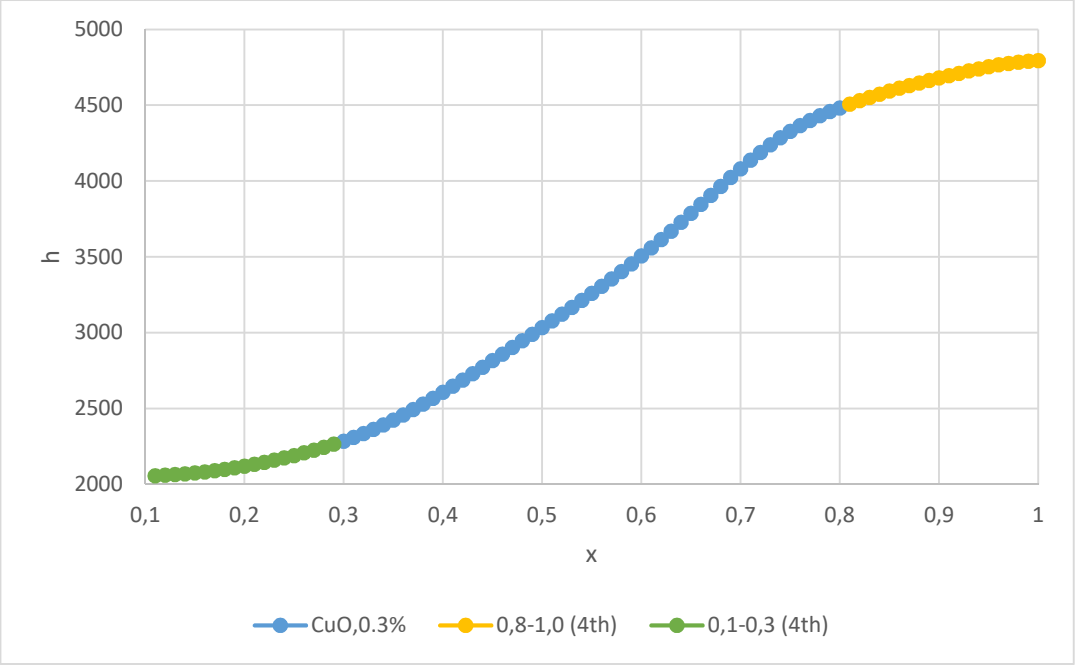

Figure D.9 0.3% mass fraction of R141b-CuO

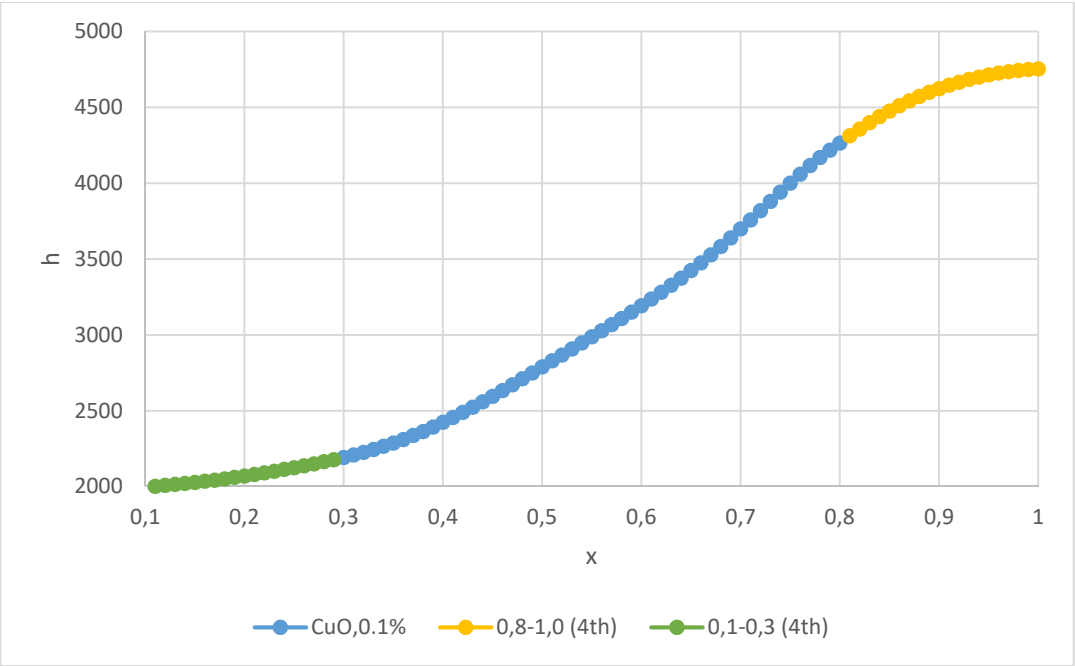

Figure D.10 0.1% mass fraction of R141b-Al_2O_3

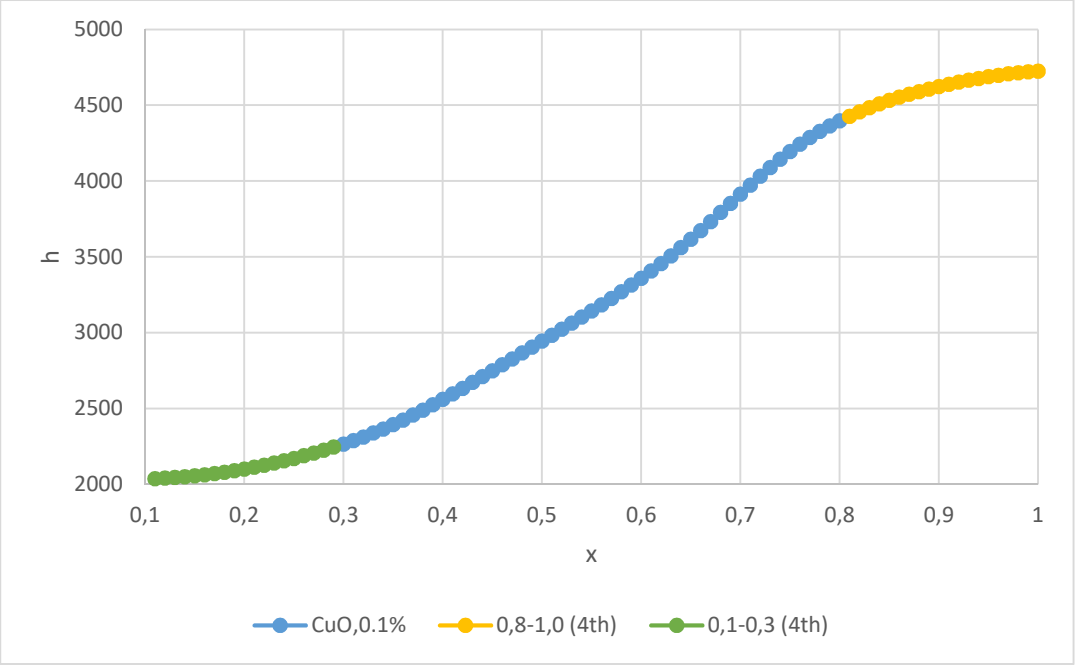

Figure D.11 0.2% mass fraction of R141b-Al_2O_3

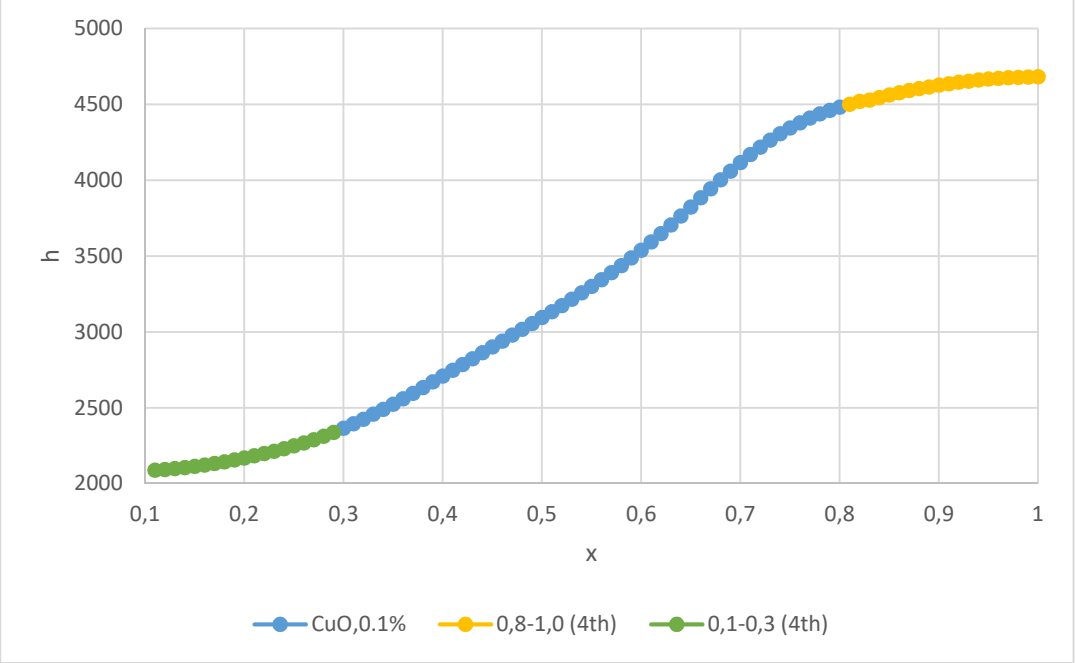

Figure D.12 0.3% mass fraction of R141b-Al_2O_3 e

CURRICULUM VITAE

Surname, Name: Tekin, Bilgehan

EDUCATION

Degree	Institution	Year of Graduation
MS	METU Mechanical Engineering	2011
BS	METU Mechanical Engineering	2008
High School	Gazi Anadolu High School, Ankara	2003

FOREIGN LANGUAGES

Advanced English, Intermediate German, Pre-intermediate Spanish

PUBLICATIONS

1. Tekin, B., Yazıcıoğlu, A.G., Kerpiççi, H., Kakaç, S. 2010. Experimental Investigation of Heat Transfer and Pressure Drop for Two-Phase R-134A Flow in a 1.65 MM Copper Tube, ASME ESDA, ESDA2010-25432, July 12-24.

2. Tekin, B., Yazıcıoğlu, A.G., Kerpiççi, H., Kakaç, S. 2011. 1.65 mm'lik Bir Bakır Miniboruda İki Fazlı R134a Akışının Deneysel Olarak İncelenmesi, 18. ULUSAL ISI BİLİMİ ve TEKNİĞİ KONGRESİ, ULIBTK'11, September 7-10.

3. Tekin, B., Yazıcıoğlu, A.G., 2016. Thermophysical Properties of Two-Phase Refrigerant Based Nanofluids in a Refrigeration Cycle, ASME 2016 SHTC, HT2016-7192, July 10-14.

INTERESTS

Basketball, Travelling, Reading, Puzzle